Università
Ca'Foscari
Venezia

Master's Degree Programme in

Sustainable Chemistry and

Technologies

Final Thesis

Manganese(II) and lanthanide(III) luminescent coordination compounds with ligands based on pentavalent phosphorous

Supervisor
Prof. Marco Bortoluzzi

Graduand
Andrea DI Vera
Matricolation number
848732

Academic Year
2018 / 2019

To my mother, my father and my brother.

INDEX

1. INTRODUCTION

1.1 d-block luminescence

In last decades research made huge progresses in the area of luminescence-based devices and their applications. Great developments have been made on OLEDs (organic light emitting diodes), LEDs (light emitting diodes) and similar devices due the high demand of new light systems such as monitors and displays. Probes and sensors using luminescent materials are currently of interest because of their high sensitivity and specificity. Remote sensors in fiber optic based systems are used for measuring oxygen, pH, pCO_2, temperature, and for immunoassays. Response is monitored by changes in luminescence intensity, lifetime (τ) or spectral distribution. An increasingly important class of sensor materials is based on luminescent transition metal complexes, especially with Ru, Os, Re, Rh, and Ir as metal centres. Long lifetimes of these species afford simpler and less expensive measurements compared to traditional organic fluorophores, which have typically nanoseconds lifetimes.

Differently from lanthanide complexes, that will be treated on this assay, luminescence properties of d-group species are strongly influenced by the ligand field. It is possible to distinguee four main mechanisms involved in luminescence of d-metal complexes: MC (metal centred), MLCT (metal to ligand charge transfer), LMCT (ligand to metal charge transfer) and LLCT (ligand to ligand charge transfer), depicted in Fig. 1.

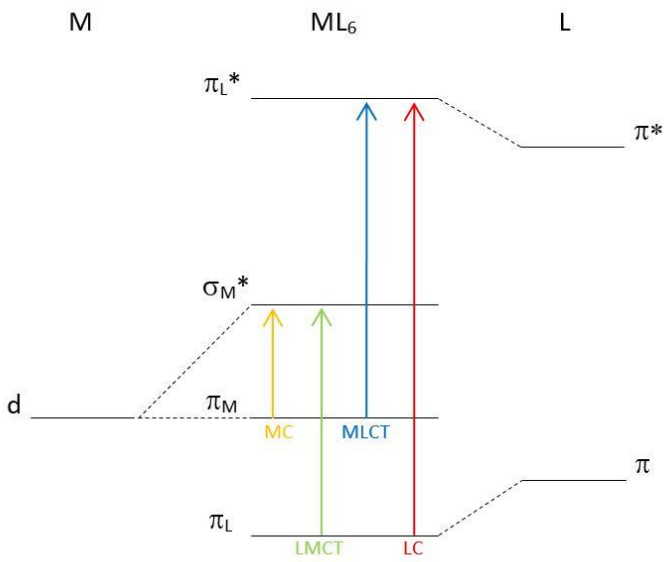

Figure 1. Molecular orbitals diagram for a generic octahedral complex of a transition metal ML_6 and possible electronic transitions: MC (yellow arrow), LMCT (green arrow), MLCT (blue arrow) and LC (red arrow) mechanisms.

The first two mechanisms are the most common for compounds of technological interest. In order to the determine the working mechanism, it's to be considered the oxidation state and the electronic configuration of the metal. Late transition metal complexes with d^6, d^8 e d^{10} configurations usually follow a MLCT mechanisms, and typical centres are Re(I), Ru(II), Os(II), Ir(III), Pt(II), Au(I) and Au(III).

This type of mechanism arises from transfer of electrons from MOs with metal-like character to empty orbitals with ligand-like character, followed by the radiative return to the ground state. For this reason, luminescent properties can be widely tuned by modifying the π system of the ligands, thus influencing both the absorption and the emission features. On considering MLCT mechanisms for ground-state singlet molecules, the emitting excited state can have both singlet or triplet multiplicity, depending upon the efficiency of intersystem crossing. For heavy metals the common situation is related to the $T_1 \rightarrow S_0$ transition.[1] There is an astonishing number of examples about luminescent complexes falling in this category, some of them with huge technological application fields. In Fig. 2 are reported some examples of luminescent complexes.

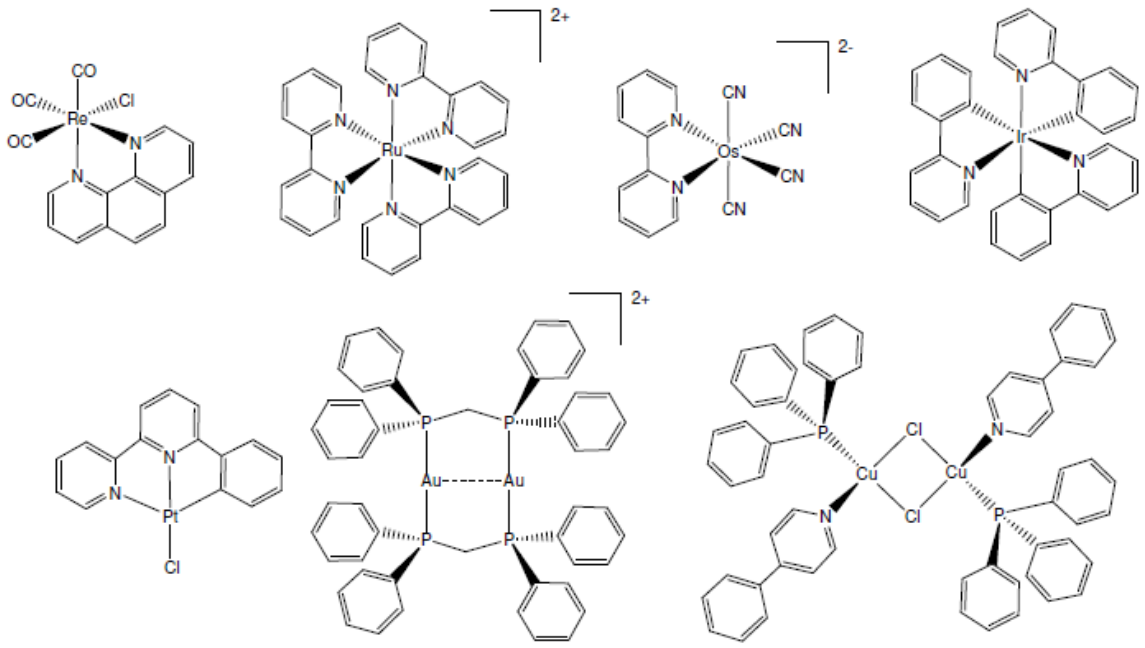

Figure 2. Some examples of luminescent complexes of transition elements.

For what concerns selected examples, recently Ru(II) diimine complexes conjugated to biomolecules were deeply investigated for biomedical applications, focusing the attention on the development of probes for the investigation of membrane dynamics. According to E. Rosenberg (2019), the study shows a strong dependence on the environment of these probes in both liposomes and nanodiscs.[2] Stable luminescent iridium(III) complexes with bis(N-heterocyclic carbene) display strong emission in deaerated solutions at room temperature with photoluminescence quantum yields up to 89% and emission lifetimes up to 96 μs.[3] Iridium(III) derivatives can be used, among all, to realize information self-encryption and anti-counterfeiting systems due the tuneable luminescence response to the electric field.[4] Ru(II) polypyridines and cyclometalated Ir(III) complexes are currently the most prominent ^{3}MLCT emitters with d^6 electron configuration [5], but early studies already indicated that Cr(0) arylisocyanides have the potential to become earth-abundant alternatives to these precious metals.[6] Several platinum(II) and gold(III) heteroleptic complexes with polydentate ligands and strong σ-donor moieties showed interesting tuneable luminescence for OLEDs systems, whose general structure is depicted in Fig. 3.[7]

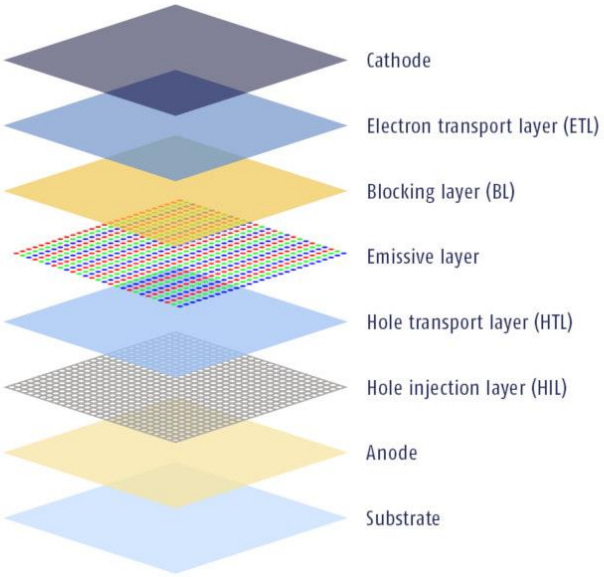

Figure 3. Schematic representation of an OLED.

Luminescent complexes can also be prepared with d^{10} centres, and the lack of d-d transitions caused by this configuration can be useful to limit the non-radiative decay. As a matter of fact, many copper(I) and gold(I) complexes show photoluminescent behaviour related to MLCT mechanism. Good examples are Cu(I) homoleptic complexes with 2,9 bis-substituted phenanthroline derivates, having general formula $[Cu(phen^{R2})_2]^+$.[8] In Fig. 4 are reported some phenanthroline-based ligands used for Cu(I) luminescent complexes.

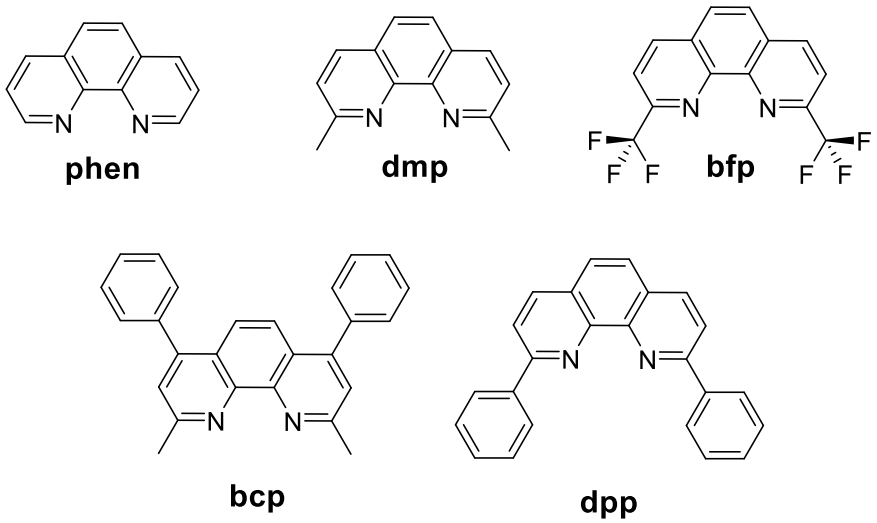

Figure 4. Examples of phenanthroline derivates.

The presence of ligands with well-designed steric bulk is necessary to reduce the probability of non-radiative decays, associated in the case of Cu(I) derivatives to the

distortion of the tetrahedral geometry moving from the ground state (formally d^{10}) to the excited state (formally d^9). The quantum yield is usually improved moving towards heteroleptic compounds with phosphines in the coordination sphere, such as $[Cu(^{R2}phen)(pop)][BF_4]$ (pop = bis(2(diphenylphosphino)phenyl)phenyl]ether.[9]

In the case of metal-centred emission the light absorbed populates an exited state of the metal, usually after a multiplicity change, and the process is followed by emission of light. Such a mechanism is limited to few metal ions, because usually d-d transitions are efficiently saturated by fast non-radiative decay routes. MC emissions occur when the geometry of the emitting excited state and that of the ground state are roughly similar. Chromium(III) complexes are good examples of this type of mechanism. Luminescent Cr(III) complexes such as $[Cr(bpy)_3]^{3+}$ (bpy = 2,2′-bipyridine), $[Cr(phen)_3]^{3+}$ (phen = 1,10-phenanthroline), or $[Cr(tpy)_2]^{3+}$ (tpy = 2,2′:6′,2″-terpyridine) were first studied more than 40 years ago.[10] Recently, Heinze, Resch-Genger and coworkers prepared a new tridentate polypyridine ligand capable to chelate the metal ion and afford a very strong crystal field (see Fig. 5). In the resulting $[Cr(L)_2]^{3+}$ complex the nearly perfect octahedral coordination is associated to striking quantum yield and high lifetime[11] once compared to bpy, phen and tpy systems.

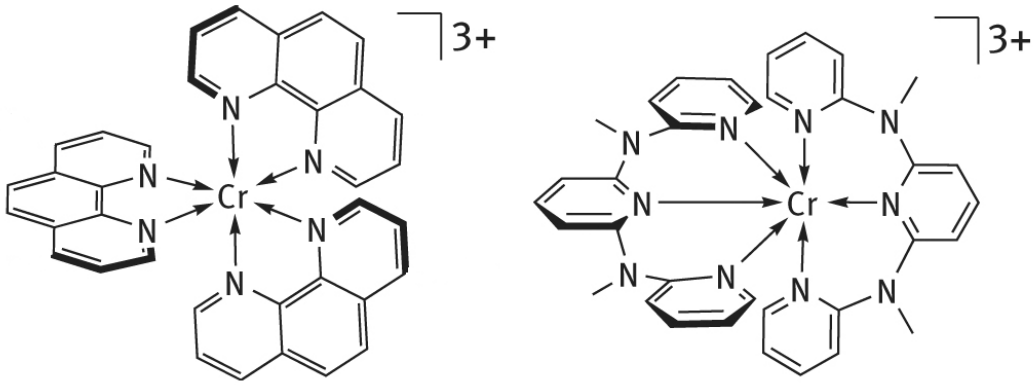

Figure 5. Homoleptic octahedral complexes of Cr(III) with phenanthroline on the left, 2,6-di(N-pyridin-2-yl-N-methyl-amino)pyridine on the right.

Despite the fact that second and third transition row elements are commonly used for luminescence purposes together with lanthanides, their cost and toxicity prompted the researchers in the recent years to find more sustainable alternatives. Promising

candidates for this replacement may be represented by chromium(III) and manganese(II) species because of their low toxicity and cost. Thanks to the high abundance and strong luminescent behaviour, manganese could represent a promising choice for future studies.

1.2 Manganese luminescence

Among the elements of the first transition series, manganese plays a central role for the preparation of luminescent compounds, and several inorganic luminescent derivatives are known for the oxidation states Mn(II), Mn(IV) and Mn(V).[12] The key features of manganese luminescence are to be referred to its electronic structure. Manganese has an incomplete d-shell in the previously summarized oxidation states and the crystal field has a strong influence on the properties of the complexes. Tetravalent manganese is usually used as a dopant into solid state materials such as gadolinium and gallium garnets to obtain red-yellow emission. Recently Senden *et al*. synthetized a manganese(IV) material for warm white LEDs. [13]
One outstanding example of luminescent mineral with NIR emission based on manganese(V) is the magmatic apatite, where some phosphate ions are replaced by tetrahedral $[MnO_4]^{3-}$.[14] On considering very recent studies, it is worth noting that manganese(III) displays an interesting cyan-blue luminescence in a tetranuclear cyanide-bridged Mn^{III}–Fe^{III} complex, as reported by Donmez and co-workers in 2018.[15]
The divalent state is however probably the most interesting oxidation state in terms of luminescence of discrete molecules. For what concerns recent advanced in luminescent ionic materials, many older fluorescent lamps, as well as lamps that have recently been produced by some non-Chinese lamp manufacturers contain the halophosphate phosphor $(Sr,Ca)_{10}(PO_4)_6(Cl,F)_2:Sb^{3+},Mn^{2+}$.[16] Ultralong lasting red to NIR luminescence originates from Mn(II) centres in doped sodium gallium aluminium germanate glasses and (Al,Ga)-albite glass-ceramics.[17] Manganese(II) is a hard Lewis acid and its coordination chemistry mostly concerns O- and N-donor ligands and halide ions.
Manganese(II) is a d^5 centre and for the high spin configuration the term symbol of the ground state is ^6S (L= 0). The electronic configuration of the ground state indicates a spherical distribution of the electron density around the metal centre, without sublevels

separation due the crystal field strength and absence of d-d absorptions between levels with the same multiplicity. Excitation of the Mn(II) ion is therefore related to multiplicity change, in particular from sextet to quartet with the coupling of two electrons. The transition involved is forbidden by the Laporte's rule and the consequence is a small absorption coefficient. The first excited state is ^4G, composed by 9 sublevels which lose their degeneracy because of the crystal field. For cubic symmetries the sublevels are separated in four groups, $^4T_1$, $^4T_2$, $^4A_1$ and ^4E. The emission is a phosphorescence with the lifetime much longer than a common fluorescence.

The Tanabe-Sugano diagram for the d^5 configuration is the most common tool to comprehend the influence of the crystal field strength on luminescence. As observable in Fig. 6, the diagram shows two main regions which identify the low and high spin configurations.

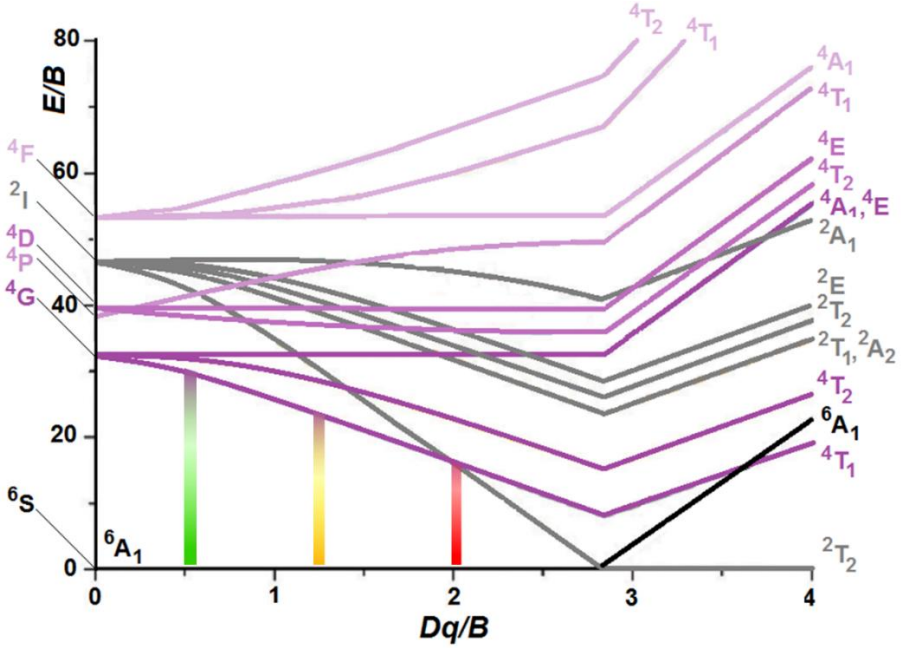

Figure 6. Tanabe-Sugano diagram for d^5 electron configuration.

In the case of low crystal field strength, *i.e.* the common situation for Mn(II) derivatives, the high spin configuration prevails because of the reduction of interelectronic repulsion and the stability given by the exchange interaction among parallel electrons. The energy gap between the first exited and the ground state is strongly dependant on the geometry and the electronic features of the first coordination sphere. In the case of octahedral complexes, the energy gap between the $^4T_1$ (^4G) and $^6A_1$ (^6S) levels

generates emission in the yellow-red part of the spectra, while in the presence of a tetrahedral geometry the energy gap is higher because of the smaller crystal field strength and consequently green emission is observed. The reduction of the emission energy on increasing the crystal field strength can be easily understood on considering that the d-orbitals closer to the ligands are more populated in the ground state rather than in the excited state.

The coordination geometry not only influences the energy gap, but also the emissions lifetimes. In octahedral complexes the emissions are parity and spin forbidden, while in tetrahedral complexes the partial p-nature of the molecular orbitals involved in the transition makes the emission only spin forbidden, and consequently shorter lifetimes are measured. The participation of d-and p-type metal orbitals to the same MOs is shown for clarity in Fig. 7.

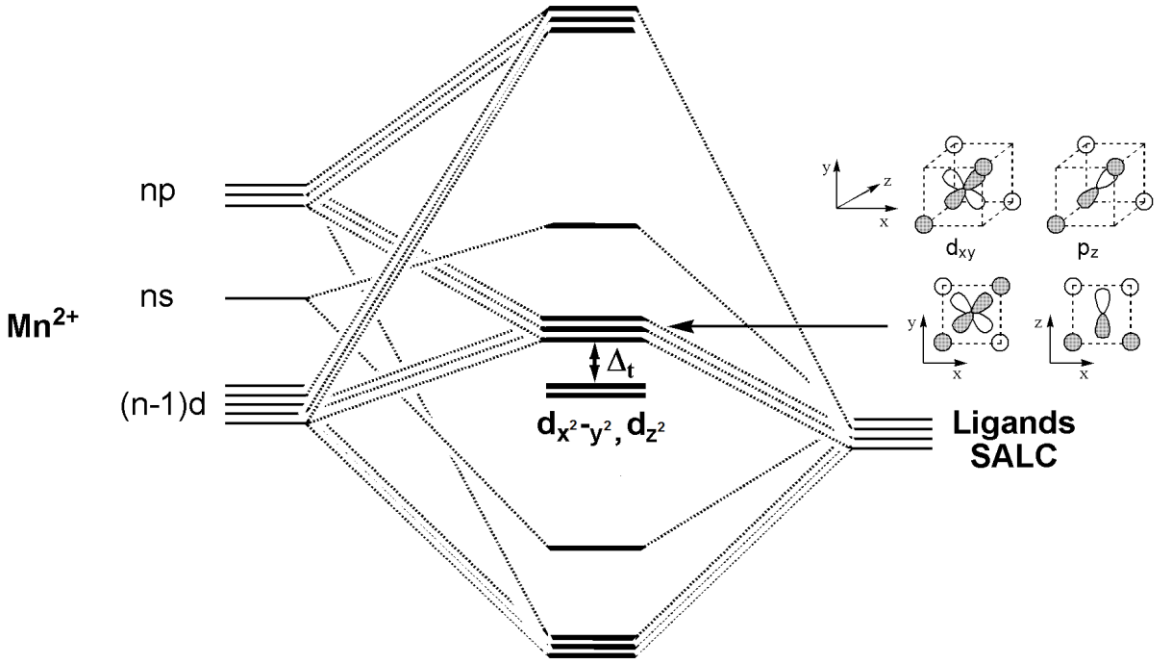

Figure 7. Ligand field diagram for σ-interactions in tetrahedral complexes.

1.3 Manganese complexes

Focusing the attention on the divalent oxidation state, the emission is associated to the $^4T_1(^4G) \rightarrow {}^6A_1(^6S)$ transition. The studies concerning luminescent Mn(II) complexes were initially concentrated on tetrahedral green-emitting species such as $[MnX_4]^{2-}$ (X = Cl, Br, I) and $[MnBr_2(O=PPh_3)_2]$,[18] described for the first time during the sixties (Fig. 8).[19] Besides photoluminescence, also triboluminescence was observed for some of these compounds. Luminescence in the yellow-red range is instead usually associated to the presence of octahedral coordination sphere surrounding the metal ion and it is observed for several Mn(II)-containing minerals, inorganic materials, coordination polymers and nanoclusters.[20]

Advances in luminescent Mn(II) compounds were reported in the last years. Green-emitting tetrahedral complexes having general formula $[MnX_2(O=PPh_2\text{-}Ph\text{-}O\text{-}Ph\text{-}Ph_2P=O)]$ (X = Cl, Br, I; $O=PPh_2\text{-}Ph\text{-}O\text{-}Ph\text{-}Ph_2P=O$ = bis[2-(diphenylphosphino)-phenyl] ether dioxide) showed promising luminescence features, strongly influenced by the nature of the anionic ligands (Fig. 8).[21] $[NH_2{}^iPr_2]_2[MnBr_4]$ (^{i}Pr = isopropyl) is a material of interest for electronic application that exhibits green luminescence.[22] Strong luminescence was observed also for complexes having formulae $[MnX_2\{O=P(NMe_2)_2R\}_2]$ (X = Br, I; R = NMe_2, Ph), with photoluminescence lifetimes in the range 100–1000 μs, strongly dependent upon the choice of the halide.[23] Early studies indicate that the presence of heavy halides in the coordination sphere leads an acceleration of the radiative decay. As proposed by Wrighton and Ginley in 1974, the effect can be ascribed to an increase of the spin–orbit coupling value, while differences in the degree of covalency in metal-halide bonds are negligible. The halide orbitals are close to those involved in the spin-forbidden transition $^4T_1(^4G) \rightarrow {}^6A_1(^6S)$, and it is likely to suppose some mixing among metal and ligand orbitals.[24]

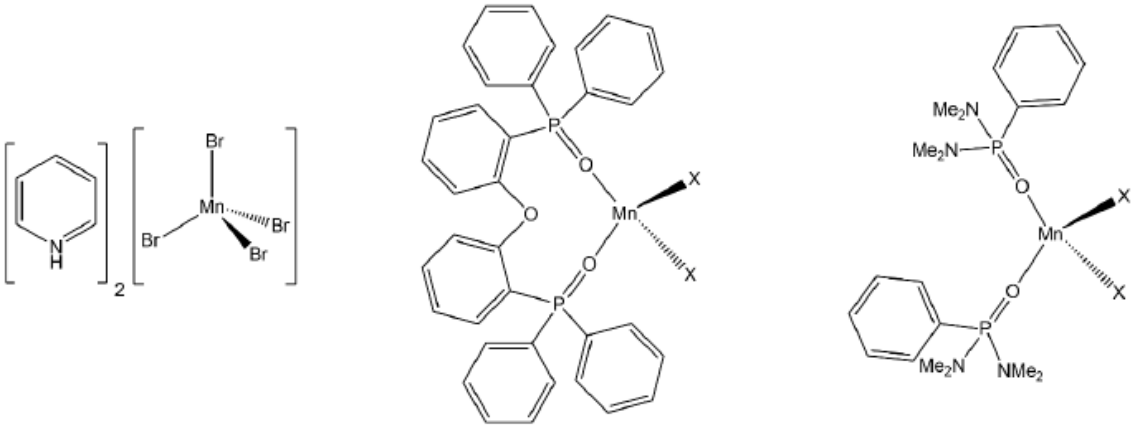

Figure 8. Examples of luminescent tetrahedral complexes of Mn(II)

Current examples of red-emitting species are coordination polymers such as $([NH_2C_4H_8][MnX_3])_\infty$ (X = Cl, Br; $[NH_2C_4H_8]^+$ = pyrrolidinium ion), $([NH_2C_4H_6][MnCl_3])_\infty$ ($[NH_2C_4H_6]^+$ = 3-pyrrolinium ion), and $([Me_3NCH_2Cl][MnCl_3])_\infty$ ($[Me_3NCH_2Cl]^+$ = trimethylchloromethyl ammonium ion), where the manganese centre is coordinated by six halide ions.[25] Another coordination polymer synthesized from the reaction between $Mn(ClO_4)_2{\cdot}6H_2O$ and 1,2,4,5-tetrakis(diphenylphosphinyl) benzene in dimethylformamide showed red luminescence at temperatures below 200 K.[26] The reaction between manganese(II) halides and tris(2-aminoethyl)amine in acidic medium afforded derivatives containing penta- and hexacoordinated Mn(II) centres with emission maxima between 573 and 590 nm.[27] Strong orange photoluminescence was detected for octahedral cationic complexes having formulae $[Mn(dppmO_2)_3]^{2+}$ and $[Mn(dppeO_2)_3]^{2+}$ ($dppmO_2$ = bis(diphenylphosphino)methane dioxide; $dppeO_2$ = 1,2-bis(diphenylphosphino)ethane dioxide). The emission intensity of these compounds is about six time higher than that of the well-known orange-luminescent complex $[Ru(bpy)_3]Cl_2$ under the same experimental conditions. One-dimensional coordination polymers obtained from the reaction of $MnBr_2$ with $dppeO_2$ exhibited luminescent vapochroism by reversible coordination of dimethylformamide, changing the coordination geometry from tetrahedral to trigonal bipyramidal.[28] Fig. 9 shows the two species involved.

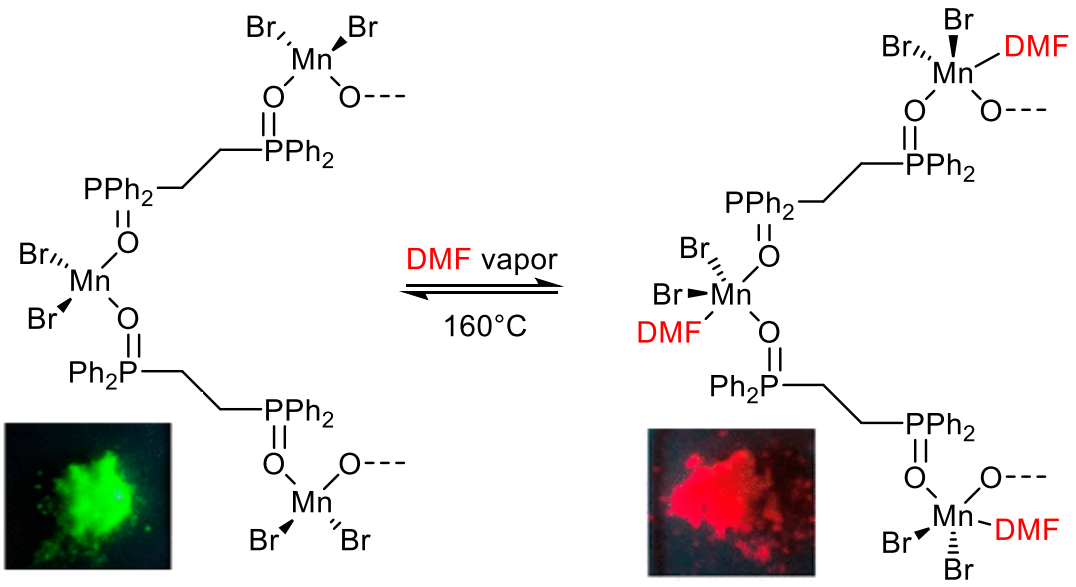

Figure 9. Luminescent vapochroism of Mn(II) with dppeO_2 as ligand by reversible coordination of DMF.

Further compounds with remarkable luminescence in the yellow to red range are neutral and ionic six- and seven-coordinated complexes prepared from the reaction between 18-crown-6 ether and $MnBr_2$.[29] A mononuclear manganese(II) complex with a chelating pyrazine-pyrimidine ligand showed excitation wavelength-dependent emission, with ligand-centred and metal-centred transitions.[30] In 2019 the first observation of luminescence for Mn(II) complexes with a square-pyramidal geometry (C_{4v}) of the metal was reported. The complexes of such type are halide derivatives with the ligand NMe_2-$CH(Ph_2P{=}O)_2$ (Fig.10) and showed at ambient temperature red photoluminescence with millisecond lifetimes. The emission for this non-O_h and non-T_d geometry is related to the spin-forbidden transition $^4E(^4G) \rightarrow 6A_1(^6S)$.[31]

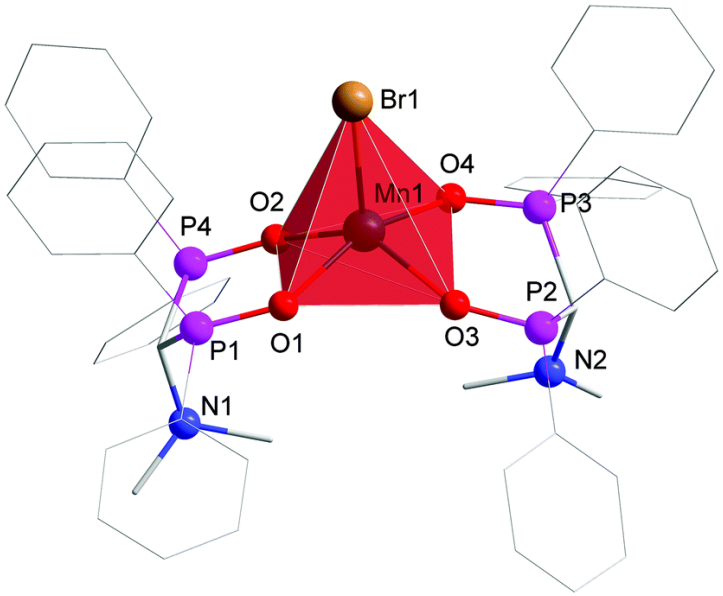

Figure 10. The structure of the cation in [MnBr(L)$_2$]Br (L= NMe$_2$-CH(Ph$_2$P=O)$_2$).

Phosphoramides, phenylphosphonic diamides and phosphine oxides appear suitable ligands for the preparation of luminescent Mn(II) complexes. These species can be modified with the introduction of suitable light-harvesting substituents, and the skeleton of the ligands can be made more rigid in order to reduce the non-radiative decay. For instance, an enhancement of Mn(II) luminescence was recently observed by using ligands such as 1,3-dimethyl-2-phenyl-1,3-diazaphospholidine-2-oxide, O=P(NMeCH$_2$CH$_2$NMe)Ph, and *N*,*N*,*N*',*N*'-tetramethyl-*P*-indol-1-ylphosphonic diamide, O=P(NMe$_2$)$_2$Ind (Ind = indol-1-yl).[32] Studies currently in progress have shown that the replacement of the phenyl ring with naphtyl substituents in arylphosphonic diamide ligands affords the unexpected formation of red-emitting Mn(II) complexes.[33] Such a result highlights the strong dependence of Mn(II) coordination sphere upon small variations of the electronic and steric properties of the ligands.

Another class of comparable species that have not been yet considered as ligands for Mn(II) is that of neutral organophosphates. Very recently, the complex having formula [MnBr$_2${O=P(OPh)$_3$}$_2$] has shown bright red emission upon excitation with near-UV light, with luminescence lifetime longer than 10 ms, but its structure is not yet known.[34]

1.4 Lanthanides

The lanthanides series, from cerium to lutetium, is composed by 14 elements called “rare-earths”. Despite the remind of this name, lanthanides are not so rare as it can be thought. In fact, the scarcest of the lanthanides, thulium, is more abundant than arsenic or mercury, elements not so rare if compared to many others. On the other hand, cerium, the most abundant of the lanthanides, has an abundance greater than that of tin (see Fig. 11). The real meaning of this appellative is to be referred to the difficult extraction and separation required for pure elements.[35]

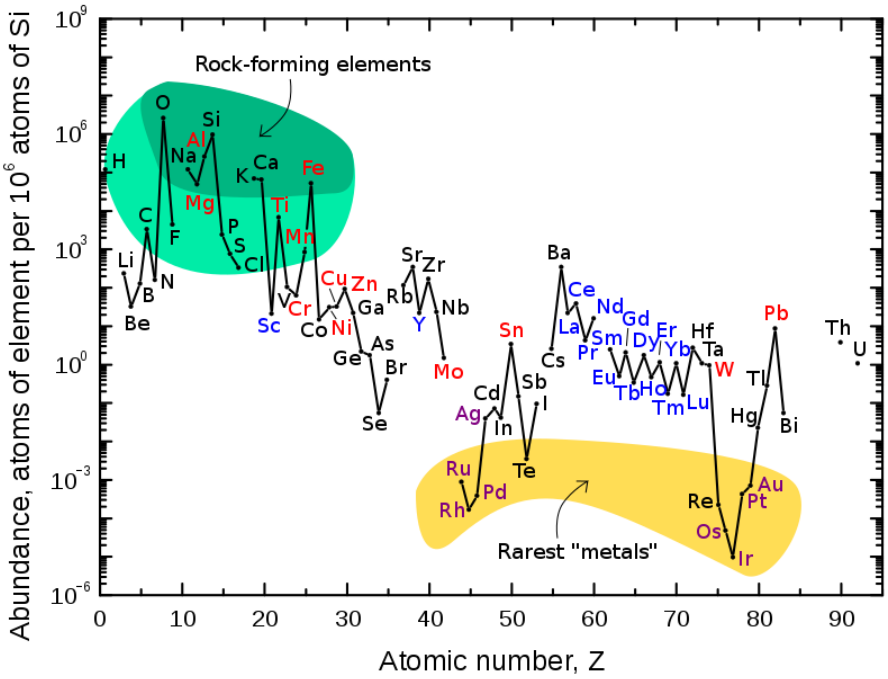

Figure 11. Abundance of elements related to the atomic numbers. Group 3 and lanthanide elements in blue.

Most of lanthanides can be extracted from phosphate minerals such as $LnPO_4$ (xenotime, monazite), aluminosilicate and fluoride-carbonates such as $LnFCO_3$ (bastnaesite). The reason why the purification of those elements is so difficult is the low influence on the reactivity of the partially occupied “4f shell” in the common oxidation state, 3+. Such an oxidation state is formally related to the loss of all the s and d electrons with respect to the element. The f-type orbitals are reported in Fig. 12.

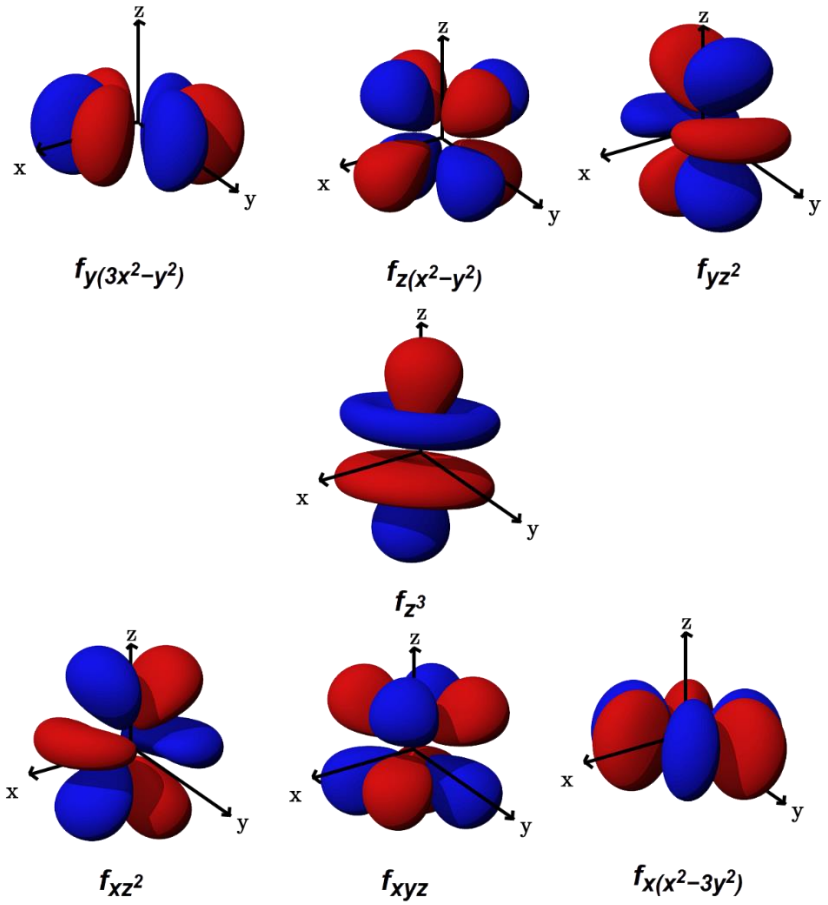

Figure 12. Representation of the f-type atomic orbitals.

There are few examples of 4+ species, in particular for cerium and terbium, while samarium, europium and ytterbium can be isolated with 2+ as oxidation state. The particular electronic configuration of the series in trivalent ions causes the strong contraction of the 4f electron cloud. These electrons are therefore excluded from the reactivity of the species in which the lanthanide ion is found. Another particular property of the series is the so-called *lanthanide contraction*. The inefficient nuclear shielding given by 4f orbitals is responsible of the decrease of the atomic radius along the series (Fig. 13). The difference between La^{3+} and Lu^{3+} is more than 20%.[36]

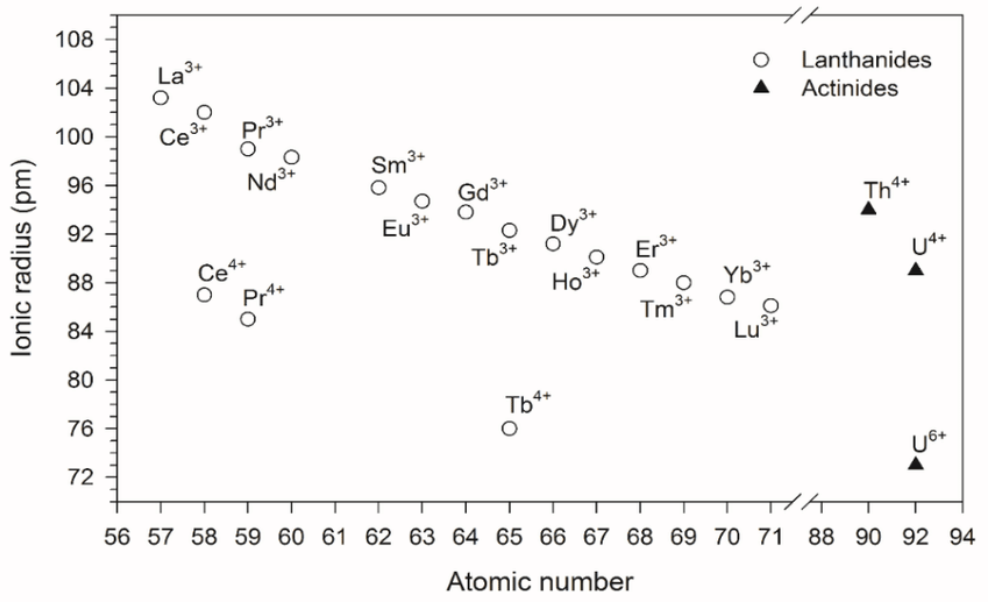

Figure 13. Ionic radii (pm) of lanthanide ions through the series. Selected actinides are included for comparison.

The coordination chemistry of trivalent lanthanides is meaningfully different with respect to the transition elements. The absence of the crystal field stabilization energy in trivalent ions, related to 4f shell contraction, plays a key role on the coordination properties. The 4f orbitals are not involved in the metal-ligands bonds, therefore magnetic and electronic properties, which depend on f orbitals, are not affected by the coordination sphere. Orbitals involved in chemical bonds are the 6s, 6p and 5d. Trivalent lanthanide ions are paramagnetic with La^{3+} and Lu^{3+} ($4f^0$ e $4f^{14}$) as exceptions.

The dominant energy component that affects the electronic structure of lanthanide ions is the spin-orbit interaction. The magnetic spin moment of the electrons is affected by the magnetic field generated from their own apparent motion around the nucleus. The potential energy related to the interaction between the spin angular momentum S and the orbital angular momentum L depends on the scalar product of S and L, the Z atomic number and the nucleus-electron distance:

$$V_{inter} \propto \frac{Z}{r^3} L \cdot S$$

Spin-orbit coupling is described from a quantum mechanical point of view by another quantum number, J, assuming values from $|L+S|$ to $|L-S|$. The high atomic numbers (from 58 to 71) and the relatively small radius due the contraction of the series make the spin-orbit interaction a component of paramount importance to define the energy

levels of trivalent lanthanides. The spectroscopic terms can be defined with three quantum numbers: S, L and J. The Dieke diagram (Fig. 14) represents the relative energies of the spin-orbit levels in Ln^{3+} cations. It is worth noting that the same diagram can be applied for coordinated ions because of the negligible influence of the first coordination sphere.

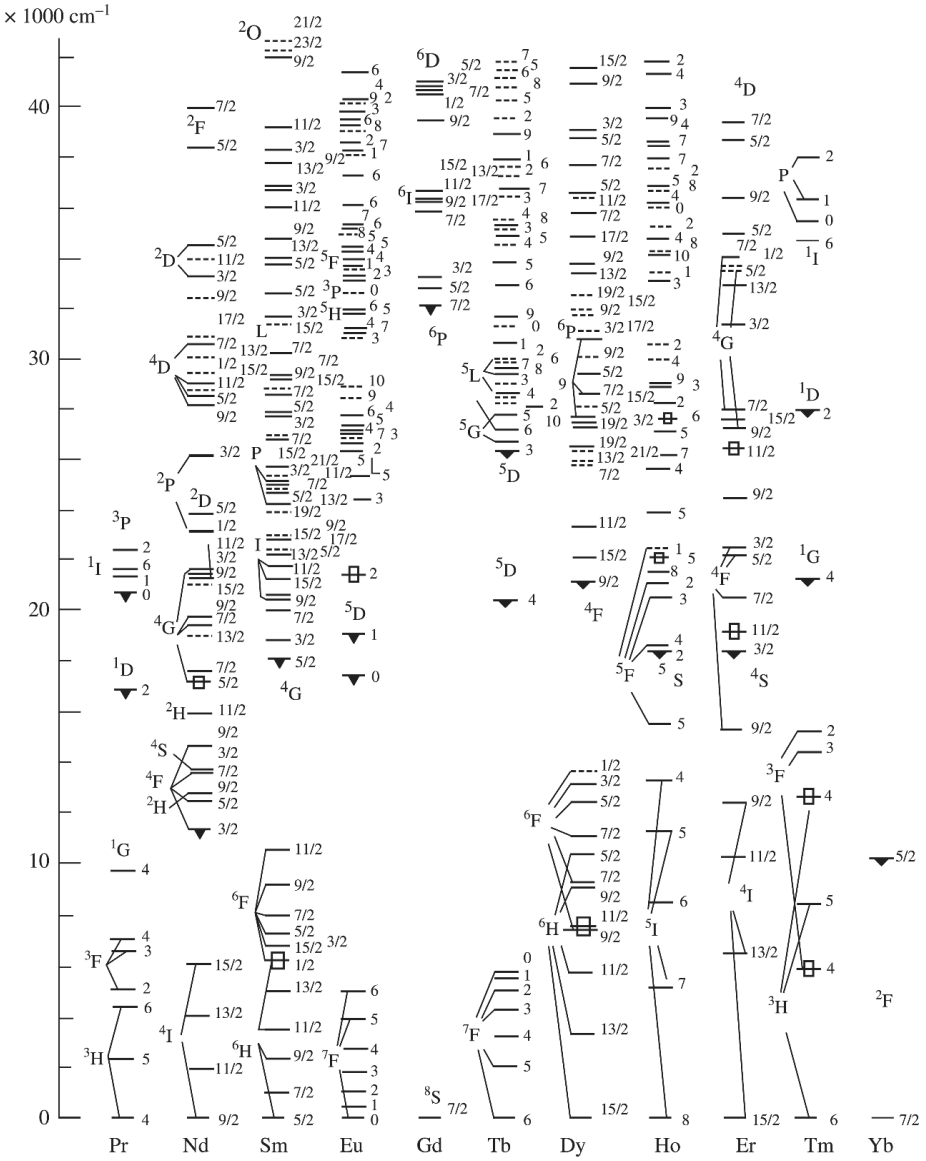

Figure 14. Dieke diagram for Ln^{3+} ions.

The coupling energy of the spin-orbit interaction is in the 10^3 cm^{-1} range, therefore there is usually a significant gap between the ground state and spin-orbit levels with different J values.

As states before, the influence of crystal field is so poor that can be neglected for most of the applications. Nevertheless, the symmetry of the first coordination sphere causes

another and smaller separation of levels in up to 2J+1 states, known as Stark effect. The energy gap in this case is around 100 cm^{-1}. The following (Fig. 15) are the typical energy separations caused by change of multiplicity and orbit term, spin-orbit interaction and crystal field (Stark effect).

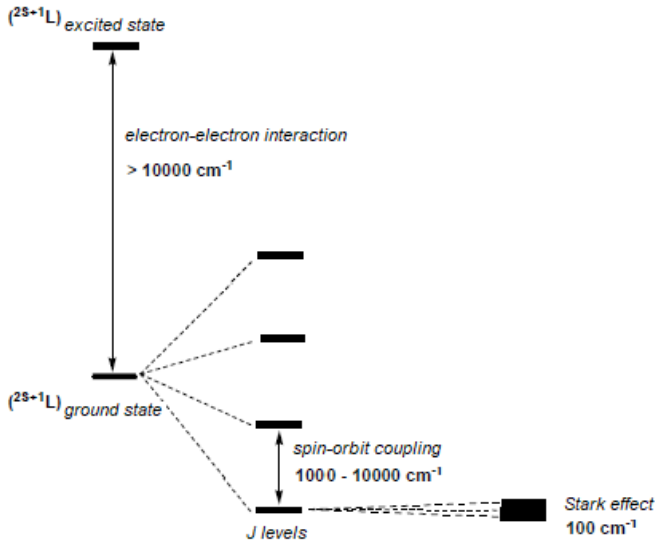

Figure 15. Levels separations for a generic Ln^{3+} ion caused by the change of multiplicity, spin-orbit interaction and Stark effect.

1.5 Lanthanides luminescence

When Ln^{3+} complexes display intense luminescence, applications ranging from biomedical[37] to sensing areas[38] and optical imaging[39] become achievable, based on the long-lived (milliseconds timescale) excited states of trivalent ions. The most studied complexes of Eu^{3+} and Tb^{3+} exhibit quite intense visible line-like emissions. The photophysical properties of near infrared (NIR) lanthanide emitters such as Sm^{3+}, Dy^{3+}, Pr^{3+}, Ho^{3+}, Yb^{3+}, Nd^{3+}, and Er^{3+} have been less investigated in early times.[40] However, a massive interest towards these complexes is registered in more recent years, which stems from their possible use in biomedical and telecommunication fields and for various photonic applications.[41] Longer-wavelength emissions are more efficient to penetrate the human tissue than visible light, so convenient medical diagnostic procedures can be based on long-wave emitters. Similarly, NIR luminescence from ions such as Nd^{3+}, Yb^{3+} and Er^{3+} proves to be very useful when employed as optical signal amplifier in telecommunication networks.[42] Regarding Nd^{3+}, it has found

applications from a long time within laser systems such as Nd:YAG.[43] Similarly, useful lasing properties are observed also for other Ln^{3+} centres[44] such as Tb^{3+}, Eu^{3+}, Dy^{3+} and Sm^{3+} that, coupled with suitable antennas, can be incorporated in stable and transparent inorganic hosts, for instance silica layers.[45] Fig. 16 summarizes typical fields of application of lanthanide derivatives depending upon the emission range.

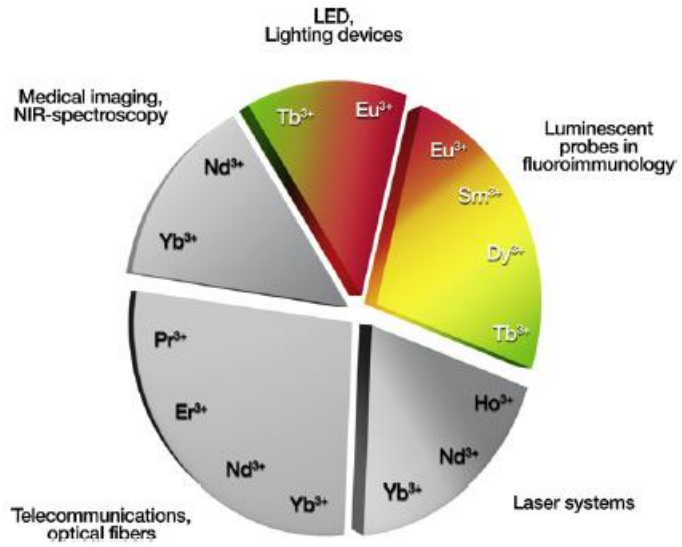

Figure 16. Type of emission and related applications of lanthanides

Antenna ligands are surely the most accessible choice in order to enhance the luminescence behaviour of lanthanides ions. The first case of antenna effect was observed by Weissman for β-diketonate complexes.[46] Antenna effect is associated to the intense absorption of energy by the ligands, followed by an energy transfer to the exited state of the metal ion and subsequently by the f-f radiative transition (Fig.17). This mechanism allows to obtain high-end luminescent species without the direct excitation of the trivalent lanthanide ions, well-known for the low absorption coefficients. The mechanism can be summarized in three main steps: (i) population of the lowest-lying singlet excited state (S) of the organic chromophore, (ii) subsequent intersystem crossing (ISC) to its triplet level (T) and (iii) energy transfer to the Ln^{3+} centre.

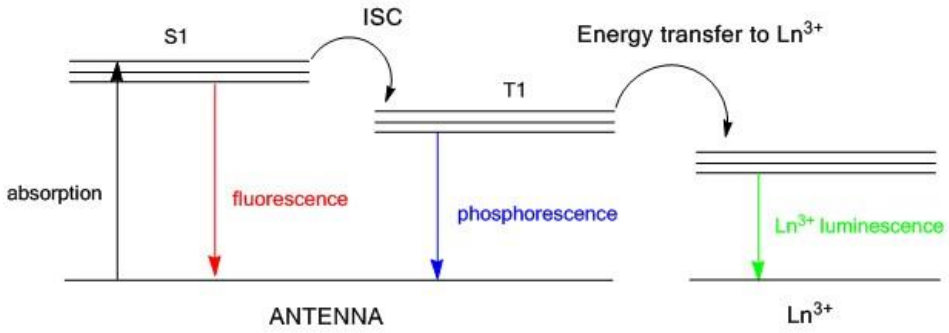

Figure 17. The antenna effect for sensitization of the luminescence in lanthanide cations.

In general, the antenna can be any aromatic or hetero-aromatic highly π-conjugated system characterized by high efficiency of light absorption (high extinction coefficient ε) and high efficiencies of intersystem crossing and energy transfer processes, these last related to the coordination to the heavy atom. Besides all, the efficiency of a chromophore as sensitizer is related to the energy of its triplet excited state, which should be at least 1850 cm^{-1} higher than the lowest emitting levels of the Ln^{3+} cation (Latva's rule).[47] When the energy gap is higher, the energy transferred from the triplet arrives to the resonance level of Ln^{3+} crossing higher-energy exited states by non-radiative pathways. On the contrary, a lower energy gap strongly limits the emission quantum yield because of thermal deactivation from ligand-centred orbitals due to back energy transfer. Selected triplet energy levels for aromatic compounds are reported as examples in Fig. 18 in order to highlight the role of the π-delocalization. It is worth noting that in the case of species able to bind lanthanide ions, the energies of the excited states are deeply influenced by the coordination.

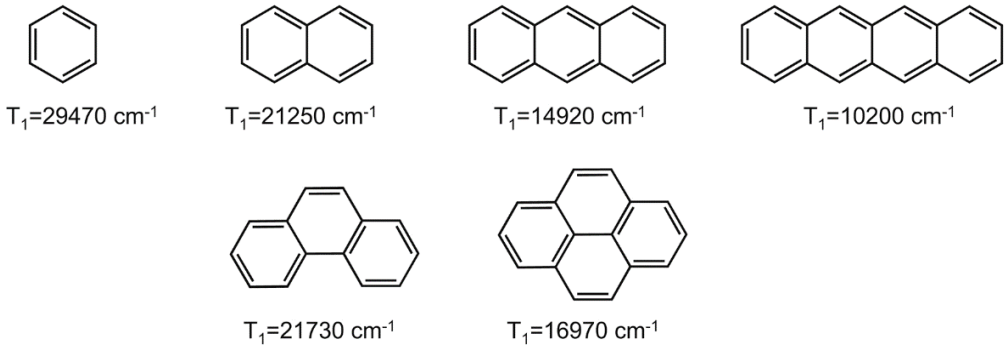

Figure 18. Triplet energy levels of selected aromatic compounds.

The energy transfer process can occur either by Förster[48] or Dexter[49] mechanisms, the first one associated to electron exchange between ligand and metal, while the second to electric dipole interaction. One of the most relevant term is the distance

between the antenna ligand and the metal cation: the energy transfer is enhanced when antenna is directly coordinated to lanthanides. Examples of ligands with a good antenna behaviour are aza-aromatic compounds (bipyridine, phenanthroline, azatriphenylene, terpyridine) or phenolate aromatics [2-hydroxyisophthalamide (IAM), 1-hydroxypyridin-2-one (1,2-HOPO)].

One of the most relevant features of trivalent lanthanide luminescence is the sharpness of the emission lines. The 4*f* orbitals are shielded from the surrounding by the filled $5s^2$ and $5p^6$ orbitals, as observable from the 4*f* radial distribution function reported in Fig. 19. In a configurational coordinate diagram, the levels related to 4*f* configurations appear as parallel parabolas because the 4*f* electrons are well shielded from the surrounding (Fig.19). Therefore, emission transitions are sharp lines (full-width at half-maximum, FWHM <10 nm) in different spectra, a much different result with respect to quantum dots, transition metal derivatives and organic molecules (in a large-stokes-shift case: FWHM >50 nm).[50]

Transitions associated to the 4^{fi} inner shell of free ions are forbidden because they do not correspond to a change in orbital parity. However, the transitions that are forbidden because of the lack of parity change become partially allowed by the mixing of the 4*f* and 5*d* orbitals through the ligand field. Since the selection rule is only weakly relaxed, the lifetime of the excited state is long (τ_{rad} > 100 μs).

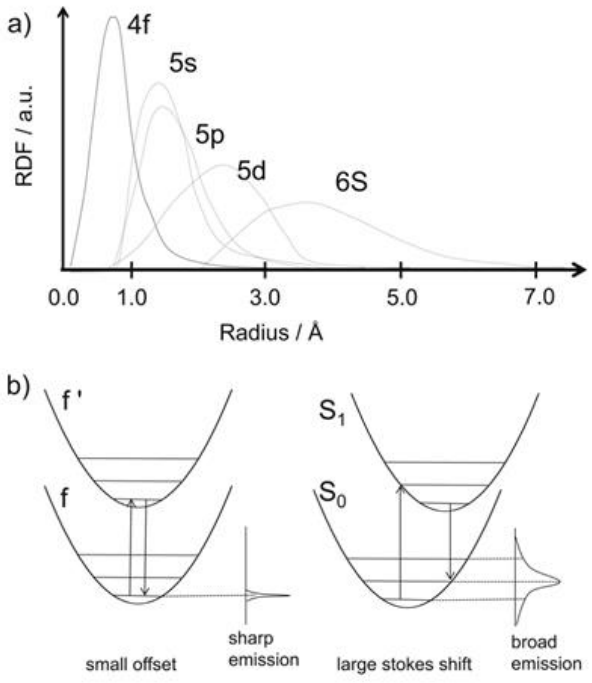

Figure 19. (a) Radial distribution of 4f, 5s, 5p, 5d, 6s orbitals in Ln^{3+} ions; (b) Configurational coordinate diagram for the emission from a lanthanide ion (left) and an organic chromophore (right).

Many Ln^{3+} emissions fall in the visible region of the spectrum (see Fig.20): orange emission for Sm^{3+} ($^4G_{5/2}\rightarrow{}^6H_J$, J=5/2-11/2), red for Eu^{3+} ($^5D_0\rightarrow{}^7F_J$, J=0-4), green for Tb^{3+} ($^5D_4\rightarrow{}^7F_J$, J=6-3) and yellow for Dy^{3+} ($^4F_{9/2}\rightarrow{}^6H_J$, J=15/2-11/2). Sm^{3+}, Dy^{3+} and some other ions such as Nd^{3+}, Ho^{3+}, Er^{3+}, Yb^{3+} and Pr^{3+} show also emissions in the NIR region, while Gd^{3+} in the UV. The intensity of the transitions depends upon selection rules based on the quantum number J of the excited and the ground state. In Eu^{3+} for example, all the transitions $^5D_0\rightarrow{}^7F_J$ with J =0 – 6 can be seen, but the $^5D_0\rightarrow{}^7F_2$ around 615 nm is the most intense in poorly symmetrical environments.[36] The emissions from a lanthanide ion can be roughly derived in electric dipole (ED) and magnetic dipole (MD) transitions. Differently from the transitions having mainly MD character, those with dominant ED character have relative intensity deeply influenced by symmetry and polarizability of the ligand field. Hypersensitive bands are the ones with particularly strong response to changes in the coordination sphere.[51] As an example, for europium(III) the hypersensitive transition is the $^5D_0\rightarrow{}^7F_2$.

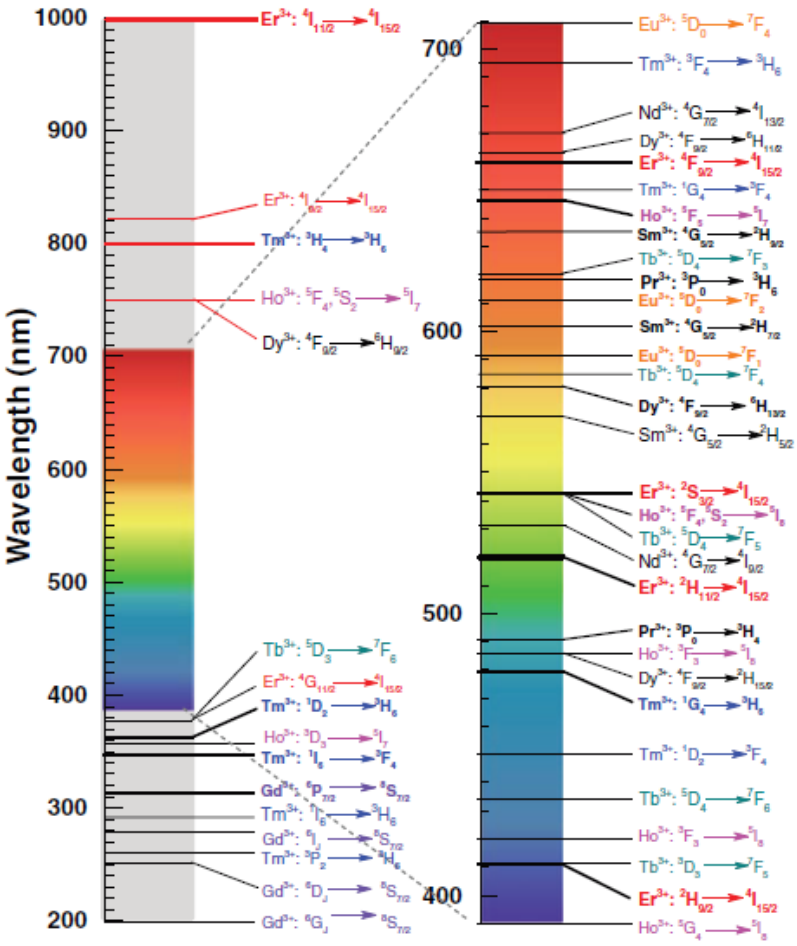

Figure 20. Wavelength distribution of Ln^{3+} transitions from 200 to 1000 nm.

Intrinsic quantum yield (Q_i) and lifetime indicate the efficiency of radiative decay on considering the relation between radiative and non-radiative processes:

$$Q_i = \frac{k_r}{k_r + k_{nr}} = \frac{\tau_{obs}}{\tau_{rad}}$$

where k_r and k_{nr} are the rate constants for the radiative and non-radiative process, respectively. The observed lifetime is usually indicated as τ_{obs}. τ_{rad} is a roughly constant value for the same lanthanide ion in comparable coordination spheres. Selected proposed values are 4.75 ms for Tb^{3+}, 3 ms for Sm^{3+} and 0.4 ms for Dy^{3+}.[52]

The quantum yield can also be written as the ratio between observed lifetime and radiative lifetime. On the basis of the energy gap rule, lower Q_i values are expected for lanthanides having spin-orbit transitions falling in the NIR range and in the presence of high-energy oscillators close to the lanthanide ion. When the overall efficiency is questioned, the overall quantum yield (Q_o) should be considered and it is the ratio between absorbed and emitted photons. In this case additional aspects of the complex need to be investigated, such as the efficiency of the energy transfer between ligand and metal ($Q_o = \eta_t Q_i$, where η_t represents the efficiency). Moreover, the molar extinction coefficient of the ligand and the position of the absorbance bands play a crucial role to determine the luminescence performances.[53]

1.6 Lanthanides complexes

Trivalent lanthanide ions are considered hard Lewis acids following Pearson's "Hard and Soft Acids and Bases" (HSAB) theory.[54] Hard anionic ligands with electronegative atoms such as fluorine, oxygen and nitrogen have strong affinity for the coordination of Ln^{3+} ions.

As mentioned before, the sensitization of lanthanide luminescence is manly promoted by π-conjugated organic chromophores as ligands.[55] Ligands such as β-diketonates are the most used to enhance the luminescence behaviour due the versatile modulation of their electronic and steric features. In Fig. 21 are reported some examples of ligands in neutral form.

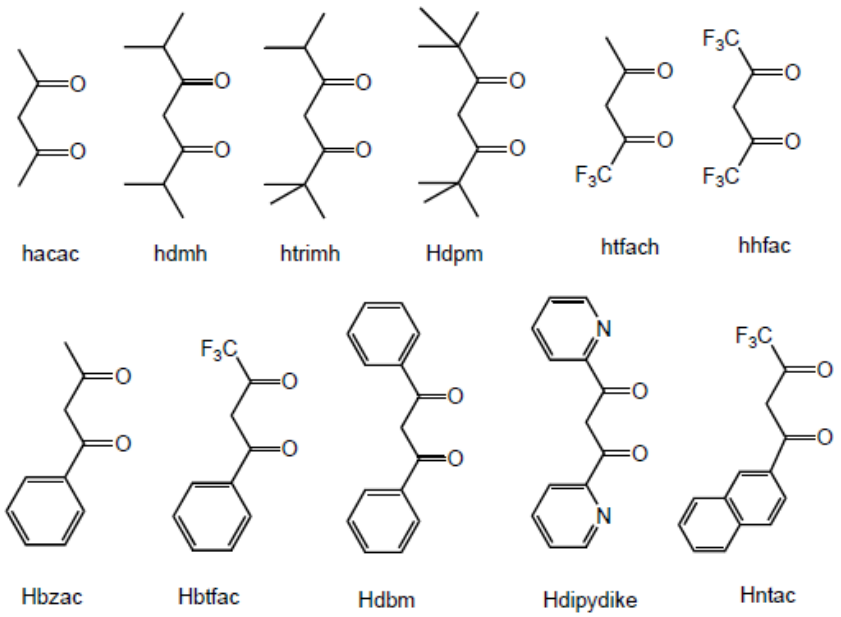

Figure 21. Common β-diketones.

Three main types of lanthanide complexes with β-diketonates can be identified: systems with three ligands [Ln(β-dike)$_3$], Lewis adducts of the tris complexes and tetrakis complexes [Ln(β-dike)$_4$]$^-$. The first category summarizes compounds that are usually coordinatively unsaturated. Because of this, the metal centre can coordinate other Lewis bases, water or solvent molecules, or polymerization to achieve coordination polymers can occur. Only few examples of octahedral mononuclear complexes are reported, one of these being the Lu(III) derivate of the bulky 2,2,6,6-tetramethylheptane-3,5-dionate.[56]

Tetrakis complexes are anions of general formula [Ln(β-dike)$_4$]$^-$, usually balanced by quaternary ammonium ions or alkali ions. Common geometries in eight-coordinated compounds with β-diketonates are the square antiprismatic or the dodecahedral. Complexes of general formula [Ln(β-dike)$_3$L$_n$] (L = Lewis base) represent the most efficient and diffuse molecules with β-diketonates. One of the most common Lewis bases is 1,10-phenantroline (phen), but many other N- and O-donor ligands such as 2,2'-bipiridine, 2,2',6',2''-terpyridine, phosphine oxides, sulphoxides and polydentate ethers can be used (Fig. 22).

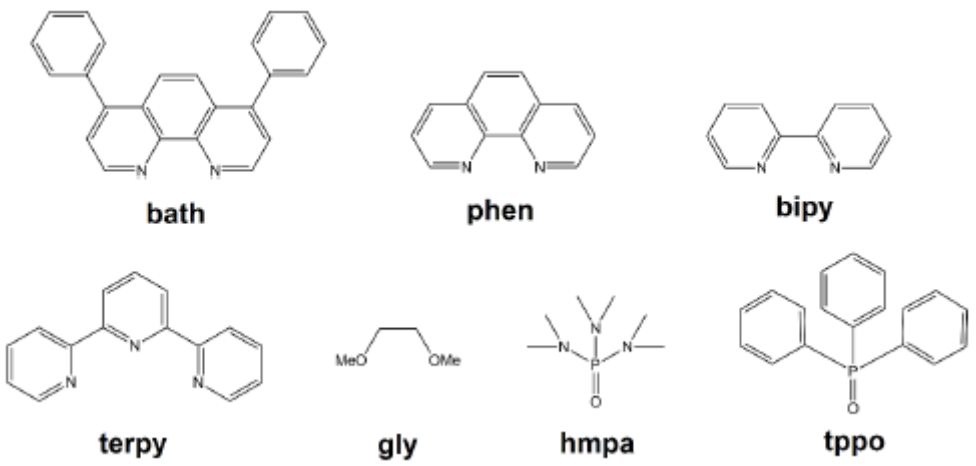

Figure 22. Examples of ligands used in combination with β-diketonates for luminescence porpoises.

Different substituents on the ligand skeletons can be used in order to modulate the triplet state energy of the β-diketonates and enhance the intersystem crossing between singlet and triplet states. Usually β-diketonates with unsymmetrical aromatic and aliphatic substituents in the coordination sphere show higher efficiency in the energy transfer mechanisms and higher luminescence of the relative complexes, probably because of the non-symmetric environment around the metal ion thus achieved.[57] Steric properties of the first coordination sphere can also heavily modify the luminescent behaviour of the species by reducing the interactions with solvent molecules, thus avoiding the quenching of radiative transitions. In this context, organic fluorinated chains create a hydrophobic shell around the complex, avoiding the interaction with water.

On considering different ancillary ligands, cyclens and cryptand-like ligands can coordinate Ln^{3+} and saturate the coordination sphere. In some cases, the structure of these ligands avoids the coordination of further species such as water and blocks the formation of polynuclear species, improving in this sense the luminescence properties. Cyclens and tris-bipyridine cryptates have also been functionalized with amides, carboxylates, phosphates, and the respective complexes can be neutral, anionic or cationic depending on the ligand charge.[58]

The coordination sphere of Ln^{3+} ions is easily saturated by [N,O,O]-donor ligands such as the dipicolinate anion (dipic), *i.e.* the conjugate base of 2,6-pyridinedicarboxylic acid. Compounds having formula $[Ln(dipic)_3]^{3-}$ exhibit intense luminescence also in water solution, being the metal centre protected from water.[59]

Another example of saturation on the coordination sphere is given by the poly(pyrazolyl)borates, called *scorpionates*[60] Substitutions on 3 and 5 positions of the pyrazole rings offer the possibility of high modulation for optic porpoises. The first examples had the general formula $[Ln(HBPz_3)_3]$ (Pz = pyrazol-1-yl) and are sketched in Fig. 23.[61]

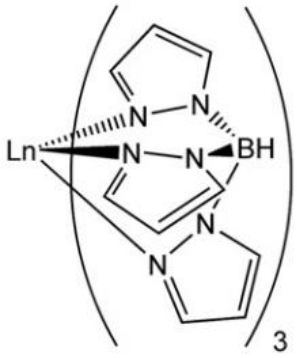

Figure 23. Coordination mode of tris(pyrazol-1-yl)borate in homoleptic lanthanide complexes.

Ligands with [P=O] as donor moiety represent a suitable choice for the coordination of Ln^{3+} ions due to the hardness behaviour as Lewis bases.

Several visible- and NIR-emitting lanthanide complexes with triphenylphosphine oxide (tppo) and anionic ligands in the coordination sphere have been studied. [62] Furthermore, chelating phosphine oxide ligands such bis(2-(diphenylphosphino)phenyl)ether (dpepo) have been explored affording luminescent complexes with exceptional high photoluminescence quantum yields in solution and in poly(methyl methacrylate).[63]

Hexamethylphosphoramide (hmpa) and its derivatives have been widely used as ligands in the chemistry of lanthanide elements. The first examples date back 40 years ago, when $[LnCl_3(hmpa)_3]$ and $[Ln(hmpa)_6](ClO_4)_3$ have been prepared and studied.[64] Similar ligands, arylphosphonic diamide species in particular, were investigated for extraction processes. [65] Examples of luminescent Ln^{3+} complexes with phosphoroamides and arylphosphonic diamides are $[Tb(dbm)(NO_3)_2(hmpa)_2]$ (dbm = dibenzoylmethanate), $[Eu(NO_3)_3(hmpa)_3]$, [Eu(β-dike)$_3$L] and [Eu(β-dike)$_3$L'$_2$] (β-dike = dibenzoylmethanate, tenoyltrifluoroacetonate; L = $OP(NMe_2)_2R$, where R = indol-1-yl, carbazole-1-yl, phenyl, 1-naphtyl and 2-naphtyl; L'= 1,3-dimethyl-2-phenyl-1,3-diazaphospholidine-2-oxide). [66] Magneto-optic materials have been developed in

recent years such [Ln(depma)$(NO_3)_3$$(hmpa)_2$] (depma = 9-diethylphosphono-methylanthracene; Ln = Dy, Gd).[67]

Neutral organophosphate derivates are employed from a long time for the extraction and purification of lanthanides, the tributyl phosphate molecule *in primis.*[68] However, the coordination chemistry of neutral organophosphate ligands towards lanthanide ions for luminescence porpoises was poorly explored.

1.7 Materials and matrices

The possibility of incorporating lanthanide complexes into plastic matrices has been explored a lot during the last decades. There are many possible systems that can embed lanthanides species in order to preserve the luminescent features. Sol-gel processes represent a common technique because of the low operating temperature, avoiding the decomposition of the complexes or the organic ligands. This route includes a series of hydrolysis and condensations reactions, starting from a silicon alkoxide in the presence of water and an acid or a base as catalyst. Matthews and co-workers back in 1993 realized the first example of doped silica gel using [Eu(tta)$_3$$(H_2O)_2$] and (pipH)[Eu(tta)$_4$] as complexes.[69] The incorporation into a matrix represent not only an easy way to preserve the photophysical properties and the chemical stability but can also enhance the luminescent features of the system. Indeed, many doped sol-gel glasses with europium β-diketonate complexes exhibited longer lifetime than the free complexes.[70] The disadvantages of these materials are their fragility, the poor solubility of the complexes and the persistence of water molecules in the inorganic network. An interesting alternative is represented by *ormosils* (*organically modified silicates*), organic/inorganic hybrid materials.[71] Zeolites have also been used for lanthanide complexes such as [Ln(β-dike)$_2$]$^+$ and [Ln(β-dike)]$^{2+}$, that replace the inorganic cations in the network.[72]

Polymers in general presents striking features in terms of flexibility, lightness and affordability. Example of polymers used are polymethylmethacrylate, polyvinyl alcohol, polystyrene, polyethylene, polyurethanes, polyesters, polyimides, polycarbonates and epoxy resins. There are many different routes for the preparation of doped polymers, and they are usually cheaper and more affordable than sol-gel derivatives.

The simplest procedure consists in the dissolution of the complex and the polymer in a solvent, which is then eliminated by slow evaporation. Alternatively, the complex

containing suitable functional groups is dissolved in a monomer solution, becoming part of the material after co-polymerization. Finally, the polymer chains can be functionalized with an antenna ligand, able to coordinate the lanthanide precursors.[73] Liquid matrices may also be the host for lanthanide complexes such as liquid-crystals. Both neutral complexes, such as $[Eu(tta)_3(phen)]$ in N-(4-methoxybenzylidene)-4-butylaniline (MBBA) and 4-n-pentyl-4-cyanobiphenyl (5CB), and anionic species, such as $[Eu(tta)_4]^-$ or $[LnCl_6]^{3-}$ in N-butyl-N'-methyl-imidazole, were successfully employed.[74]

1.8 Aim of the thesis

As stated in the previous chapters, mono- and bidentate ligands based on the phosphine oxide skeleton are among the most important for the preparation of luminescent Mn(II) and Ln(III) coordination compounds. Recent advances in this field were obtained by introducing phosphoramides, arylphosphonic diamides and 1,3-diazaphospholidine-2-oxides in the coordination sphere of these metal centres. The [P=O] donor fragment appears therefore of noticeable interest for the design of luminescent compounds. It is worth noting that the studies concerning neutral organophosphates as ligands for Mn(II) and Ln(III) are much less developed, despite some promising preliminary result indicating strong changes in the coordination environment of the related Mn(II) complexes with respect to other [P=O]-donors.

A class of ligands that was never investigated in this field of research is composed by species with mixed phosphoramide/organophosphate character, amidophosphates in particular. The aim of this thesis is the preparation of molecules belonging to this category and the synthesis and characterization of corresponding Mn(II) and Ln(III) complexes. Particular attention will be devoted to the photophysical features of the isolated compounds.

2. EXPERIMENTAL PART

2.1 Methods

All the syntheses involving metal centres were performed in a glove-box MBraun Labstar filled with N_2, equipped with an automatic pressure control system. Selected operations were carried out under N_2 in a Nautilus™ glove-box equipped for inorganic syntheses.

UV-vis spectra were registered for dichloromethane solutions with a Perkin-Elmer Lambda 35 spectrophotometer in the 235 - 700 nm range at room temperature. IR spectra were recorded between 4000 and 400 cm^{-1} with a Perkin- Elmer SpectrumOne spectrometer. In the case of air- sensitive compounds, samples were deposited and sealed between two KBr windows in glove-box.

Photoluminescence measurements (PL) were carried out with two different spectrometers. An OceanOptics Flame T spectrophotometer equipped with optic fiber and achromatic lens was used for preliminary measurements on solid samples, with excitation wavelengths of 280 nm or 375 nm obtained with LED sources. The reflected radiation was removed using suitable longpass filters. The useful range of emission was between 400 and 1035 nm. More accurate PL measurements were carried out with a Horiba Jobin Yvon Fluorolog-3 spectrofluorimeter. The same instrument was used to record excitation (PLE) spectra and for lifetime determinations. In the cases of PL and PLE measurements the instrument uses a xenon lamp as light source with continuous emission, coupled with Czerny-Turner double grating monochromator. Lifetimes measurement were obtained with a LED pulsed source centred at 377 nm. The detection system includes a single-grating monochromator iHR320 coupled with a Hamamatsu R928 photomultiplier. The Multi-Channel Scaling (MCS) techniques was used for the lifetime determinations.

NMR spectra were collected using Bruker Avance 300 and Bruker Avance 400 spectrometers, with a frequency of 300.13 MHz and 400.13 MHz for protons, respectively. ^{1}H chemical shifts are referred to the partially deuterated fraction of the solvent, itself referred to tetramethylsilane. $^{31}P\{^{1}H\}$ chemical shifts are reported with respect to 85% H_3PO_4, with downfield shifts considered positive. ^{19}F chemical shifts are referred to $CFCl_3$.

Magnetic susceptibilities were measured on solid samples at room temperature with a MK1 magnetic susceptibility balance (Sherwood Scientific Ltd) and corrected for diamagnetic contribution by means of tabulated Pascal's constants. Melting points were obtained with a modified Falc 360D apparatus, equipped with a camera.

2.2 Reagents

The commercial reagents were purchased from Sigma-Aldrich, TCI chemicals and Alfa-Aesar. Lanthanides salts were provided by Strem and ChemPur. Ln(III) nitrato-complexes were obtained by reacting Ln_2O_3 (Ln = Eu, Tb, Gd) with concentrate nitric acid. The solutions thus obtained were purified by filtration and water was removed under vacuum in the presence of phosphoric anhydride.
The organic solvents used for the syntheses were dried and purified following standard procedures and stored under inert atmosphere.[75] Deuterated solvents for NMR spectroscopy are Euriso-Top products.

2.3 Synthesis of the ligands

2.3.1 Synthesis of (1-phenyl)-N,N,N',N'-tetramethylamido phosphate, $O=P(OPh)(NMe)_2$

The synthesis was carried out under N_2 with slight modifications with respect to a reported procedure.[76] In a 50 ml flask a stochiometric quantity of potassium *tert*-butoxide K[O^{t}Bu] (0.328 g; 2.9 mmol) was added to a 20 mL EtOH solution of phenol (0.276 g; 2.9 mmol) at room temperature under stirring. The cloudy reaction mixture thus obtained was evaporated under reduced pressure and THF (10 mL) was added. The resulting solution was then added to a 50 mL flask containing a stochiometric quantity of *N,N,N',N'*- tetramethylphosphorodiamidic chloride (0.5 g; 2.9 mmol) and a small amount of THF (about 10 mL). The reaction was stopped after 24 hours and the solution obtained was centrifuged in order to eliminate insoluble by-products. The solvents were evaporated under reduced pressure and the residue was washed several times with small aliquots of Et_2O. The product is a light-brown liquid. Yield > 60%.

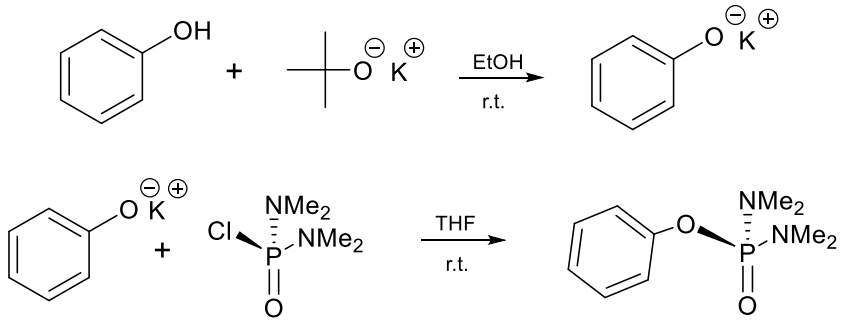

Scheme 1. Synthesis of (1-phenyl)-N,N,N',N'-tetramethylamido phosphate.

Characterization

IR *(cm^{-1}): 3065 m - 2810 m (ν_{C-H}), 1592 w (aromatic $\nu_{C=C}$), 1493 w, 1456 m (δ_{C-H}), 1308 m ($\nu_{P=O} + \nu_{C-O}$), 1237-1164 s ($\nu_{P=O} + \delta_{C-H}$), 997 s (ν_{P-O}), 918 s (ν_{P-N}).*
^{1}H NMR *($CDCl_3$, 298 K), δ: 7.33 (m, 2H, Ph), 7.21 (m, 2H, Ph), 7.14 (m, 1H, Ph), 2.75 (d, 12H, J_{PH} = 10.0 Hz, Me).* ***^{31}P {^{1}H}*** *NMR ($CDCl_3$, 298 K), δ: 15.95 (FWHM = 2 Hz).*
UV-VIS *(CH_2Cl_2, r.t., nm): 270 (ε = 3150 M^{-1}cm^{-1}), 264 (ε = 3600 M^{-1}cm^{-1}) <250.*

2.3.2 Synthesis of (2-naphthyl)-N,N,N',N'-tetramethylamido phosphate, O=P(ONaph)(NMe)$_2$

The synthesis of this ligand follows the same procedure previously described for the preparation of O=P(OPh)(NMe)$_2$. The quantities of reactants are: 2-naphtol (1.69 g; 11.7 mmol); potassium *tert*-butoxide (1.12 g; 11.7 mmol); *N,N,N',N'*-tetramethylphosphorodiamidic (2 g; 11.7 mmol). The product is liquid, with dark brown colour. Yield > 55%. It is worth noting that other synthetic approaches are present in the literature.[77]

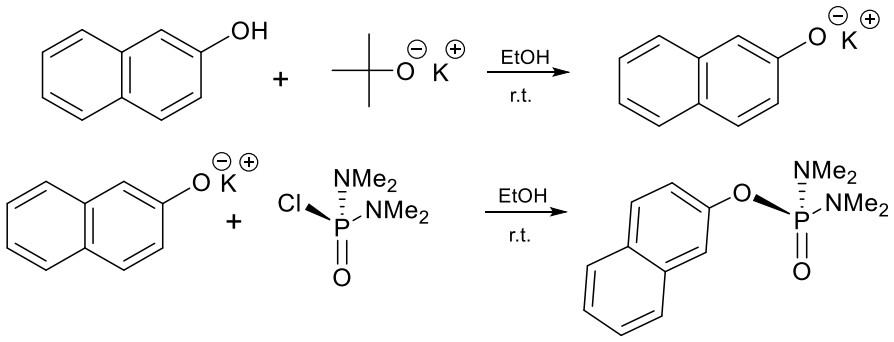

Scheme 2. Synthesis of (2-naphthyl)-N,N,N',N'-tetramethylamido phosphate.

Characterization

IR *(cm^{-1}): 3053 - 2807 m (ν_{C-H}), 1630 s, 1597 w, 1511 w, (aromatic $\nu_{C=C}$) 1465 m (δ_{C-H}), 1304 m (ν_{C-O}), 1250 -1161 s ($\nu_{P=O}$ + ν_{C-O} + δ_{C-H}), 996 (ν_{P-O}), 927 s (ν_{P-N}).*

^{1}H NMR *($CDCl_3$, 298 K), δ: 7.86 -7.77 (m, 3H, Naph), 7.68 (s, br, 1H, Naph), 7.52 – 7.35 (m, 3H, Naph), 2.78 (d, 12H, J_{PH} = 10.0 Hz, Me).* ***$^{31}P\{^1H\}$*** *NMR ($CDCl_3$, 298 K), δ: 16.25 (FWHM = 2 Hz).*

UV-VIS *(CH_2Cl_2, r.t., nm)*: 321 *(**ε= 21360 $M^{-1}cm^{-1}$**)*, 312 *(**ε= 16840 $M^{-1}cm^{-1}$**)*, 307 *(**ε= 18040 $M^{-1}cm^{-1}$**)* <250.

2.3.3 Synthesis of diphenyl N-dimethylamidophosphate, $O=P(OPh)_2(NMe_2)$

Early attempts of preparation of the title compound were reported by H. Kovache et al. in 1950.[78] In the method here described, 10.0 g of $[NH_2Me_2]Cl$ (123 mmol) and a stochiometric amount of NaOH (4.9 g) were mixed with continuous stirring into a 100 mL flask, connected to a refrigerator and a NaOH trap. The reaction mixture was put under N_2 and heated at 200°C. The stream of gaseous $NHMe_2$ was allowed to enter in second reaction flask containing a solution of phosphorochloridic acid diphenyl ester $O=PCl(OPh)_2$ (5.37 g; 20 mmol) in 30 mL of CH_2Cl_2. Once stopped the evolution of $NHMe_2$ from the first flask, the dichloromethane solution was stirred at room temperature for 5 hours, then the solvent was removed under reduced pressure and diethylether (30 mL) was added. The by-product $[NH_2Me_2]Cl$ was removed by filtration and the final product was obtained after evaporation of the solvent as colourless liquid. Yield 95%.

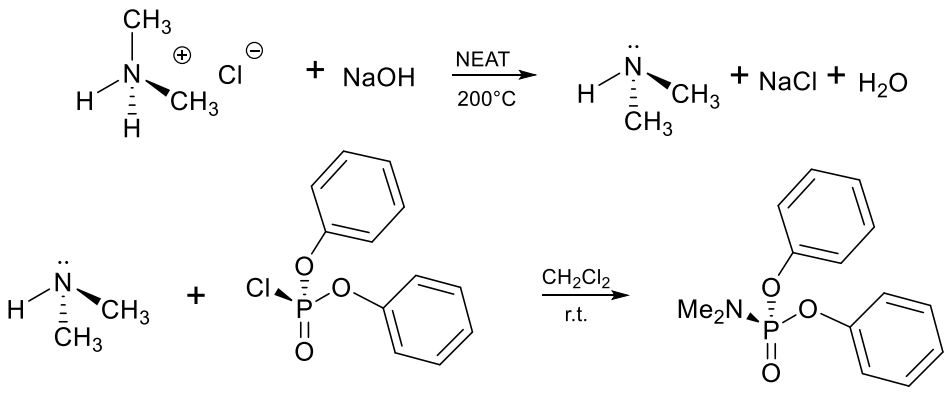

Scheme 3. Synthesis of diphenyl N-dimethylamidophosphate.

Characterization

IR *(cm^{-1}): 3070 - 2817 m (ν_{C-H}), 1590 s, 1489 s (aromatic $\nu_{C=C}$) 1465 m (δ_{C-H}), 1319 m (ν_{C-O}), 1270 -1164 s ($\nu_{P=O}$ + ν_{C-O} + δ_{C-H}), 1007 (ν_{P-O}), 925 s (ν_{P-N}).*

^{1}H NMR *($CDCl_3$, 298 K), δ: 7.32 (m, 4H, Ph), 7.26 (m, 4H, Ph), 7.14 (m, 4H, Ph), 2.78 (d, 6H, J_{PH} = 10.4 Hz, Me).* ***^{31}P {^{1}H}*** *NMR ($CDCl_3$, 298 K), δ: 1.27 (FWHM = 3 Hz).*

UV-VIS *(CH_2Cl_2, r.t., nm): 269 (ε= 12800 $M^{-1}cm^{-1}$), 263 (ε= 16100 $M^{-1}cm^{-1}$), 258 (ε= 13480 $M^{-1}cm^{-1}$) <240.*

2.3.4 Synthesis of 1,3-(N,N,N′,N′-tetramethyldiamidophosphoryloxy benzene), $O=P(NMe_2)_2(res)(NMe_2)_2P=O$ and 1,2-(N,N,N′,N′-tetramethyldiamidophosphoryloxy benzene) $O=P(NMe_2)_2(cat)(NMe_2)_2P=O$

A solution of 0.322 g (30 mmol) of 1,3-dihydroxybenzene (resorcin) or 1,2-dihydroxybenzene (catechol) in 50 mL of EtOH was slowly added to a flask containing two equivalents of potassium *tert*-butoxide (0.562 g; 60 mmol) in 20 mL of EtOH under stirring. After 4 hours the solvent was evaporated under reduced pressure. The oil thus obtained was then dissolved in 50 mL of THF and 1.0 g of *N,N,N′,N′*-tetramethylphosphorodiamidic (60 mmol) was added to the solution under stirring. After 12 hours the cloudy solution was purified by centrifugation. The solvents were evaporated under reduced pressure and the residue was washed several times with small aliquots of Et_2O. The result is a light brown liquid. Yield 70% in both cases.

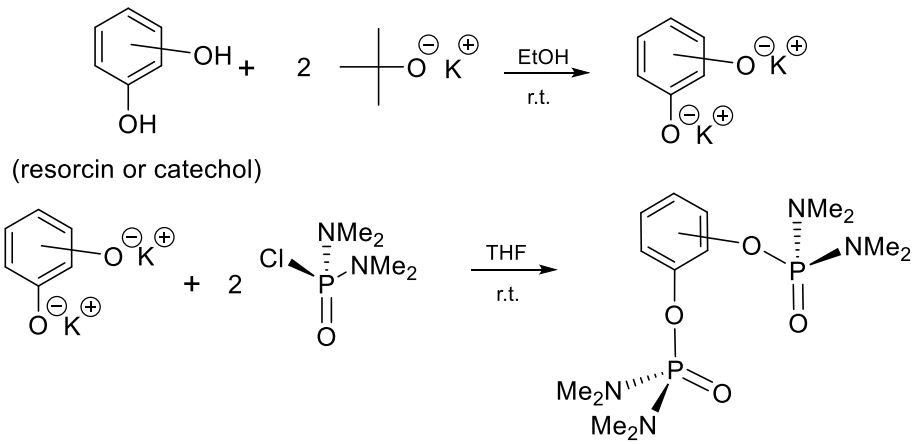

Scheme 4. Synthesis of 1,2-(N,N,N′,N′-tetramethyldiamidophosphoryloxy benzene) and 1,2-(N,N,N′,N′-tetramethyldiamidophosphoryloxy benzene)

Characterization of $O=P(NMe_2)_2(res)(NMe_2)_2P=O$

IR *(cm^{-1}): 3070 - 2817 m (ν_{C-H}), 1590 s, 1489 s (aromatic $\nu_{C=C}$) 1465 m (δ_{C-H}), 1319 m (ν_{C-O}), 1270 -1164 s ($\nu_{P=O} + \nu_{C-O} + \delta_{C-H}$), 1007 ($\nu_{P-O}$), 925 s ($\nu_{P-N}$).*
^{1}H NMR *($CDCl_3$, 298 K), δ: 7.26 (t, 1H, J_{HH} = 8.1 Hz, Ph), 7.17 (m, br, 1H, Ph), 6.97 (b, 2H, J_{HH} = 8.1 Hz, Ph), 2.74 (d, 24H, J_{PH} = 10.0 Hz, Me).* ***^{31}P {^{1}H}*** *NMR ($CDCl_3$, 298 K), δ: 16.20 (FWHM = 4 Hz).*
UV-VIS *(CH_2Cl_2, r.t., nm): 272 (ε = 4700), 266 (ε = 4650) <250.*

Characterization of $O=P(NMe_2)_2(cat)(NMe_2)_2P=O$

IR *(cm^{-1}): 3070 - 2820 m (ν_{C-H}), 1499 s (aromatic $\nu_{C=C}$) 1461 m (δ_{C-H}), 1313 m (ν_{C-O}), 1262 -1175 s ($\nu_{P=O} + \nu_{C-O} + \delta_{C-H}$), 1005 ($\nu_{P-O}$), 934 s ($\nu_{P-N}$).*
^{1}H NMR *($CDCl_3$, 298 K), δ: 7.46 (m, 2H, Ph), 7.07 (m, 2H, Ph), 2.75 (d, 24H, J_{PH} = 10.2 Hz, Me).* ***^{31}P {^{1}H}*** *NMR ($CDCl_3$, 298 K), δ: 16.40 (FWHM = 3 Hz).*

2.4 Synthesis of manganese(II) complexes

2.4.1 Synthesis of [$MnBr_2${O=P(OPh)$(NMe)_2$}$_2$]

In a 50 mL flask were mixed together under stirring 1 mmol (0.215 g) of anhydrous $MnBr_2$ and two equivalents of O=P(OPh)$(NMe)_2$ (2 mmol, 0.456 g) in 25 mL of EtOH. After 12 hours under stirring at room temperature the solution was taken to dryness under reduced pressure and the obtained compound was triturated with Et_2O (10 mL). The whitish product was filtered, washed with diethylether and dried under vacuum. Yield 75%.

Characterization of [$MnBr_2${O=P(OPh)$(NMe)_2$}$_2$]

***IR** (cm^{-1}): 3059 - 2822 w (ν_{C-H}), 1591 m, 1490, 1456 s (aromatic $\nu_{C=C}$), 1314 m (ν_{C-O}), 1213 -1166 s ($\nu_{P=O}$ + ν_{C-O} + δ_{C-H}), 1006 s (ν_{P-O}), 933 s (ν_{P-N}).*

***mp:** 112°C.*

***χ^M_{corr}** (M = 671.46 g mol^{-1}, c.g.s.u.): 1.36 · 10^{-2}.*

***PL** (solid sample, r.t., $\lambda_{excitation}$ = 375 nm, nm): 513 ($^4T_1(^4G)\rightarrow{}^6A_1(^6S)$, FWHM = 2000 cm^{-1}).*

2.4.2 Synthesis of [MnX_2{O=P(OPh)$_2$(NMe)}$_2$] {X = Cl, Br, I}

The syntheses of [MnX_2{O=P(OPh)$_2$(NMe)}$_2$] complexes were conducted with the same procedure above described for [MnX_2{O=P(OPh)$(NMe)_2$}$_2$], using O=P(OPh)$_2$(NMe_2) and the proper anhydrous MnX_2 salt as reactants. In the case of the chloro-complex iso-hexane was used instead of diethylether to avoid decomposition. Yield > 50% in all the cases.

Characterization of [$MnCl_2${O=P(OPh)$_2$(NMe)}$_2$]

***IR** (cm^{-1}): 3068 - 2819 w (ν_{C-H}), 1586 m, 1484 s (aromatic $\nu_{C=C}$), 1319 m (ν_{C-O}), 1233 - 1158 s ($\nu_{P=O}$ + ν_{C-O} + δ_{C-H}), 1014, 1002 s (ν_{P-O}), 977 s (ν_{P-N}).*

***mp:** 122°C.*

***χ^M_{corr}** (M = 750.90 g mol^{-1}, c.g.s.u.): 1.59 · 10^{-2}.*

PL *(solid sample, r.t., $\lambda_{excitation}$ = 368 nm, nm): 647 ($^4T_1(^4G)\rightarrow{}^6A_1(^6S)$, FWHM = 2700 cm^{-1}). PL (solid sample, r.t., $\lambda_{excitation}$ = 304 nm, nm): 647 ($^4T_1(^4G)\rightarrow{}^6A_1(^6S)$, FWHM = 2700 cm^{-1}).*

PLE *(solid sample, r.t., $\lambda_{emission}$ = 647 nm, nm): 303 ($^4F\leftarrow{}^6A_1(^6S)$), 368 ($^4P,^4D\leftarrow{}^6A_1(^6S)$), 477 ($^4G\leftarrow{}^6A_1(^6S)$). PLE (solid sample, r.t., $\lambda_{emission}$ = 600 nm, nm): 303 ($^4F\leftarrow{}^6A_1(^6S)$), 368 ($^4P,^4D\leftarrow{}^6A_1(^6S)$), 477 ($^4G\leftarrow{}^6A_1(^6S)$).*

τ (solid sample, r.t., $\lambda_{excitation}$ = 377 nm, $\lambda_{emission}$ = 647 nm, ms): 1.5.

Characterization of $[MnBr_2\{O=P(OPh)_2(NMe)\}_2]$

IR *(cm^{-1}): 3059 - 2830 w (ν_{C-H}), 1586 m, 1484 s (aromatic $\nu_{C=C}$), 1318 m (ν_{C-O}), 1228 - 1154 s ($\nu_{P=O}$ + ν_{C-O} + δ_{C-H}), 1013 (ν_{P-O}), 948 s (ν_{P-N}).*

mp*: 125°C.*

χ^{M}_{corr} (M = 769.52 g mol^{-1}, c.g.s.u.): 1.42 · 10^{-2}.

PL *(solid sample, r.t., $\lambda_{excitation}$ = 320 nm, nm): 513 ($^4T_1(^4G)\rightarrow{}^6A_1(^6S)$, FWHM = 2200 cm^{-1}).*

Characterization of $[MnI_2\{O=P(OPh)_2(NMe)\}_2]$

IR *(cm^{-1}): 3066 - 2814 w (ν_{C-H}), 1586 m, 1486 s (aromatic $\nu_{C=C}$), 1315 m (ν_{C-O}), 1227 - 1160 s ($\nu_{P=O}$ + ν_{C-O} + δ_{C-H}), 1013 (ν_{P-O}), 954 s (ν_{P-N}).*

mp: *107°C.*

χ^{M}_{corr} (M = 863.52 g mol^{-1}, c.g.s.u.): 1.54 · 10^{-2}.

PL *(solid sample, r.t., $\lambda_{excitation}$ = 315 nm, nm): 513 ($^4T_1(^4G)\rightarrow{}^6A_1(^6S)$, FWHM = 2100 cm^{-1}).*

PLE *(solid sample, r.t., $\lambda_{emission}$ = 570 nm, nm): 293, 303, 315 ($^4F\leftarrow{}^6A_1(^6S)$), 372, 391-420 ($^4P,^4D,^4G\leftarrow{}^6A_1(^6S)$).*

τ (solid sample, r.t., $\lambda_{excitation}$ = 377 nm, $\lambda_{emission}$ = 520 nm, μs): 86.

2.4.3 Synthesis of $[MnX_2\{O=P(NMe_2)_2(res)(NMe_2)_2P=O\}]_n$ {X = Br, I}

The syntheses of the following manganese complexes were conducted with the same procedure above described for $[MnX_2\{O=P(OPh)(NMe)_2\}_2]$, using $O=P(NMe_2)_2(res)(NMe_2)_2P=O$ as ligand. Yield > 60% in both the cases.

Characterization of $[MnBr_2\{O=P(NMe_2)_2(res)(NMe_2)_2P=O\}]_n$

***IR** (cm^{-1}): 3078 - 2821 w (ν_{C-H}), 1598 - 1456 s (aromatic $\nu_{C=C}$), 1310 m (ν_{C-O}), 1183 -1129 s ($\nu_{P=O}$ + ν_{C-O} + δ_{C-H}), 1013 (ν_{P-O}), 980 s (ν_{P-N}).*

***mp:** 167°C.*

***χ^M_{corr}** (M = 593.35 g mol^{-1}, c.g.s.u.): 1.47 · 10^{-2}.*

***PL** (solid sample, r.t., $\lambda_{excitation}$ = 300 nm, nm): 521 ($^4T_1(^4G)\rightarrow{}^6A_1(^6S)$, FWHM = 2200 cm^{-1}).*

***PLE** (solid sample, r.t., $\lambda_{emission}$ = 570 nm, nm): 292, 304, 316 ($^4F\leftarrow{}^6A_1(^6S)$), 369, 386-450 ($^4P,^4D,^4G\leftarrow{}^6A_1(^6S)$).*

τ (solid sample, r.t., $\lambda_{excitation}$ = 377 nm, $\lambda_{emission}$ = 522 nm, ms): 0.7.

Characterization of $[MnI_2\{O=P(NMe_2)_2(res)(NMe_2)_2P=O\}]$

***IR** (cm^{-1}): 3015 - 2811 w (ν_{C-H}), 1579 - 1475 s (aromatic $\nu_{C=C}$), 1362 m (ν_{C-O}), 1172 -1124 s ($\nu_{P=O}$ + ν_{C-O} + δ_{C-H}), 982 (ν_{P-O}), 930 s (ν_{P-N}).*

***mp:** 149°C.*

***χ^M_{corr}** (M = 687.35 g mol^{-1}, c.g.s.u.): 1.49 · 10^{-2}.*

***PL** (solid sample, r.t., $\lambda_{excitation}$ = 280 nm, nm): 529 ($^4T_1(^4G)\rightarrow{}^6A_1(^6S)$, FWHM = 2100 cm^{-1}).*

2.5 Synthesis of lanthanide(III) complexes

2.5.1 Synthesis of $[Eu(tta)_3L_2]$ {L= $O=P(OPh)(NMe_2)_2$, $O=P(OPh)_2(NMe_2)$, $O=P(NMe_2)_2(res)(NMe_2)_2P=O$}

In a 100 mL flask, 1 mmol of anhydrous $EuCl_3$ was dissolved in 20 mL of THF. In another flask potassium *tert*-butoxide (3 mmol, 0.34 g) was slowly added under stirring to a 50 mL THF solution of thenoyltrifluoroacetone (tta, 3 mmol, 0.67 g). The obtained solution was added to the flask containing $EuCl_3$. After 6 hours two equivalents of the proper monodentate phosphoroamidic ligand (2 mmol) or 1 mmol of $O=P(NMe_2)_2(res)(NMe_2)_2P=O$} were slowly added to the β-diketonate complex solution. After 12 hours the solvent was evaporated under reduced pressure. The solid obtained was dissolved in the minimum amount of CH_2Cl_2 and the solution was cleared by centrifugation. Once removed the solvent under reduced pressure, the products

were precipitated by addition of Et_2O and collected by filtration. Yield > 85% in all the cases.

Characterization of $[Eu(tta)_3\{O=P(OPh)(NMe_2)_2\}_2]$

IR *(cm^{-1}): 1636-1302 s (ν_{tta}), 1183 s, 1138 s ($\nu_{P=O} + \delta_{C-H}$), 1008 m (ν_{P-O}), 934 m (ν_{P-N}).*

^{1}H NMR *(DMSO-d_6, 298 K), δ: 7.45 (s, br, 3H, tta), 7.40-7.11 (m, 10H, Ph), 6.52 (s, br, 3H, tta), 6.36 (s, br, 3H, tta), 3.80 (s, br, 3H, tta), 2.63 (d, 24H, J_{PH}= 10.2Hz, Me).* ***^{31}P{^{1}H}*** *NMR (DMSO-d_6, 298 K), δ: 15.93 (FWHM = 10 Hz).* ***^{19}F*** *NMR (DMSO-d_6, 298 K), δ: -78.33, -78.40.*

PL *(solid sample, r.t., $\lambda_{excitation}$ = 375 nm, nm): 579 ($^5D_0 \rightarrow {}^7F_0$, 1.1%), 590, 595 ($^5D_0 \rightarrow {}^7F_1$, 5.6%), 612, 615, 617 ($^5D_0 \rightarrow {}^7F_2$, 85.0%), 651, 656 ($^5D_0 \rightarrow {}^7F_3$, 2.9%), 690, 701, 705 ($^5D_0 \rightarrow {}^7F_4$, 5.4%).*

Characterization of $[Eu(tta)_3\{O=P(OPh)_2(NMe_2)\}_2]$

IR *(cm^{-1}): 1635-1306 s (ν_{tta}), 1184 s, 1140 s ($\nu_{P=O} + \delta_{C-H}$), 1012 m (ν_{P-O}), 950 m (ν_{P-N}).*

^{1}H NMR *(DMSO-d_6, 298 K), δ: 7.48- 7.19 (m, 23H, Ph + tta), 6.52 (s, br, 3H, tta), 6.36 (s, br, 3H, tta), 3.80 (s, br, 3H, tta), 2.72 (d, 12H, J_{PH}= 10.4 Hz, Me).* ***^{31}P{^{1}H}*** *NMR (DMSO-d_6, 298 K), δ: 1.64 (FWHM = 2 Hz).* ***^{19}F*** *NMR (DMSO-d_6, 298 K), δ: -78.33, -78.40.*

mp*: 90°C.*

χ^M_{corr} *(M = 1373.02 g mol^{-1}, c.g.s.u.): $4.31 \cdot 10^{-3}$.*

PL *(solid sample, r.t., $\lambda_{excitation}$ = 375 nm, nm): 579 ($^5D_0 \rightarrow {}^7F_0$, 1.5%), 589, 591, 596 ($^5D_0 \rightarrow {}^7F_1$, 5.0%), 610, 613, 615, 620, 623 ($^5D_0 \rightarrow {}^7F_2$, 79.7%), 649, 652, 655 ($^5D_0 \rightarrow {}^7F_3$, 4.5%), 688, 691, 696, 700 ($^5D_0 \rightarrow {}^7F_4$, 9.3%).*

PLE *(solid sample, r.t., $\lambda_{emission}$ = 614 nm, nm): < 500 (ligands excitation, max 388), 464 ($^5D_2 \leftarrow {}^7F_0$), 533 ($^5D_1 \leftarrow {}^7F_1$).*

τ (solid sample, r.t., $\lambda_{excitation}$ = 377 nm, $\lambda_{emission}$ = 614 nm, μs): 570.

Characterization of [Eu(tta)$_3${O=P(NMe$_2$)$_2$(res)(NMe$_2$)$_2$P=O}]

IR *(cm^{-1}): 1637-1305 s (ν_{tta}), 1182 s, 1132 s ($\nu_{P=O}$ + δ_{C-H}), 1001 m, 981 m (ν_{P-O}), 930 m (ν_{P-N}).*

^{1}H NMR *(DMSO-d$_6$, 298 K), δ: 7.44 (m, 1H, res), 7.33 (t, 1H, J_{HH} = 8.3 Hz, res), 7.00 (s, 2H, res), 6.95 (d, 2H, J_{HH}= 8.3 Hz, res), 6.51 (s, 3H, tta), 6.35 (s, 3H, tta) , 3.81 (s, br, 3H, tta), 2.62 (d, 12H, J_{PH}= 10.1 Hz, Me).* ***^{31}P{^{1}H}*** *NMR (DMSO-d$_6$, 298 K), δ: 16.01 (FWHM = 13 Hz).* ***^{19}F*** *NMR (DMSO-d$_6$, 298 K), δ: -78.34.*

mp: *108°C.*

χ^M_{corr} *(M = 1196.85 g mol^{-1}, c.g.s.u.): 4.09 · 10^{-3}.*

PL *(solid sample, r.t., $\lambda_{excitation}$ = 375 nm, nm): 579 ($^5D_0 \rightarrow {}^7F_0$, 1.0%), 588, 591, 595 ($^5D_0 \rightarrow {}^7F_1$, 5.6%), 611, 614, 619 ($^5D_0 \rightarrow {}^7F_2$, 74.9%), 649, 655 ($^5D_0 \rightarrow {}^7F_3$, 5.2%), 690, 700 ($^5D_0 \rightarrow {}^7F_4$, 13.3%).*

PLE *(solid sample, r.t., $\lambda_{emission}$ = 614 nm, nm): < 500 (ligands excitation, max 388), 464 ($^5D_2 \leftarrow {}^7F_0$), 535 ($^5D_1 \leftarrow {}^7F_1$).*

τ (solid sample, r.t., $\lambda_{excitation}$ = 377 nm, $\lambda_{emission}$ = 614 nm, μs): 499.

2.5.2 Synthesis of [Eu(dbm)$_3${O=P(OPh)$_2$(NMe$_2$)}]

The synthesis was carried out following the procedure already described for [Eu(tta)$_3${O=P(OPh)$_2$(NMe$_2$)}$_2$], using dibenzoylmethane (3 mmol, 0.68 g) instead of thenoyltrifluoroacetone. Yield = 85% calculated on Eu.

Characterization of [Eu(dbm)$_3${O=P(OPh)$_2$(NMe$_2$)}]

IR *(cm^{-1}): 1607-1306 s (ν_{dbm}), 1224-1159 s ($\nu_{P=O}$ + δ_{C-H}), 1022 m (ν_{P-O}), 940 m (ν_{P-N}).*

^{1}H NMR *(DMSO-d$_6$, 298 K), δ: 7.42 (t, 2H,J_{HH}= 7.7 Hz, OPh), 7.24 (s, 3H, dbm), 7.23 (m, 3H, OPh), 6.82 (t, 6H, J_{HH}= 7.2 Hz, dbm), 6.68 (t, 12H, J_{HH}= 7.2 Hz, dbm), 5.72 (d, 12H, J_{HH}= 7.2 Hz, dbm) , 2.72 (d, 6H, J_{PH}= 10.4 Hz, Me).* ***^{31}P{^{1}H}*** *NMR (DMSO-d$_6$, 298 K), δ: 1.64 (FWHM = 2 Hz).*

mp: *153°C.*

χ^M_{corr} *(M = 1102.09 g mol^{-1}, c.g.s.u.): 4.85 · 10^{-3}.*

PL *(solid sample, r.t., $\lambda_{excitation}$ = 375 nm, nm): 579 ($^5D_0 \rightarrow {}^7F_0$, 1.5%), 593, 596 ($^5D_0 \rightarrow {}^7F_1$, 4.3%), 610, 612, 619, 623, 625 ($^5D_0 \rightarrow {}^7F_2$, 82.6%), 650, 654 ($^5D_0 \rightarrow {}^7F_3$, 5.8%), 687, 690, 699, 701, 706 ($^5D_0 \rightarrow {}^7F_4$, 5.8%).*

PLE *(solid sample, r.t., $\lambda_{emission}$ = 614 nm, nm): < 510 (ligands excitation, max 388), 464 ($^5D_2 \leftarrow {}^7F_0$), 532 ($^5D_1 \leftarrow {}^7F_1$).*

τ (solid sample, r.t., $\lambda_{excitation}$ = 377 nm, $\lambda_{emission}$ = 612 nm, μs): 241.

2.5.3 Synthesis of $[Tb(acac)_3L_2]$ {L= $O=P(OPh)(NMe_2)_2$, $O=P(OPh)_2(NMe_2)$, $O=P(NMe_2)_2(res)(NMe_2)_2P=O$}

The synthesis of Tb(III) complexes were conducted with the same procedure employed for the analogous europium-tta species, starting from anhydrous $TbCl_3$. Acetylacetone was employed as β-diketone. Yield > 65% in all the cases.

Characterization of $[Tb(acac)_3\{O=P(OPh)(NMe_2)_2\}_2]$

IR *(cm^{-1}): 1601-1402 s (ν_{acac}), 1218 s, 1184 s ($\nu_{P=O} + \delta_{C-H}$), 1002 m (ν_{P-O}), 919 m (ν_{P-N}).*

PL *(solid sample, r.t., $\lambda_{excitation}$ = 375 nm, nm): 486, 490, 496 ($^5D_4 \rightarrow {}^7F_6$, 14.2%), 545 ($^5D_4 \rightarrow {}^7F_5$, 66.5%), 582, 590 ($^5D_4 \rightarrow {}^7F_4$, 9.9%), 619, 623 ($^5D_4 \rightarrow {}^7F_3$, 5.9%), 642-692 ($^5D_4 \rightarrow {}^7F_2$, $^5D_4 \rightarrow {}^7F_1$, $^5D_4 \rightarrow {}^7F_0$, 3.5%).*

Characterization of $[Tb(acac)_3\{O=P(OPh)_2(NMe_2)\}_2]$

IR *(cm^{-1}): 1599-1397 s (ν_{acac}), 1258 s, 1182 s ($\nu_{P=O} + \delta_{C-H}$), 1015 s (ν_{P-O}), 934 m (ν_{P-N}).*

mp: *128°C.*

χ^M_{corr} (M = 1013.80 g mol^{-1}, c.g.s.u.): $6.08 \cdot 10^{-2}$.

PL *(solid sample, r.t., $\lambda_{excitation}$ = 330 nm, nm): 485, 492, 496 ($^5D_4 \rightarrow {}^7F_6$, 15.1%), 542, 548 ($^5D_4 \rightarrow {}^7F_5$, 63.9%), 583, 590, 592, 597 ($^5D_4 \rightarrow {}^7F_4$, 9.6%), 616, 618, 622 ($^5D_4 \rightarrow {}^7F_3$, 7.2%), 638-683 ($^5D_4 \rightarrow {}^7F_2$, $^5D_4 \rightarrow {}^7F_1$, $^5D_4 \rightarrow {}^7F_0$, 4.2%).*

PLE *(solid sample, r.t., $\lambda_{emission}$ = 548 nm, nm): < 410 (ligands excitation, max 379, 329).*

τ (solid sample, r.t., $\lambda_{excitation}$ = 377 nm, $\lambda_{emission}$ = 548 nm, μs): 648.

Characterization of [Tb(acac)$_3${O=P(NMe$_2$)$_2$(res)(NMe$_2$)$_2$P=O}]

***IR** (cm^{-1}): 1603-1367 s (ν_{acac}), 1260 m ($\nu_{P=O} + \delta_{C-H}$), 1017 s (ν_{P-O}), 921 m (ν_{P-N}).*

***PL** (solid sample, r.t., $\lambda_{excitation}$ = 375 nm, nm): 488, 495 ($^5D_4 \rightarrow {}^7F_6$, 10.1%), 543, 549 ($^5D_4 \rightarrow {}^7F_5$, 69.5%), 583, 594, 598 ($^5D_4 \rightarrow {}^7F_4$, 9.6%), 620 ($^5D_4 \rightarrow {}^7F_3$, 6.9%), 641-660 ($^5D_4 \rightarrow {}^7F_2$, $^5D_4 \rightarrow {}^7F_1$, 3.9%).*

2.5.4 Synthesis of [Dy(acac)$_3${O=P(OPh)$_2$(NMe$_2$)}$_2$]

The synthesis of Dy(III) complex with two equivalents of *O=P(OPh)$_2$(NMe$_2$)* was conducted with the same procedure previously described for the Tb(III) derivative. Yield > 60%.

Characterization of [Dy(acac)$_3${O=P(OPh)$_2$(NMe$_2$)}$_2$]

***IR** (cm^{-1}): 1597-1395 s (ν_{acac}), 1258 s, 1182 s ($\nu_{P=O} + \delta_{C-H}$), 1015 s (ν_{P-O}), 933 m (ν_{P-N}).*

***mp:** 118 °C.*

χ^{M}_{corr} (M = 1017.38 g mol^{-1}, c.g.s.u.): 6.68 · 10^{-2}.

***PL** (solid sample, r.t., $\lambda_{excitation}$ = 375 nm, nm): 480, 490 ($^4F_{9/2} \rightarrow {}^6H_{15/2}$, 11.5%), 574, 579 ($^4F_{9/2} \rightarrow {}^6H_{13/2}$, 76.9%), 668 ($^4F_{9/2} \rightarrow {}^6H_{11/2}$, 7.3.%), 755 ($^4F_{9/2} \rightarrow {}^6H_{9/2}$, 4.3%).*

2.6 X-ray structures determination

The crystallographic data were collected at CACTI (Universidade de Vigo) by the research group of prof. Castro using a Bruker D8 Venture Photon 100 CMOS detector and Mo-Kα radiation (λ = 0.71073 Å) generated by a Incoatec high brilliance IμS microsource. Reflections were collected at low temperature using a CryoStream 800 apparatus. Crystal data and structure refinement parameters are summarized in Tables 1-2-3.

Table 1. Structure refinement parameters of $[MnI_2\{O=P(OPh)_2(NMe_2)\}_2]$.

Compound	**$[MnI_2\{O=P(OPh)_2(NMe_2)\}_2]$**
Empirical formula	C28 H32 I2 Mn N2 O6 P2
Formula weight	863.23
Temperature	100(2) K
Wavelength	0.71073 Å
Crystal system	Monoclinic
Space group	$P2_1/n$
Unit cell dimensions	a = 10.0153(8) Å
	b = 17.3133(14) Å
	c = 19.6665(16) Å
	alpha = 90º
	beta = 103.495(3)º
	gamma = 90º
Volume	3316.0(5) $Å^3$
Z	4
Density (calculated)	1.729 Mg/m^3
Absorption coefficient	2.398 mm^{-1}
F(000)	1692
Crystal size	0.191 x 0.091 x 0.069 mm
θ range for data collection	2.353 to 28.383 º.
Index ranges	$-13 \leq h \leq 13$
	$-23 \leq k \leq 23$
	$-26 \leq l \leq 26$
Reflections collected	57360
Independent reflections	8266 [R_{int} = 0.0424]
Reflections observed (>2σ)	7001
Data Completeness	0.993
Absorption correction	Semi-empirical from equivalents

Max. and min. transmission	0.7457 and 0.6383
Refinement method	Full-matrix least-squares on F^2
Data / restraints / parameters	8266 / 0 / 374
Goodness-of-fit on F^2	1.052
Final R indices [I>2σ(I)]	R_1 = 0.0555
	wR_2 = 0.2282
R indices (all data)	R_1 = 0.0664
	wR_2 = 0.2369
Largest diff. peak and hole	2.706 and -2.445 e.Å^{-3}

Table 2. Structure refinement parameters of [MnI_2{O=P(NMe_2)$_2$(res)(NMe_2)$_2$P=O}].

Compound	[MnI_2{O=P(NMe_2)$_2$(res)(NMe_2)$_2$P=O}]
Empirical formula	C14 H28 I2 Mn N4 O2 P2
Formula weight	655.08
Temperature	100(2) K
Wavelength	0.71073 Å
Crystal system	Monoclinic
Space group	$P2_1/n$
Unit cell dimensions	a = 11.1151(9) Å
	b = 14.0317(12) Å
	c = 16.0386(14) Å
	α = 90°
	β = 100.395(3)°
	γ = 90°
Volume	2460.4(4) Å^3
Z	4
Density (calculated)	1.768 Mg/m^3
Absorption coefficient	3.190 mm^{-1}
F(000)	1268
Crystal size	0.265 x 0.238 x 0.205 mm
θ range for data collection	2.362 to 28.345°
Index ranges	-14 ≤ *h* ≤ 14
	-18 ≤ *k* ≤ 18
	-20 ≤ *l* ≤ 21
Reflections collected	50220
Independent reflections	6143 [R_{int} = 0.0425]
Reflections observed (>2σ)	5510
Data Completeness	0.999
Absorption correction	Semi-empirical from equivalents

Max. and min. transmission	0.7457 and 0.5007
Refinement method	Full-matrix least-squares on F^2
Data / restraints / parameters	6143 / 0 / 252
Goodness-of-fit on F^2	1.093
Final R indices [I>2σ(I)]	R_1 = 0.0395
	wR_2 = 0.0960
R indices (all data)	R_1 = 0.0458
	wR_2 = 0.0986
Largest diff. peak and hole	1.946 and -2.470 e.Å^{-3}

Table 3. Structure refinement parameters of [Eu(dbm)$_3${O=P(OPh)$_2$(NMe$_2$)}].

Compound	[Eu(dbm)$_3${O=P(OPh)$_2$(NMe$_2$)}]
Empirical formula	C_{59} H_{49} Eu N O_9 P
Formula weight	1098.92
Temperature	100(2) K
Wavelength	0.71073 Å
Crystal system	Triclinic
Space group	*P*-1
Unit cell dimensions	a = 10.2787(19) Å
	b = 11.247(2) Å
	c = 23.022(4) Å
	α = 100.074(5)°
	β = 100.205(5)°
	γ = 97.719(4)°
Volume	2541.1(8) Å^3
Z	2
Density (calculated)	1.436 Mg/m^3
Absorption coefficient	1.325 mm^{-1}
F(000)	1120
Crystal size	0.112 x 0.035 x 0.027 mm
θ range for data collection	2.242 to 25.423°
Index ranges	-12 ≤ h ≤ 12
	-13 ≤ k ≤ 13
	-27 ≤ l ≤ 27
Reflections collected	35098
Independent reflections	9207 [R_{int} = 0.0798]
Reflections observed (>2σ)	6958
Data Completeness	0.979
Absorption correction	Semi-empirical from equivalents

Max. and min. transmission	0.7452 and 0.5228
Refinement method	Full-matrix least-squares on F^2
Data / restraints / parameters	9207 / 6 / 527
Goodness-of-fit on F^2	1.353
Final R indices [$I>2\sigma(I)$]	R_1 = 0.1132
	wR_2 = 0.2283
R indices (all data)	R_1 = 0.1441
	wR_2 = 0.2379
Largest diff. peak and hole	1.909 and -3.643 e.Å^{-3}

2.7 Computational details

Geometry optimizations of Mn(II) bromo-complexes were carried out using the range-separated hybrid functional ωB97X[79] in combination with the Ahlrichs' split-valence triple-zeta polarized basis set.[80] The C-PCM solvation model was added, considering ethanol as continuous medium.[81] Sextet ground-state was considered, therefore the unrestricted DFT approach was used.[82] All the calculations were performed with ORCA 4.0.1.2.[83] The output, converted in .molden format, was analysed with MultiWfn, version 3.5.[84]

3. RESULTS AND DISCUSSIONS

3.1 Ligands and Mn(II) complexes

The internship activity started with the preparation of amidophosphate compounds to be considered as ligands towards hard metal centres such as Mn(II) and Ln(III). The design of the ligands was oriented towards species containing aromatic O-bonded fragments, in order to verify possible antenna-effect. The synthetic approaches were based on substitution reactions involving the P-Cl bonds of commercially available precursors, in particular *N,N,N′,N′*-tetramethylphosphorodiamidic chloride O=PCl(NMe$_2$)$_2$ and phosphorochloridic acid diphenyl ester O=PCl(OPh)$_2$. In the case of O=PCl(NMe$_2$)$_2$ the compound was reacted with aryloxides, obtained from the deprotonation of the corresponding neutral species with potassium *tert*-butoxide. The

conjugate bases of phenol, β-naphtol, resorcin and cathecol were successfully used for the displacement of P-bonded chloride. On the other hand, $O=PCl(OPh)_2$ was reacted with an excess of gaseous dimethylamine, obtained *in situ* from $[NH_2Me_2]Cl$ and NaOH. The reactions are summarized in Scheme 5 for clarity. As stated in the Experimental section, the species containing only one [P=O] fragment were already reported in the literature, even if using different experimental conditions. On the other hand, the compounds $O=P(NMe_2)_2(cat)(NMe_2)_2P=O$, 1,2-(*N*,*N*,*N*',*N*'-tetramethyldiamidophosphoryloxy benzene), and $O=P(NMe_2)_2(res)(NMe_2)_2P=O$, 1,3-(*N*,*N*,*N*',*N*'-tetramethyldiamidophosphoryloxy benzene), were never synthesized before.

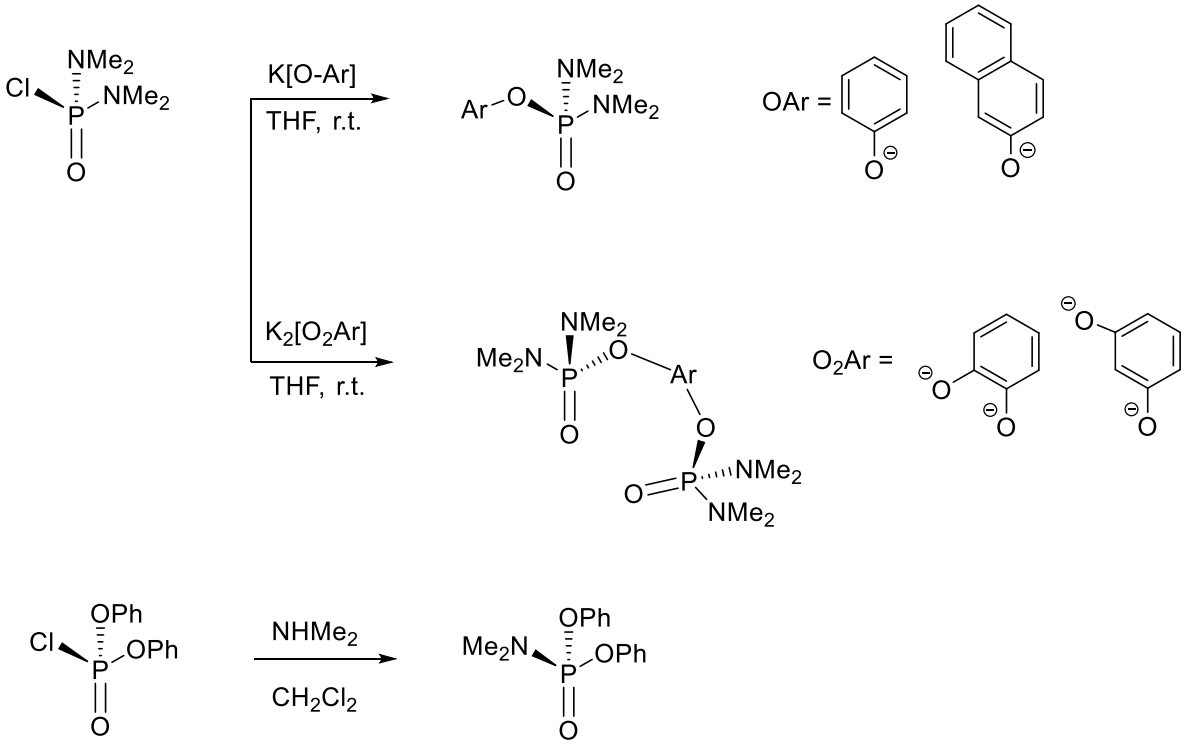

Scheme 5. General scheme for the synthesis of ligands.

In all the cases the ^1H NMR spectra confirmed the proposed formulae showing, besides the aromatic resonances, a doublet related to the N-bonded methyl groups in the low frequency region, with $^3J_{PH}$ coupling constant around 10 Hz. The ^{31}P $\{^1H\}$ NMR spectra are all characterized by a single sharp resonance. The NMR spectra are provided in Figs. 24-28 for clarity.

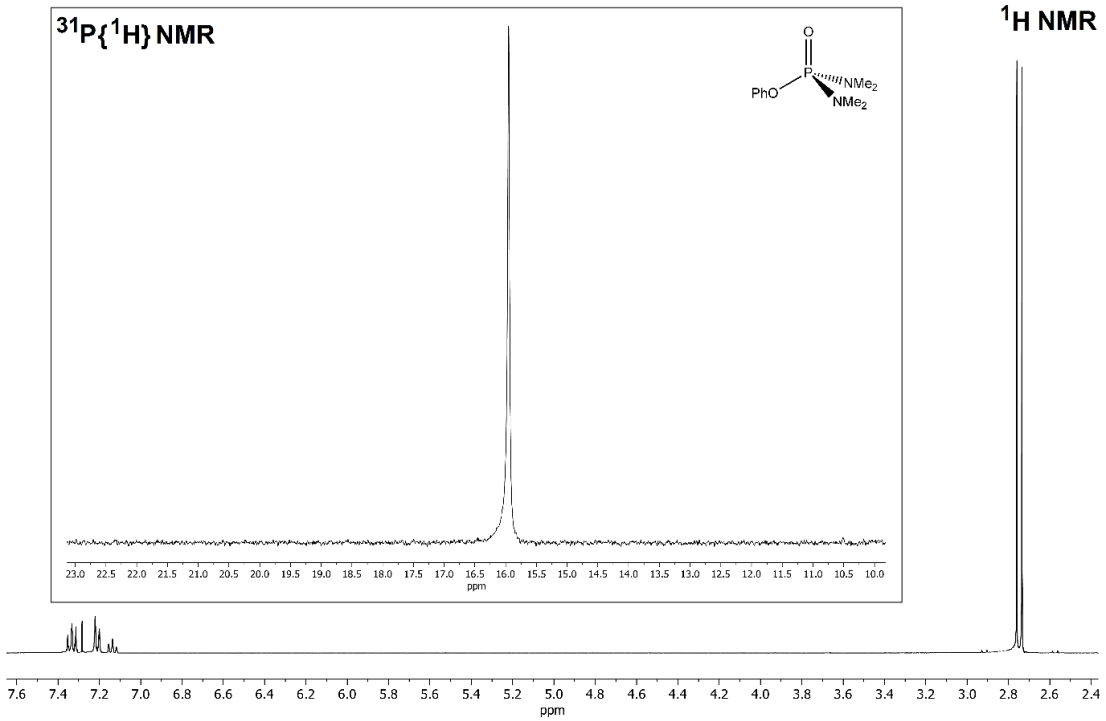

Figure 24. ^{1}H NMR spectrum of $O=P(OPh)(NMe_2)_2$. Inset: $^{31}P\{^{1}H\}$ NMR spectrum. $CDCl_3$, 298 K.

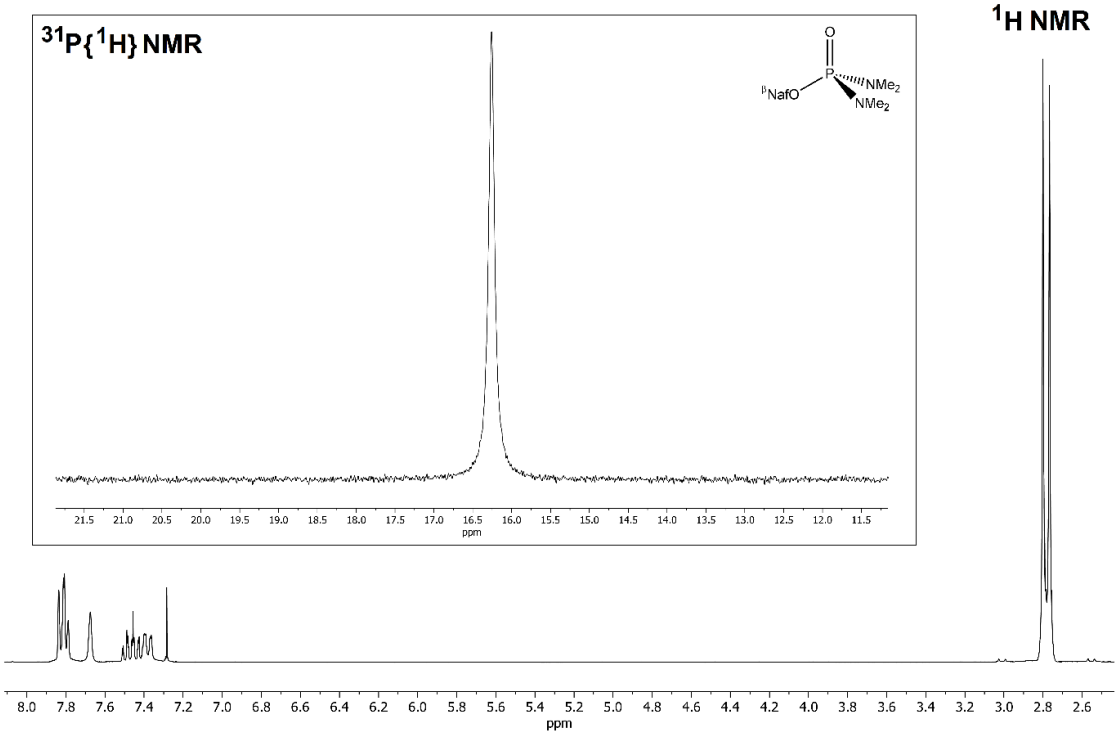

Figure 25. ^{1}H NMR spectrum of $O=P(ONaph)(NMe)_2$. Inset: $^{31}P\{^{1}H\}$ NMR spectrum. $CDCl_3$, 298 K

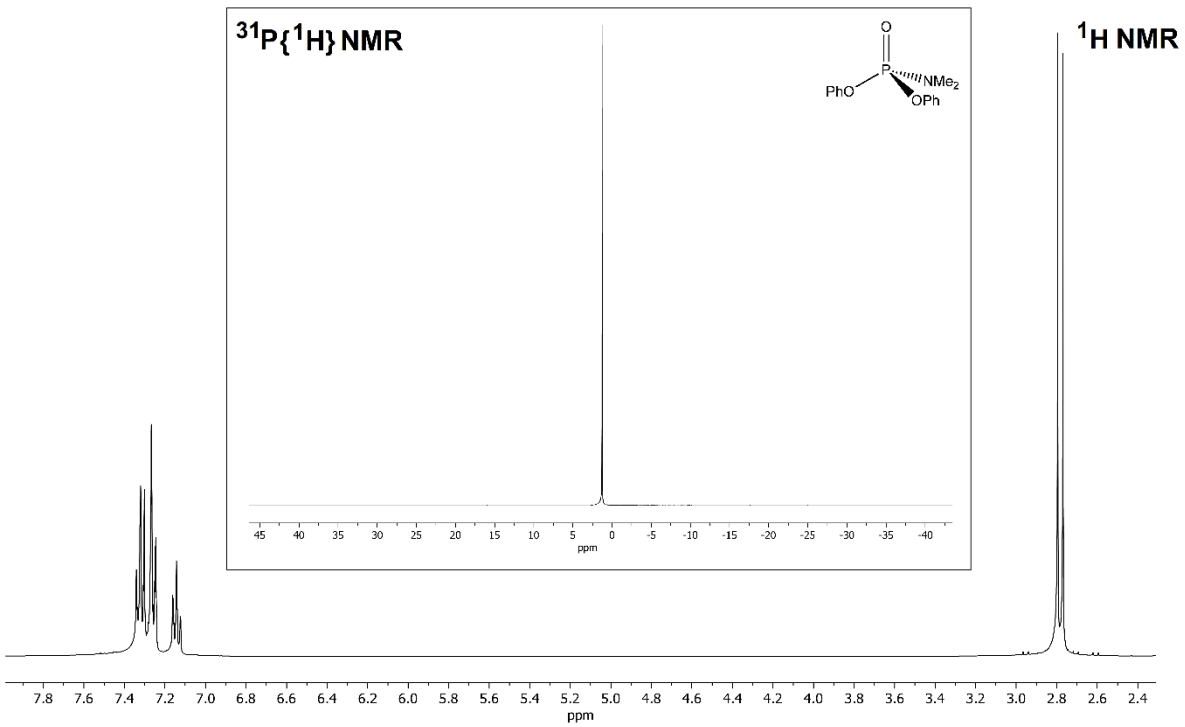

Figure 26. ^{1}H NMR spectrum of $O=P(OPh)_2(NMe_2)$. Inset: $^{31}P\{^{1}H\}$ NMR spectrum. $CDCl_3$, 298 K.

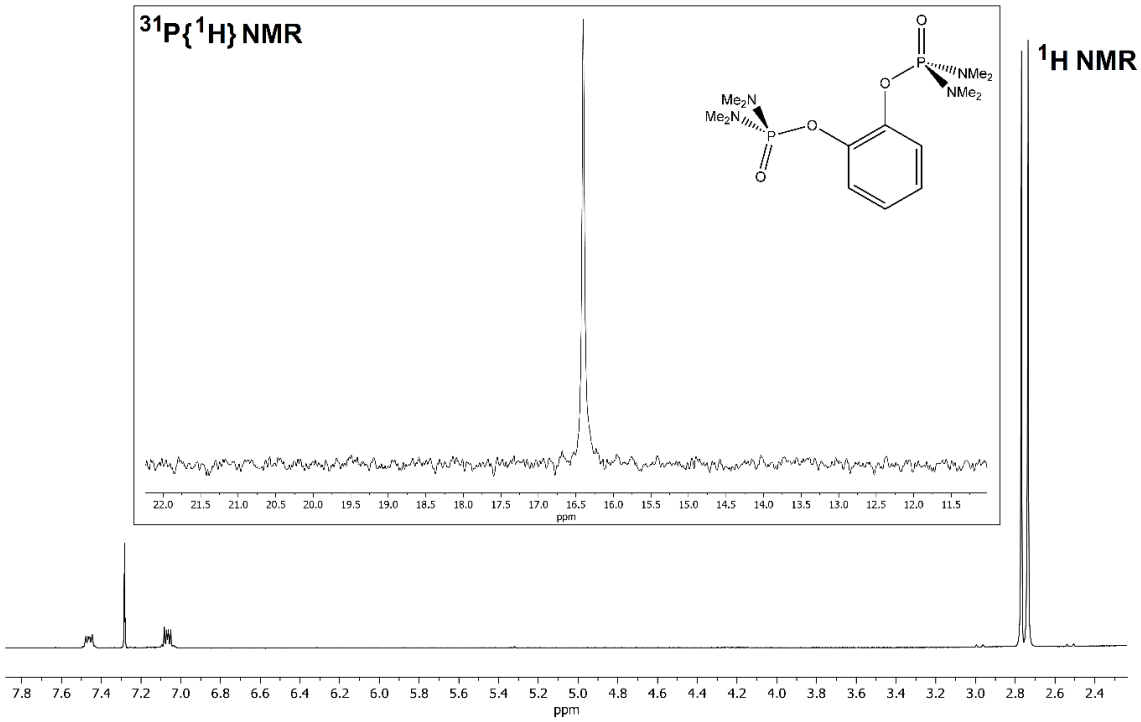

Figure 27. ^{1}H NMR spectrum of $O=P(NMe_2)_2(cat)(NMe_2)_2P=O$. Inset: $^{31}P\{^{1}H\}$ NMR spectrum. $CDCl_3$, 298 K.

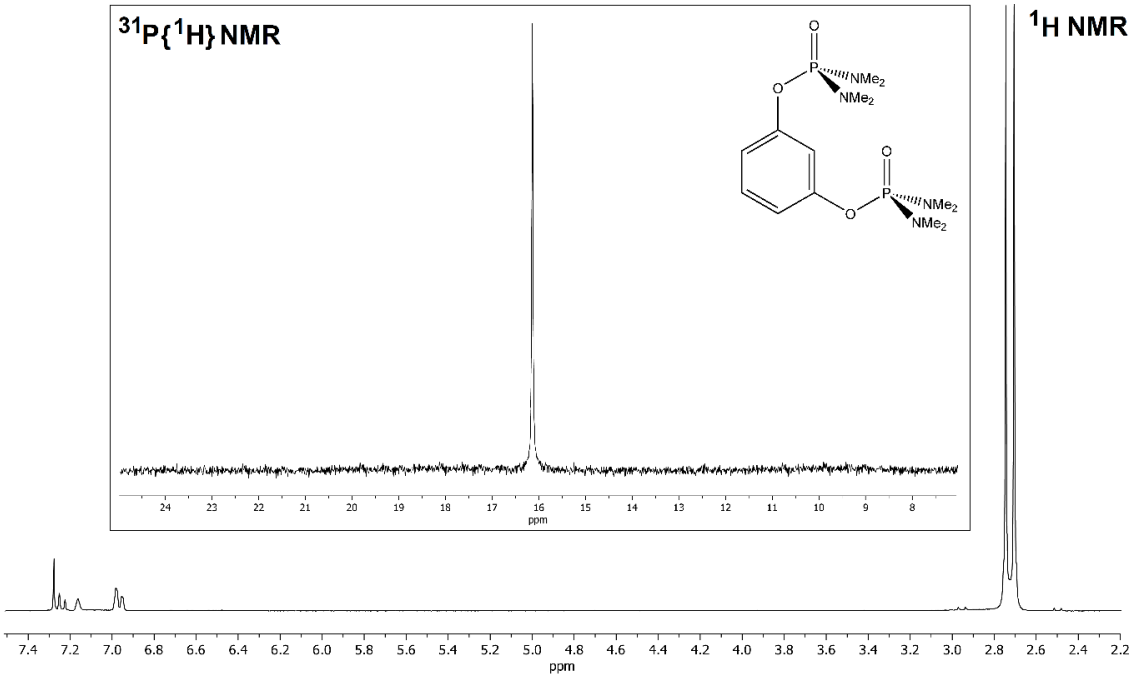

Figure 28. ^{1}H NMR spectrum of $O=P(NMe_2)_2(res)(NMe_2)_2P=O$. Inset: $^{31}P\{^{1}H\}$ NMR spectrum. $CDCl_3$, 298 K.

Diagnostic signals in the IR spectra are related to the P=O stretching, falling between 1270 and 1150 cm^{-1}. The precise assignment is in part confused by the fact that the stretching is combined with C-H bending vibrations, as confirmed by computational IR simulations. Other diagnostic signals are related to the P-O and P-N stretchings, falling respectively around 1000 and 930 cm^{-1} (see Figure 29).

All the phenyl-based ligands showed absorptions in the UV range for wavelengths below 320 nm, with a maximum around 270 nm. A slightly wider absorption range, below 350 nm, was observed as expected for the naphtyl derivative.

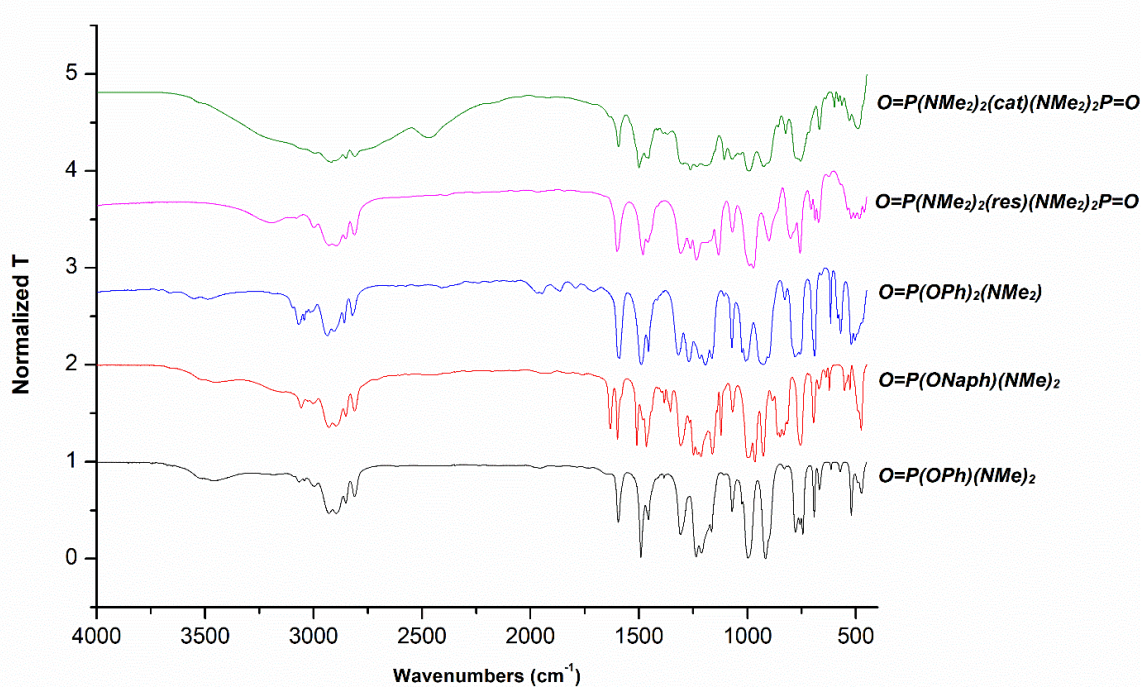

Figure 29. Comparison of the IR spectra among amidophosphate ligands.

The synthesis of the complexes started considering anhydrous Mn(II) halides MnX_2 (X = Cl, Br, I) as precursors. The reactions were carried out under controlled atmosphere using ethanol as solvent, accordingly to the procedure recently used by for the preparation of comparable phosphoramide and arylphosphonic diamide derivatives.[22/23/32] In the case of the mono-amidophosphate $O=P(OPh)(NMe_2)_2$ as ligand, the reaction worked only for X = Br, with the isolation of $[MnBr_2\{O=P(OPh)(NMe_2)_2\}_2]$ (Scheme 6). Despite all the attempts, the same reaction with $MnCl_2$ and MnI_2 afforded only untreatable oils without any appreciable luminescence. Despite the comparable steric bulk close to the metal centre, the formal replacement of the phenyl ring with β-naphtyl was detrimental for the synthesis of new Mn(II) complexes. Preliminary investigations revealed the formation of mixtures of products with all the halides here considered. It is worth noting that the non-innocent role of the naphyl substituents on the formation of Mn(II) complexes was previously observed by studying the coordination chemistry of arylphosphonic diamide ligands towards Mn(II).[33] The attention was therefore moved towards the bis-amidophosphate species $O=P(OPh)_2(NMe_2)$. In this case luminescent coordination compounds were obtained with all the Mn(II) precursors, having general formula $[MnX_2\{O=P(OPh)_2(NMe_2)\}_2]$ (X = Cl, Br, I) (see Scheme 6). Finally, different results were obtained with the bidentate ligands $O=P(NMe_2)_2(cat)(NMe_2)_2P=O$ and

$O=P(NMe_2)_2(res)(NMe_2)_2P=O$. In the first case mixture of products were obtained, while with the second ligand species having general formula $[MnX_2\{O=P(NMe_2)_2(res)(NMe_2)_2P=O\}]$ (X = Br, I) were isolated (Scheme 6).

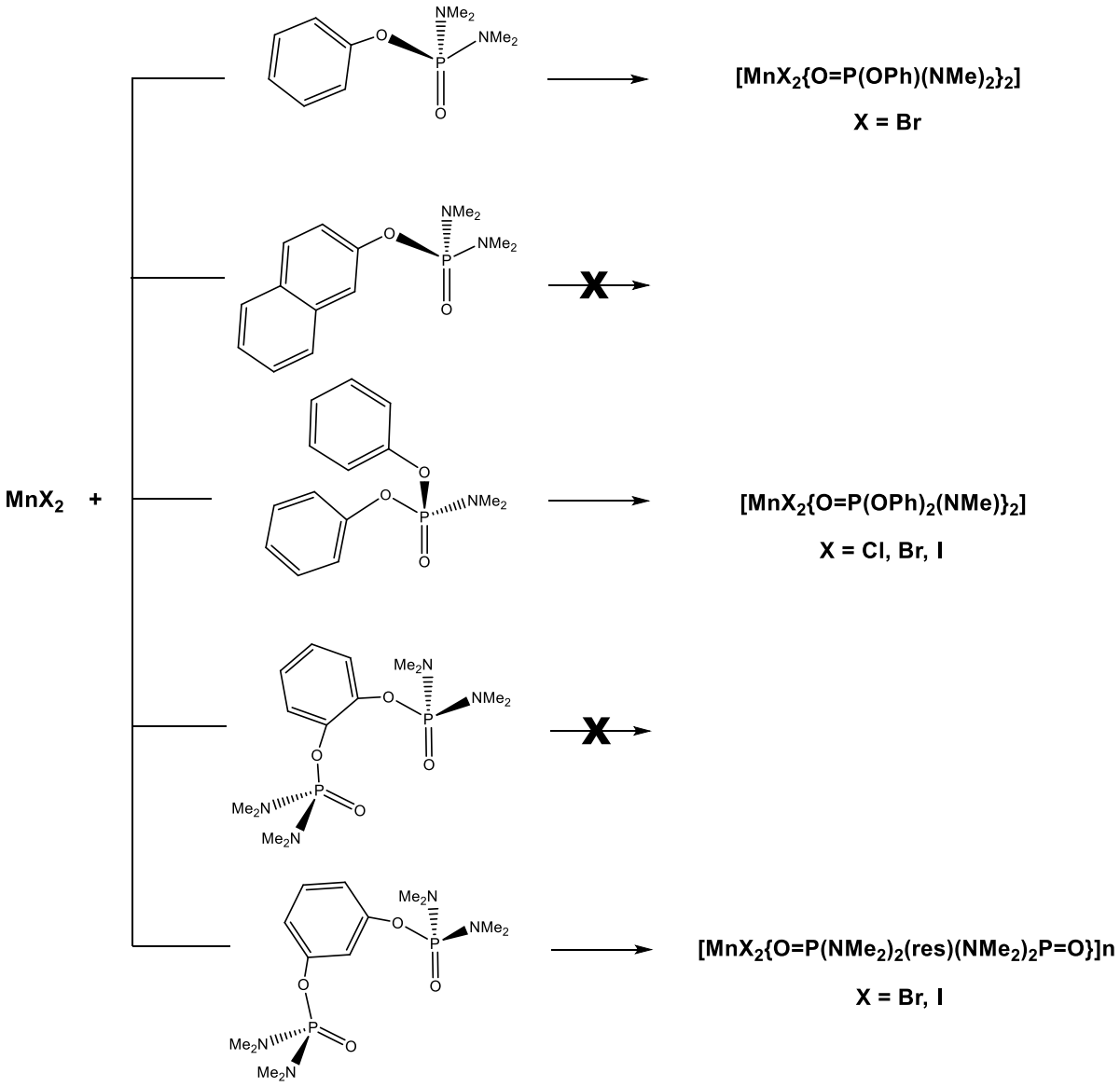

Scheme 6. Mn(II) complexes obtained with amidophosphate ligands.

All the species are moisture-sensitive. Thermal decomposition occurs in the range of 110-140° depending on the halide and the ligand considered.

Characterization data agree with the proposed formulae. In particular, magnetic measurements gave molar magnetic susceptibility values in line with magnetic moments around 5.9 BM, *i.e.* the value expected for a high-spin d^5 metal centre,

therefore confirming the molecular weights related to the formulations proposed in Scheme 6. The IR spectra show signals comparable to those of the free ligands, with slight low-frequency shift of the bands related to P=O stretching because of coordination.[32] The weakening of the P=O bond slightly enforces the P-N interactions. As an example, Fig. 30 shows the superposition of the IR spectra of $[MnI_2\{O=P(OPh)_2(NMe_2)\}_2]$ and of the corresponding free ligand.

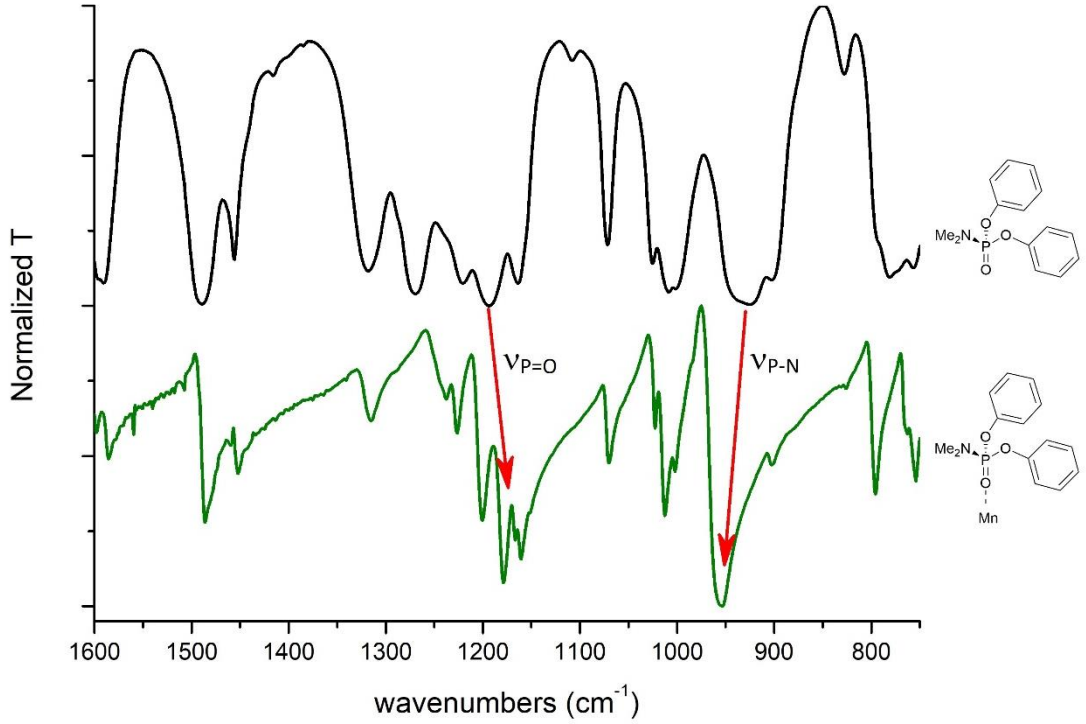

Figure 30. IR spectra comparison between $[MnI_2\{O=P(OPh)_2(NMe_2)\}_2]$ and the corresponding ligand. (P=O and P-N stretching bands evidenced).

The unambiguous characterization of the complex $[MnI_2\{O=P(OPh)_2(NMe_2)\}_2]$ was obtained from single crystal X-ray diffraction. The structure, reported in Fig. 31, clearly shows the tetrahedral coordination sphere surrounding the Mn(II) ion, as already observed for comparable derivatives with phosphoramide and phenylphosphonic diamide as ligands. The tetrahedral geometry is only slightly distorted, the τ_4 parameter being 0.94 (ideal values: 1, regular tetrahedron; 0, square planar; 0.85, trigonal pyramid).[85] The Mn-O bond lengths are in line with values previously reported for tetrahedral compounds with other [P=O]-donor ligands.[22/23/32] The coordination of $O=P(OPh)_2(NMe_2)$ is slightly bent, the Mn-O-P angles being between around 175°. The P=O distances confirm the double bond character. As previously observed for comparable Mn(II)-coordinated ligands, the nitrogen atoms are nearly trigonal planar.

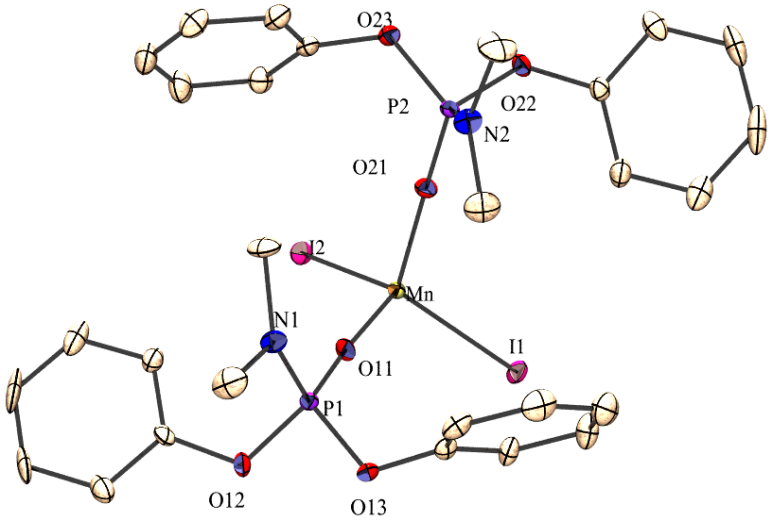

Figure 31. ORTEP view of [MnI_2{$O=P(OPh)_2(NMe_2)$}$_2$].Hydrogen atoms are omitted for clarity. Selected bond lengths (Å): Mn-O(11): 2.0023(5); Mn-O(21): 2.039(5); Mn-I(1): 2.6782(11); Mn-I(2): 2.6782(11); P(1)-O(11): 1.482(5); P(2)-O(21): 1.471(5). Selected angles (°): O(11)-Mn-O(21): 93.8(2); O(11)-Mn-I(1): 111.25(15); O(11)-Mn-I(2); O(21)-Mn-I(1): 113.48(16); O(21)-Mn-I(2): 111.26(15); I(2)-Mn-I(1): 112.25(4); Mn-O(11)-P(1): 175.6(4); Mn-O(22)-P(2): 175.4(4).

The ligand $O=P(NMe_2)_2(res)(NMe_2)_2P=O$ could hypothetically coordinate the same metal centre, forming a 10-membered metallacycle, or behave as bridging ligand between two metal ions. The second possibility was confirmed by the X-ray structure determination of $[MnI_2\{O=P(NMe_2)_2(res)(NMe_2)_2P=O\}]_n$. The compound is a coordination polymer, the unit cell and its zigzag chain growth are shown in Fig. 32. As for the previous compound, the coordination sphere surrounding Mn(II) is tetrahedral (τ_4 =0.96), with comparable Mn-O and Mn-I bond distances. The most striking difference is the bent coordination mode of the [P=O]-donor fragments, being the Mn-O=P angles comprised between 143.4(2) and 145.7(2) °.

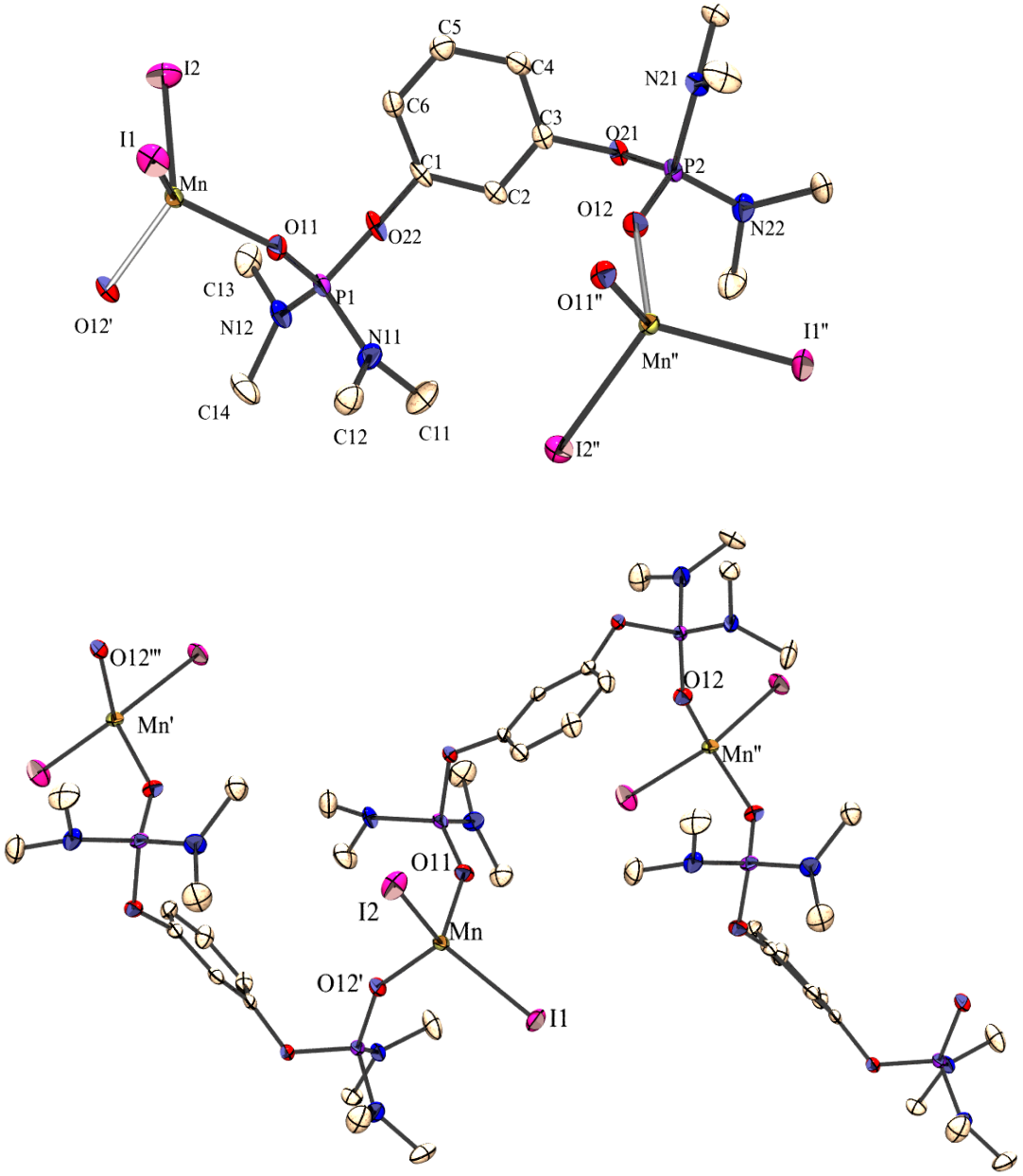

Figure 32. ORTEP view of the unit cell of $[MnI_2\{O=P(NMe_2)_2(res)(NMe_2)_2P=O\}]_n$ and its chain growth. Hydrogen atoms are omitted for clarity. Selected bond lengths (Å): Mn-O(11): 2.035(3); Mn-O(12): 2.036(3); Mn-I(1): 2.6742(7); Mn-I(2): 2.6489(7); P(1)-O(11): 1.490(3); P(2)-O(12): 1.495(3). Selected angles (°): O(11)-Mn-O(12): 99.42(13); O(11)-Mn-I(2): 107.30(9); O(12)-Mn-I(2): 112.50(9); O(12)-Mn-I(1): 111.71(9); O(11)-Mn-I(1): 110.52(9); I(2)-Mn-I(1): 114.27(2); P(1)-O(11)-Mn: 143.4(2); P(2)-O(12)-Mn: 145.7(2).

As stated in the Introduction, the tetrahedral geometry is associated to green emission from Mn(II). Excitation of the above described iodo-complexes confirmed this assumption, being the species appreciably green-emitting at the solid state. The photoluminescence spectra, reported in Fig. 33, showed the presence of a single band centred around 520 nm with FWHM of 2100 cm^{-1}. The CIE 1931 coordinates[86] are x

= 0.189, y = 0.663 for $[MnI_2\{O=P(OPh)_2(NMe_2)\}_2]$ and x = 0.294, y = 0.644 for $[MnI_2\{O=P(NMe_2)_2(res)(NMe_2)_2P=O\}]$ (Fig. 35).

The PLE spectrum reported in Fig. 33 indicates that Mn(II) luminescence is achieved only by direct excitation of the metal centre, based on the $^4F,^4P,^4D,^4G \leftarrow ^6S$ transitions. A wide band at wavelengths below 300 nm, related to the absorption of the phenyl rings, is in fact absent. Such a result leads to the conclusion that no antenna-effect occurs between Mn(II) and the aromatic substituents of amidophosphate ligands, differently to what previously observed for arylphosphonic diamides and related ligands.[22/32]. It is to be concluded that the oxygen atom between phosphorous and phenyl fragments interrupts the ligand→metal energy transfer.

Another information coming from the PLE spectrum is related to the ligand field strength. The ^4G exited state is closer to the ^4P and ^4D states with respect to the previously mentioned arylphosphonic diamide complexes, and the ^4F states fall at slightly lower wavelengths.[22/32] On considering the Tanabe-Sugano diagram shown in Fig. 6, these variations can be rationalized on the basis of lower σ-donation from amidophosphates with respect to arylphosphonic diamides, in agreement with the presence of electron-withdrawing OPh groups bonded to phosphorous.

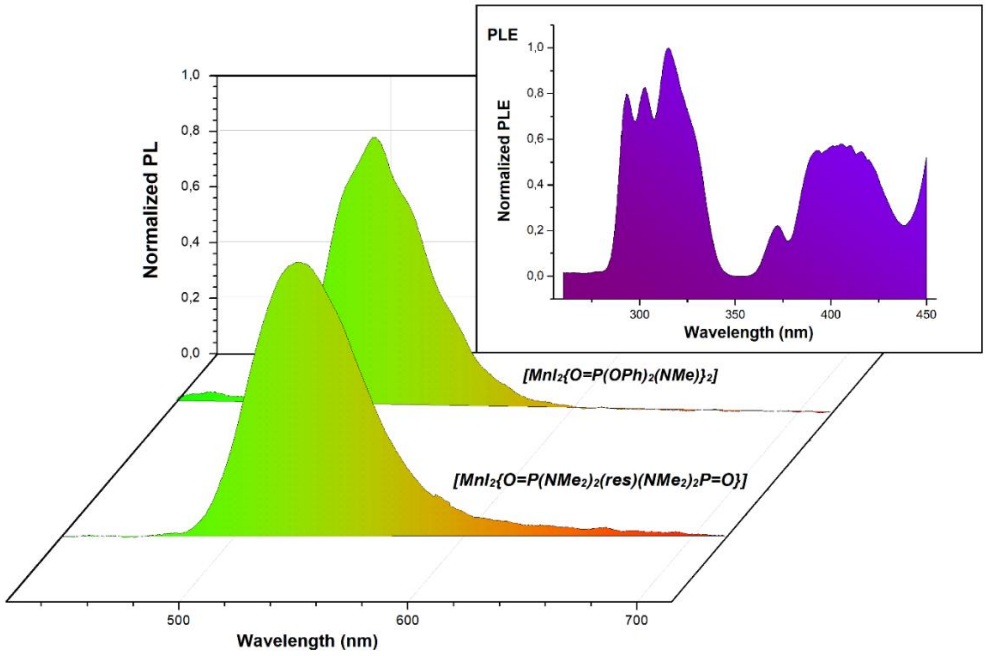

Figure 33. Normalized PL spectra of iodo-complexes. Inset: PLE spectrum of $[MnI_2\{O=P(OPh)_2(NMe_2)\}_2]$.

On the basis of the photoluminescence spectra, tetrahedral geometry is proposed also for the other green-emitting Mn(II) derivates here described, *i.e.* the bromo-complexes $[MnBr_2\{O=P(OPh)(NMe_2)_2\}_2]$, $MnBr_2\{O=P(OPh)_2(NMe_2)\}_2]$ and $[MnBr_2\{O=P(NMe_2)_2(res)(NMe_2)_2P=O\}]_n$. PL and PLE spectra are reported in Fig. 34. The bands are centred at 513 nm, with FWHM values between 2000 and 2200 cm^{-1}. The CIE coordinates are reported in Fig. 35.

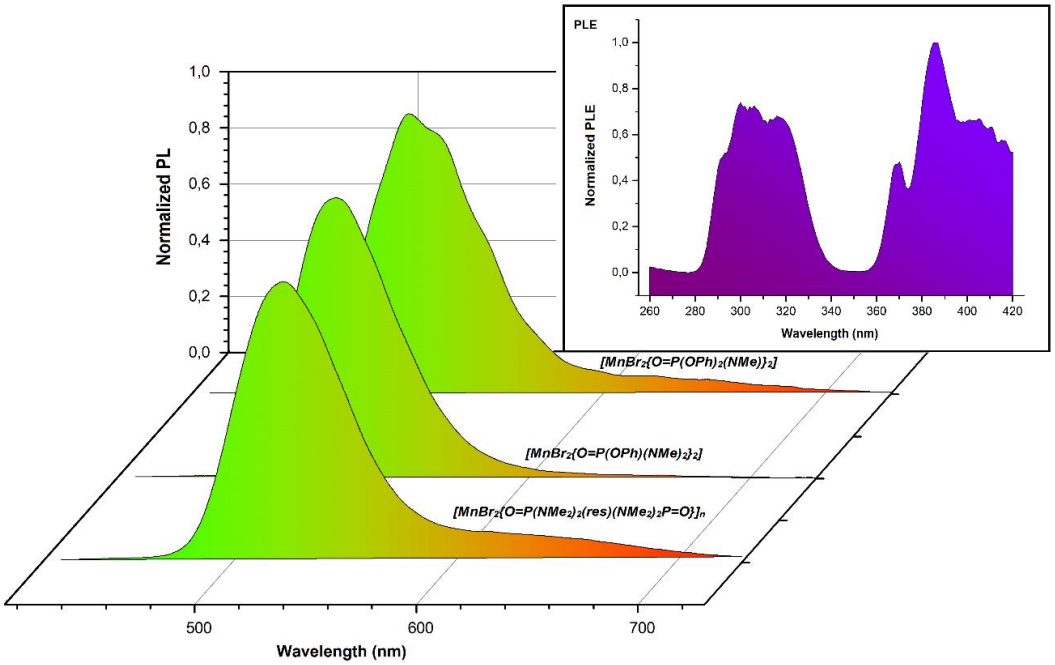

Figure 34. Normalized PL spectra of bromo-complexes. Inset: PLE of $[MnBr_2\{O=P(NMe_2)_2(res)(NMe_2)_2P=O\}]_n$.

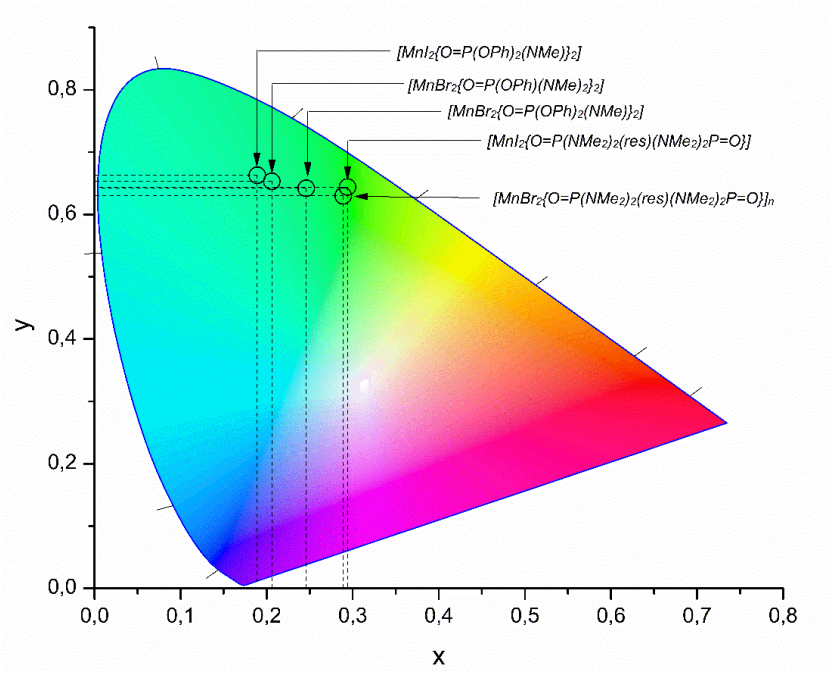

Figure 35. Chromaticity coordinates of the green-emitting Mn(II) complexes.

The PLE spectra do not show any appreciable difference with respect to those of the iodo-complexes, supporting the hypothesis of weaker σ-donation by the amidophosphates with respect to other ligands based on the [P=O]-donor fragment. This point was ascertained by means of DFT calculations on model systems having general formula $[MnBr_2L_2]$, where L is hexamethylphosphoramide $O=P(NMe_2)_3$, (1-phenyl)-*N*,*N*,*N*',*N*'-tetramethylamido phosphate $O=P(OPh)(NMe_2)_2$, diphenyl *N*-dimethylamidophosphate $O=P(OPh)_2(NMe_2)$ and triphenylphosphate $O=P(OPh)_3$. The optimized structures are depicted in Fig. 36. Salient data related to the Mn-O bond critical points (b.c.p.), obtained from the Atoms-In-Molecules (AIM) analyses on the optimized geometries, are reported in Table 4. As clearly observable, the formal replacement of $[NMe_2]$ fragments with [OPh] causes the progressive reduction of electron density ρ at b.c.p., accompanied by less negative values of potential energy density (V). Both these trends agree with the weakening of the Mn-O bonds. The slightly negative energy density (E) values and the positive Laplacian of electron density ($\nabla^2\rho$) values agree with Bianchi's definition of dative bonds.[87] Calculations on the triphenylphosphate derivative, included for comparison, indicate that the Mn-O bonds are particularly weak. It is worth noting that, differently from the other compounds, experimental evidences do not suggest tetrahedral geometry for $[MnBr_2\{O=P(OPh)_3\}]$.[34]

Table 4. Salient data related to the Mn-O bond critical points from Atoms-In-Molecules (AIM) analyses. All quantities in a.u.

Complex	ρ	V	E	$(\nabla^2\rho)$
$[MnBr_2(O=P(NMe_2)_3)_2]$	0.072	-0.114	-0.009	0.384
$[MnBr_2(O=P(OPh)(NMe_2)_2)_2]$	0.070	-0.109	-0.008	0.376
$[MnBr_2(O=P(OPh)_2(NMe_2))_2]$	0.066	-0.102	-0.007	0.346
$[MnBr_2(O=P(OPh)_3)_2]$	0.056	-0.061	-0.011	0.155

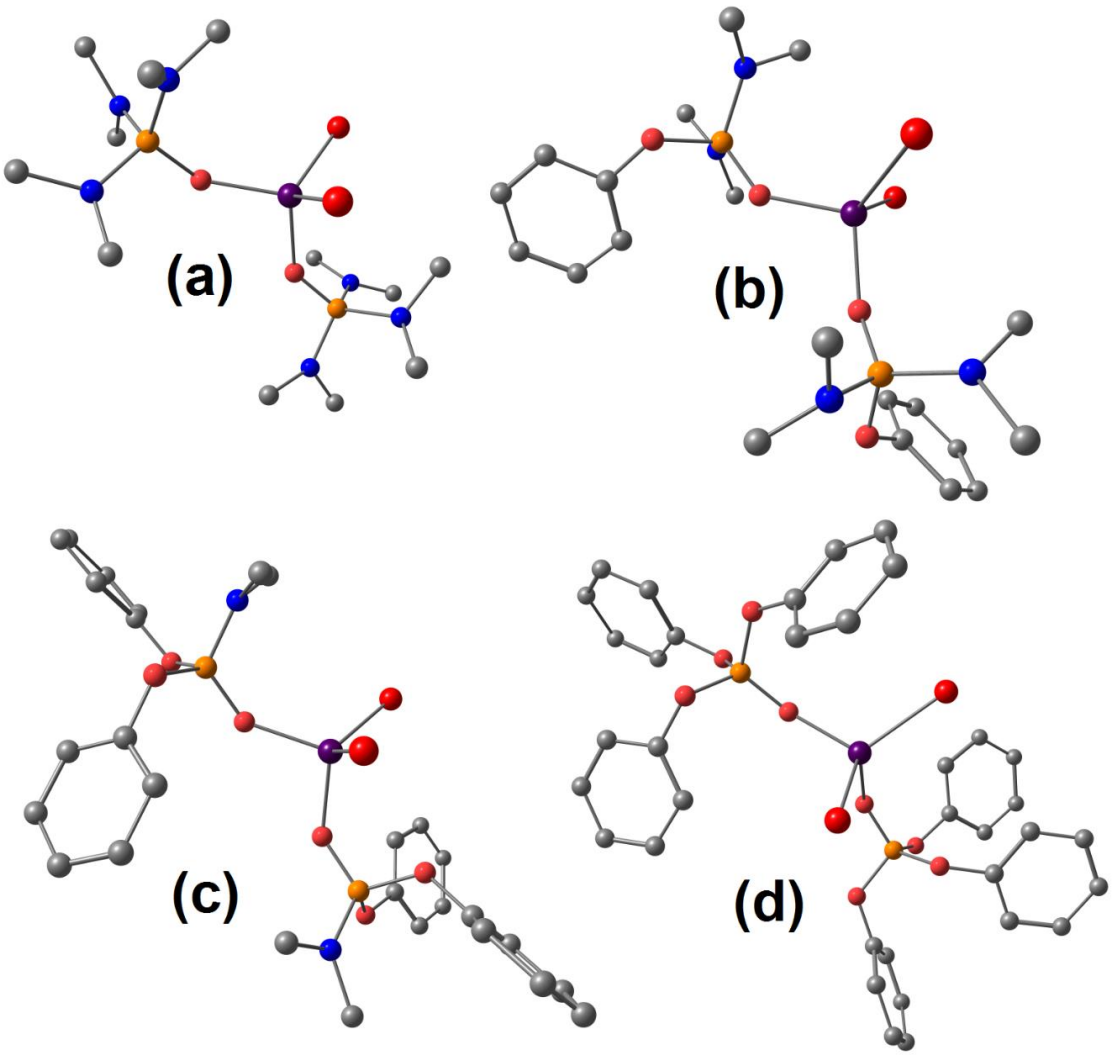

Figure 36. DFT-optimized structures of $[MnBr_2L_2]$ compounds: (a) L = $O=P(NMe_2)_3$; (b) L = $O=P(OPh)(NMe_2)_2$; (c)) L = $O=P(OPh)_2(NMe_2)$; (d)) L = $O=P(OPh)_3$. C-PCM/ωB97X/def2-TZVP calculations, ethanol as continuous medium. Colour map: Mn, violet; Br, dark red; P, orange; O, red; N, blue; C, grey. Hydrogen atoms are omitted for clarity.

The only chloro-complex that was synthesized has general formula $[MnCl_2\{O=P(OPh)_2(NMe_2)\}_2]$. As observable in Fig. 37, the species is, quite surprisingly, red-emitting (PL maximum at 647 nm, FWHM = 2700 cm^{-1}), therefore the tetrahedral geometry is ruled out. The PLE spectrum reported in Fig. 37 suggests that the emission occurs for direct Mn(II) excitation. The compound is quite unstable, for instance it reacts with diethylether to form green-emitting by-products, among all probably $[MnCl_4]^{2-}$.

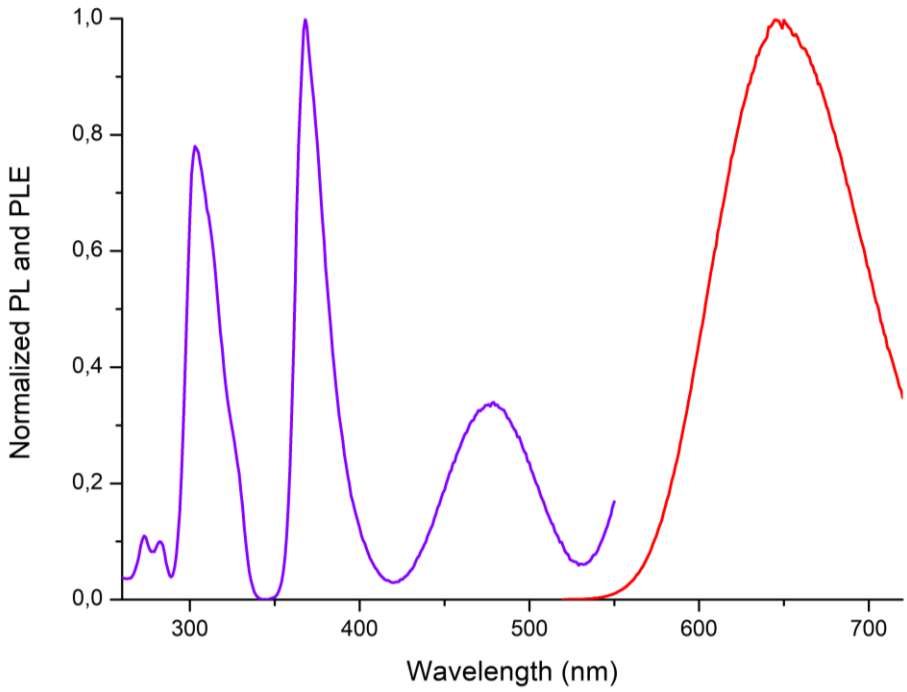

Figure 37. PL and PLE spectra [$MnCl_2\{O=P(OPh)_2(NMe_2)\}_2$].

The poor stability did not allow the isolation of crystals suitable for X-ray diffraction. The characterization data however agree with the proposed formulation, in particular the magnetic moment is in line with a high-spin d^5 configuration. The IR spectrum shows bands related to the diphenyl N-dimethylamidophosphate ligands, with P=O and P-N stretching moved at slightly lower and higher wavenumbers, respectively.

On the basis of the PL spectrum it is likely to suppose an increase of the coordination number with respect to the corresponding bromo- and iodo-complexes, perhaps attributable to bridging coordination mode of chlorides. The luminescence lifetime is 1.5 ms, higher than those measured for bromo- and iodo-complexes (see Fig. 38). Longer lifetimes are however expected for Mn(II) chloro-complexes because of the lower spin-orbit coupling,[24] therefore the τ value does not allow the unambiguous determination of the coordination number. It is however worth noting that a similar lifetime was measured for the coordination polymer $[MnBr_2(dmf)(\mu\text{-}dppeO_2)]_n$ (dmf = dimethylformamide; $doppeO_2$ = 1,2-diphenylphosphinoethane dioxide), where Mn(II) is pentacoordinated.[28]

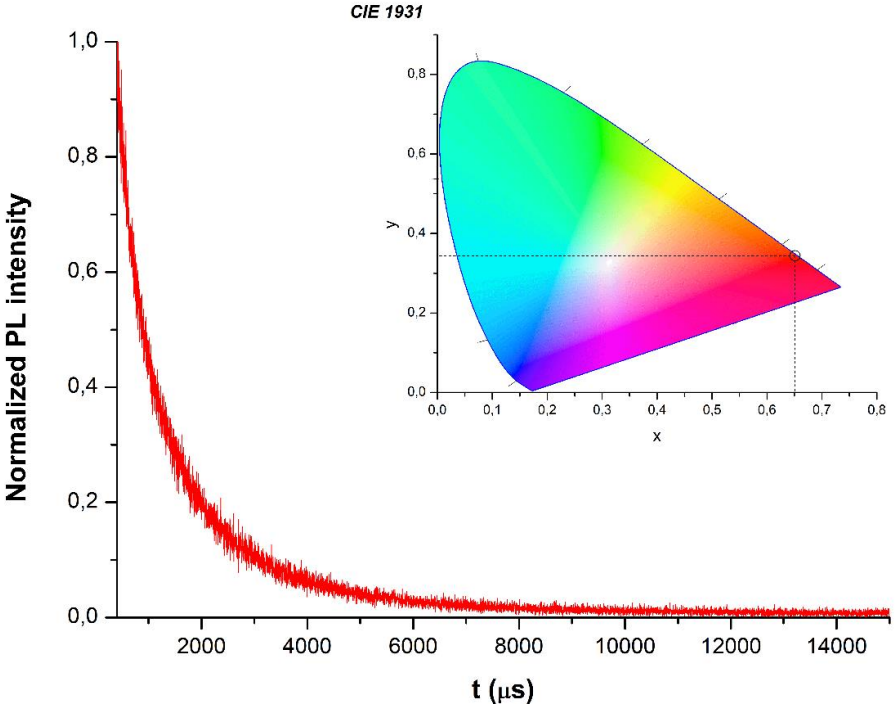

Figure 38. Luminescence decay curve of [$MnCl_2${O=P(OPh)$_2$(NMe$_2$)}$_2$] and chromaticity coordinates (x= 0.652; y= 0.347).

Preliminary studies were carried out also on another amidophosphate species, the cyclic compound *o*-phenylen-dimethylphosphoramidate, O=P(*o*-phenylen)(NMe_2). The procedure adopted during the thesis, starting from $O=PCl_3$, is summarized in Scheme 7. The compound thus obtained was reacted with $MnBr_2$ using the experimental conditions previously described, affording a green-emitting complex with proposed formula [$MnBr_2${O=P(*o*-phenylen)(NMe_2)}$_2$]. The ligand was isolated in very low yield, this avoiding the complete study of the reactions with Mn(II) precursors and the full characterization of the species. The literature however reports an improved synthetic procedure based on the reaction of hexamethylphosphoramide and catechol at high temperature.[88] The rigid structure of O=P(*o*-phenylen)(NMe_2) could potentially reduce the non-radiative decays, so the preliminary evidence of luminescence from Mn(II) with this ligand appears promising for further developments.

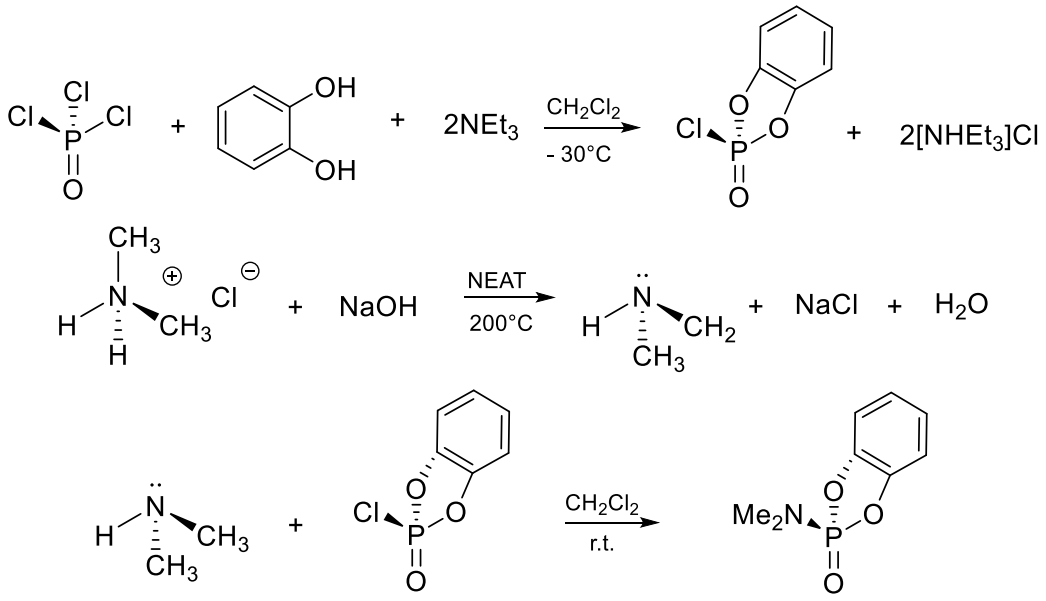

Scheme 7. Synthesis of O=P(o-phenylen)(NMe$_2$).

3.2 Lanthanide(III) complexes

The ligands that were successfully coordinated to Mn(II) were subsequently considered for the preparation of new luminescent lanthanide complexes, focusing the attention of visible-emitting metal centres, Eu(III), Tb(III) and Dy(III) in particular. Preliminary attempts to obtain new compounds starting from nitrato-precursors were unsuccessful, therefore attention was devoted to the synthesis of β-diketonate derivatives. The general synthetic procedure was based on the stepwise addition of the diketone, previously deprotonated with potassium *tert*-butoxide, and of the proper [P=O]-donor ligand to anhydrous $LnCl_3$ in THF. The β-diketones were chosen in order to optimize the luminescence of the Ln(III) centre. For this reason, in the case of Eu(III) tenoyltrifluoroacetone (H-tta) and dibenzoylmethane (H-dbm) were used, while acetylacetone (H-acac) was considered for Tb(III) and Dy(III).[73] The products isolated and characterized are sketched in Scheme 8.

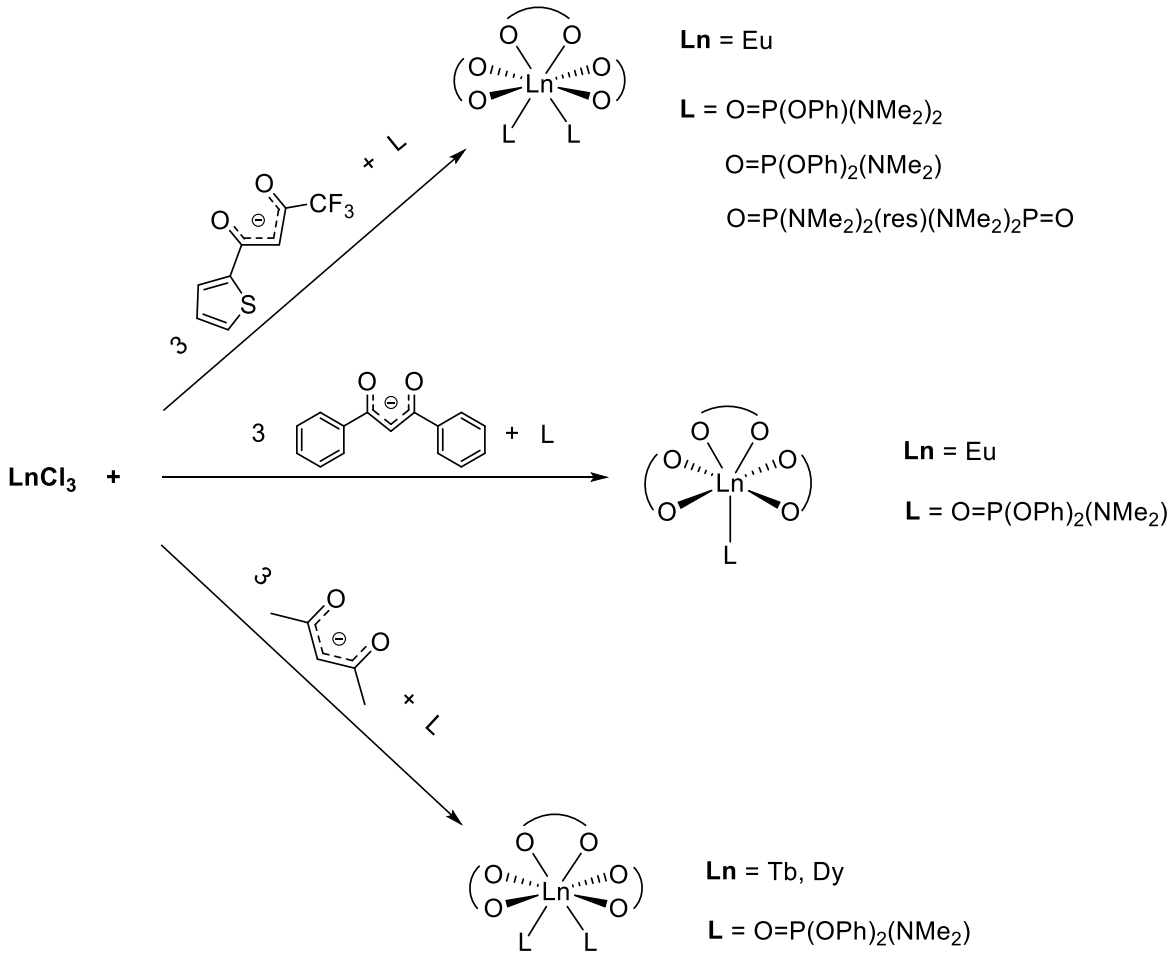

Scheme 8. Ln(III) β-diketonates with [P=O]-donor ligands.

In the case of Eu-tta complexes, the characterization data suggest the formation of 8-coordinated species having general formula $[Eu(tta)_3L_2]$. Experimental magnetic moments are all around 3.3 BM, *i.e.* the common value for Eu(III) at room temperature. The IR spectra show, besides the typical transitions of coordinated tta, the bands related to the amidophosphate ligands, with shifts of the P=O and P-N stretchings in line with those previously described for Mn(II) complexes. As an example, the IR spectrum of $[Eu(tta)_3\{O=P(OPh)_2(NMe_2)\}_2]$ is compared with that of the free ligand in Fig. 39.

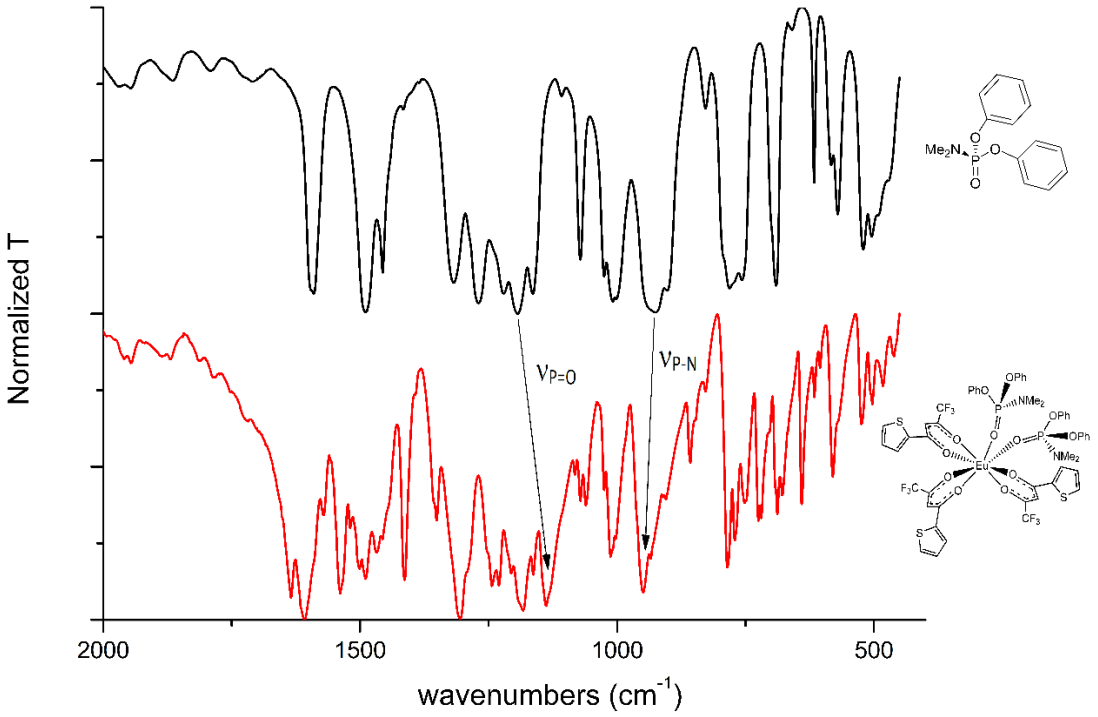

Figure 39. IR spectra comparison between $[Eu(tta)_3\{O=P(OPh)_2(NMe_2)\}_2]$ and the corrisponding ligand. (P=O and P-N stretching bands evidenced)

NMR spectra are characterized by very broad bands because of the paramagnetism of Eu(III) using solvents such as $CDCl_3$. NMR signals related the ligands were instead observed in the spectra collected in the coordinating solvent DMSO-d_6. The ^1H and $^{31}P\{^1H\}$ NMR spectra are reported in Figs. 40-42. As observable, all the ^1H NMR spectra show the typical broad bands of coordinated tta around 7.5, 6.5, 6.3 and 3.8 ppm. The presence of tta was also confirmed by ^{19}F resonances around –78 ppm. The presence of the amidophosphate ligands was confirmed by the related aromatic signals and by the doublet assigned to the N-bonded methyl groups in the aliphatic region. The $^{31}P\{^1H\}$ NMR showed in all the cases sharp singlets closely comparable with those of the free ligands, this suggesting that the [P=O]-donors here studied are displaced by DMSO, differently from what observed for arylphosphonic diamides.[89] As stated before on studying Mn(II) derivatives, amidophosphates are weaker ligands with respect to arylphosphonic diamides. Characterization data do not allow to unambiguously determine the coordination mode of the bidentate ligand $O=P(NMe_2)_2(res)(NMe_2)_2P=O$. On considering the previously described X-ray structure determination of the MnI_2 derivative, it is likely to suppose that the species acts as bridging ligand between two Eu(III) centres.

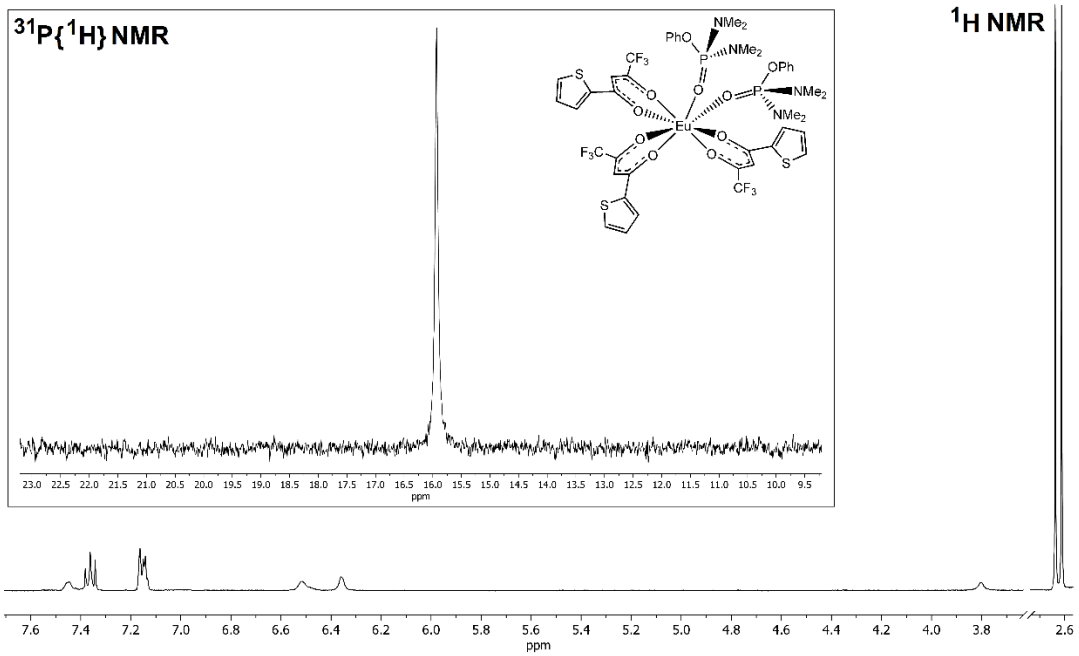

Figure 40. ^{1}H NMR spectrum of $[Eu(tta)_3\{O=P(OPh)(NMe_2)_2\}_2]$ Inset: $^{31}P\{^{1}H\}$ NMR spectrum. DMSO-d_6, 298 K.

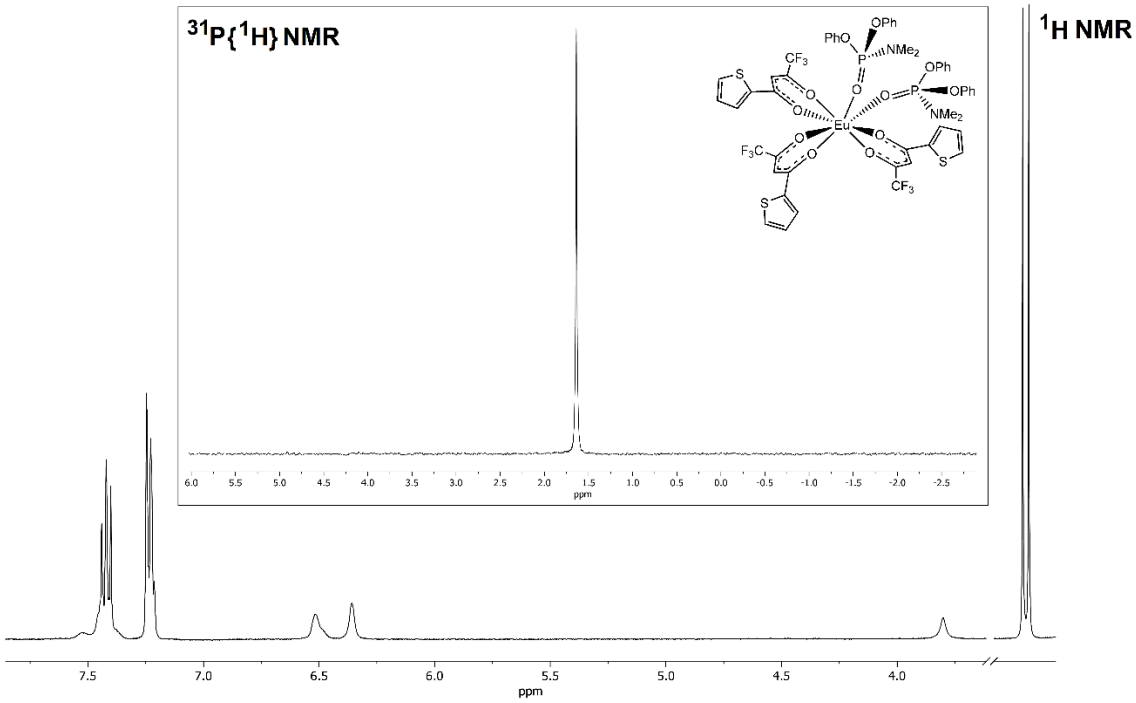

Figure 41. ^{1}H NMR spectrum of $[Eu(tta)_3\{O=P(OPh)_2(NMe_2)\}_2]$ Inset: $^{31}P\{^{1}H\}$ NMR spectrum. DMSO-d_6, 298 K.

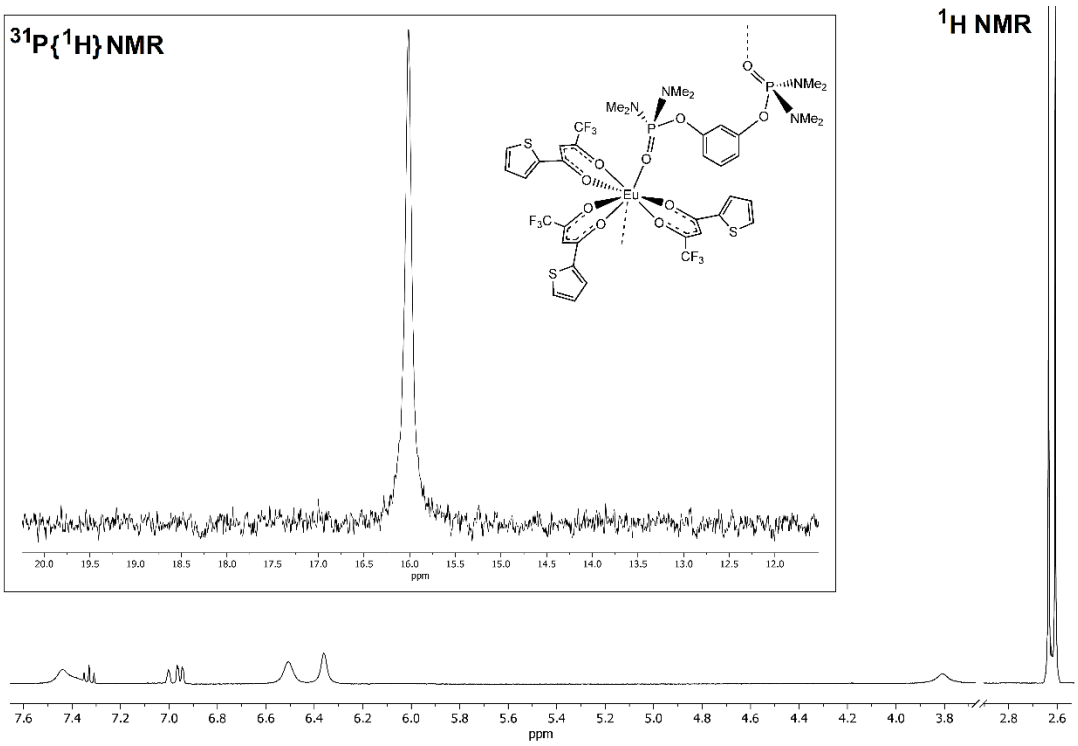

Figure 42. ^{1}H NMR spectrum of $[Eu(tta)_3\{O=P(NMe_2)_2(res)(NMe_2)_2P=O\}]$ Inset: $^{31}P\{^{1}H\}$ NMR spectrum. DMSO-d_6, 298 K.

Preliminary studies were carried out considering $O=P(OPh)_2(NMe_2)$ and dbm instead of tta as ligands. Probably because of the increased steric bulk, in this case the reaction afforded a 7-coordinated complex having formula $[Eu(dbm)_3\{O=P(OPh)_2(NMe_2)\}]$. As before, the IR spectrum showed signals related to the β-diketonate and the coordinated amidophosphate. The lower coordination number was suggested by magnetic measurements and by the integration of the ^{1}H NMR resonances (see the spectrum provided in Fig. 43).

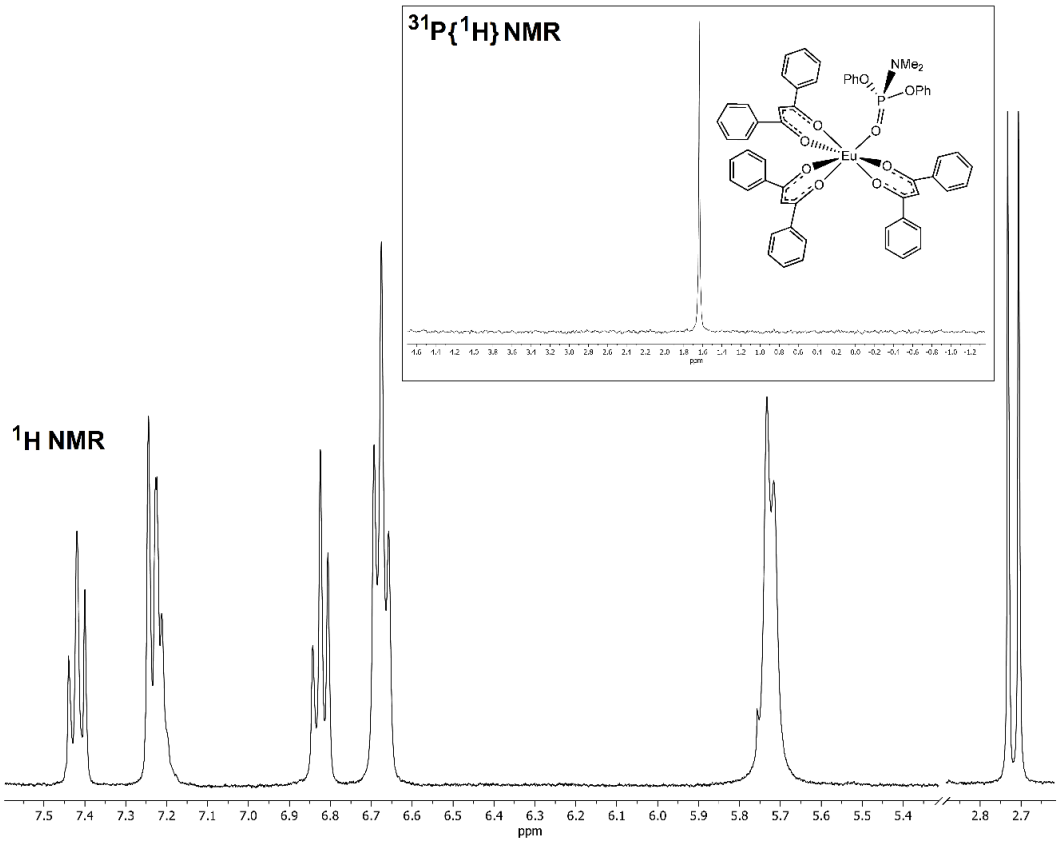

Figure 43. ^{1}H NMR spectrum of $[Eu(tta)_3\{O=P(OPh)_2(NMe_2)\}_2]$ Inset: $^{31}P\{^{1}H\}$ NMR spectrum. DMSO-d_6, 298 K.

The unambiguous determination of the structure was obtained from single crystal X-ray diffraction. An ORTEP view of the compound is reported in Fig. 44 and selected bond lengths are provided in the caption. The Eu-O(dbm) bond lengths are comprised between 2.298(9) and 2.338(8) Å, while as expected a slightly longer Eu-O distance was measured for the amidophosphate, 2.380(8) Å, probably because of the neutral charge of the last ligand. The Eu-O=P angle, 162.5(5)°, indicates slightly bent coordination mode. By using the Shape software,[90] the first coordination sphere was compared with different possible solids, in particular the heptagon (HP-7), the hexagonal pyramid (HPY-7), the pentagonal bipyramid (PBPY-7), the capped octahedron (COC-7), the capped trigonal prism (CTPR-7), the Johnson pentagonal bipyramid J13 (JPBPY-7) and the Johnson elongated triangular pyramid J7 (JETPY-7). On the basis of the output of the software, reported in Table 5, the geometry of the inner coordination sphere results close to the capped octahedron COC-7, as also observable in Fig. 44.

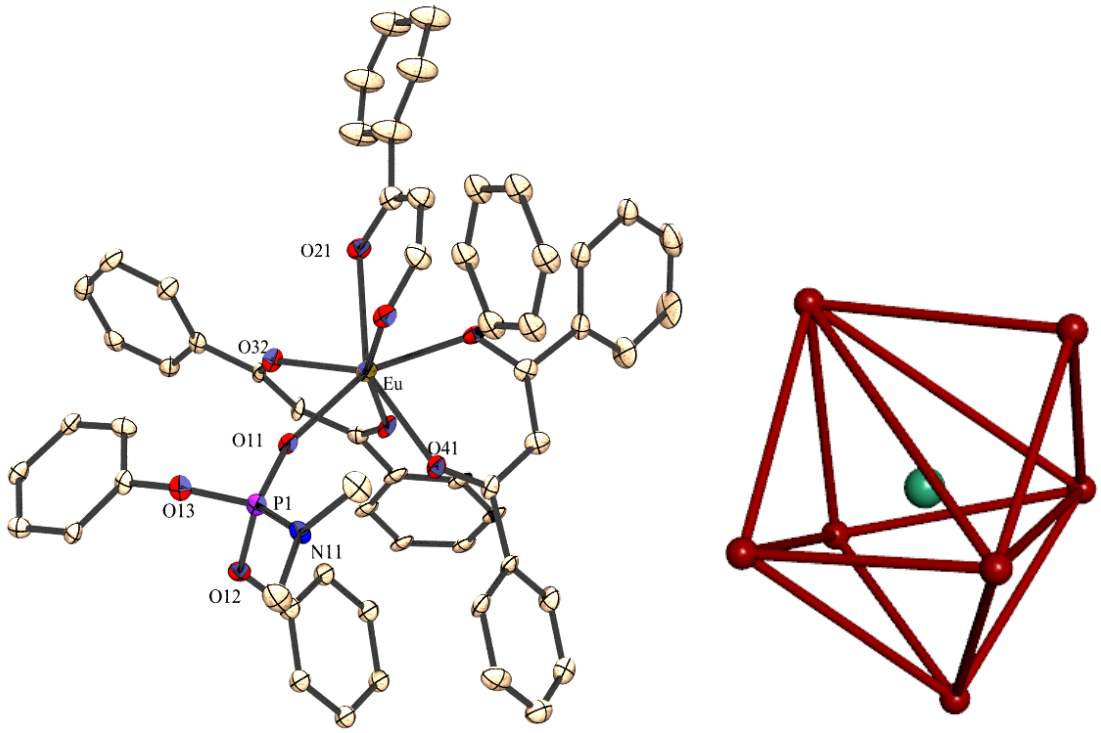

Figure 44. ORTEP view of [Eu(dbm)$_3${O=P(OPh)$_2$(NMe$_2$)] and polyhedron surrounding the Eu(III) centre. Selected bond lengths (Å): Eu-O(dbm) 2.338(8), 2.298(9), 2.328(8),2.306(9),2.347(8), 2.338(8), Eu-O(amidophosphate) 2.380(8). Selected angles (°): Eu-O=P 162.5(5).

Table 5. Output of the Shape software

Structure [ML7]	HP-7	HPY-7	PBPY-7	COC-7	CTPR-7	JPBPY-7	JETPY-7
[Eu(dbm)$_3${O=P(OPh)$_2$(NMe$_2$)]	34.959	19.778	6.267	0.727	1.492	9.855	20.449

All the Eu(III) complexes resulted bright red luminescent by excitation with near-UV and violet light. The PL spectra, reported in Figure 45, show the typical transitions from the $^5D_0$ resonance level to the ^7F_J manifold, the most intense band corresponding to J = 2 (hypersensitive). The high $^5D_0 \rightarrow {}^7F_2/{}^5D_0 \rightarrow {}^7F_1$ ratio (between 13 and 16 for the tta complexes, around 19 for the dbm derivative) and the separation in Stark sublevels of the $^5D_0 \rightarrow {}^7F_1$ transition indicate low symmetry of the complexes. Despite not conclusive, the presence of only one $^5D_0 \rightarrow {}^7F_0$ band indicates the presence of only one emitting species.[91] The PLE spectra (see for example Fig. 45) indicate antenna-effect from the coordinated ligands, superimposed to the direct excitation of the Eu(III) centre.

The range of excitation useful for Eu(III) luminescence is extended over all the UV and the blue-violet regions of the spectrum.

The luminescence lifetimes (τ) of the two O=P(OPh)$_2$(NMe) derivatives, the 7-coordinated [Eu(dbm)$_3${O=P(OPh)$_2$(NMe)}] and the 8-coordinated [Eu(tta)$_3${O=P(OPh)$_2$(NMe)}$_2$], are markedly different, being 241 and 570 μs, respectively. The role of the coordination number on the luminescence lifetimes was already observed for related species with comparable values.[66/89] The luminescence decay curves are compared in Fig. 46. The intrinsic quantum yields Q_{Eu}^{Eu} were estimated from the relative intensities of the $^5D_0 \rightarrow {}^7F_1$ transitions and the τ values accordingly to Eqn. 1.[92] The refraction index *n* was conventionally set equal to 1.5. Q_{Eu}^{Eu} resulted around 56% for the 8-coordinated tta derivative, while half of the value, 28%, was obtained for the 7-coordinated dbm complex.

$$Q_{Eu}^{Eu} = 14.65 \cdot n^3 \cdot \frac{I\left({}^5D_0 \rightarrow {}^7F_J\right)}{I\left({}^5D_0 \rightarrow {}^7F_1\right)} \cdot \tau(s)$$

The intense luminescence of the compound [Eu(tta)$_3${O=P(OPh)$_2$(NMe)}$_2$] prompted the study of its embedding in polymeric materials. In a typical preparation, 40 mg of the complex were added to 1.5 g of poly(methyl methacrylate) dissolved in the minimal amount of dichloromethane and the solution was used for the coating of commercially available near-UV LEDs (VCC VAOL-5EUV8T4, RS Components, maximum of emission at 385 nm, luminous intensity of 100 mcd). As observable in Fig. 46, the down-shifting of the radiation was successful and bright red-emitting LEDs were obtained.

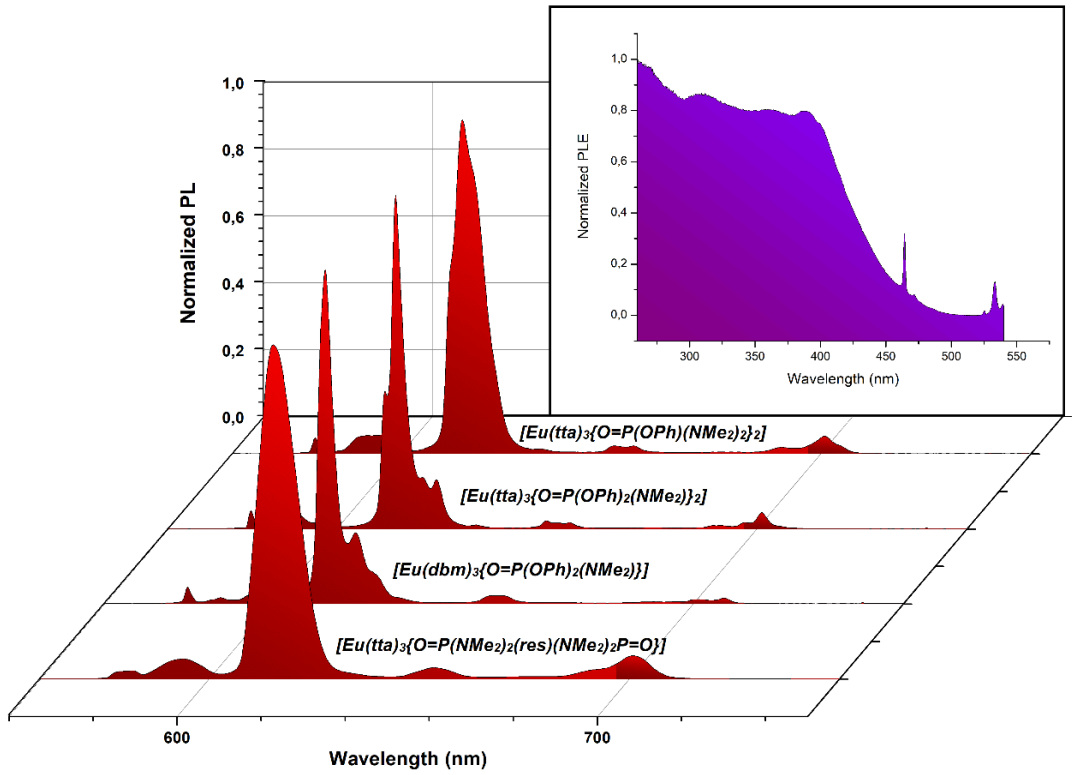

Figure 45. Normalized PL spectra of Eu complexes. Inset: PLE of $[Eu(tta)_3\{O=P(OPh)_2(NMe_2)\}_2]$.

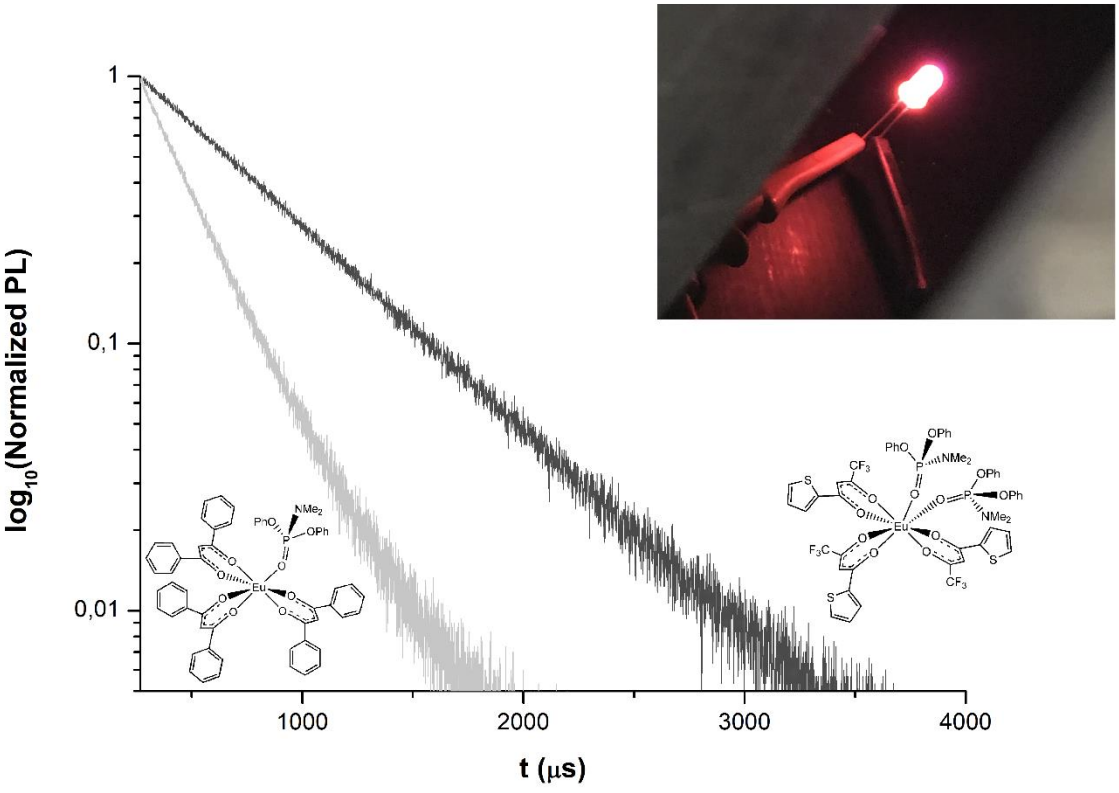

Figure 46. Semi-log plot of the luminescence decay curves of $[Eu(tta)_3\{O=P(OPh)_2(NMe_2)\}_2]$ (black) and $[Eu(dbm)_3\{O=P(OPh)_2(NMe_2)\}]$ (grey) and near-UV LED coated with $[Eu(tta)_3\{O=P(OPh)_2(NMe_2)\}_2]$@PMMA.

For what concerns the Tb(III) and Dy(III) derivatives, the general formula $[Ln(acac)_3L_2]$ was confirmed by magnetic measurements, affording values in line with those reported in the literature.[36] The IR spectra showed bands related to the coordinated ligands. The PL spectra of the Tb(III) complexes showed the typical $^5D_4 \rightarrow {}^7F_J$ transitions of the metal centre, the most intense corresponding to J = 5 centred around 547 nm, causing bright green photoluminescence of the compounds (see for instance Fig. 47). The relative energy of the $^5D_4$ resonance level is 20430 cm^{-1}, meaningfully higher than that of the Eu(III) $^5D_0$ level, 17250 cm^{-1}.[55] For this reason, Tb(III) requires ligands with quite high triplet states for its sensitization, such as acetylacetonate, this reducing the useful excitation range. As observable in Fig. 47, the PLE spectrum show bands related to antenna-effect for wavelengths below 410 nm. The luminescence lifetime measurement on $[Tb(acac)_3\{O=P(OPh)_2(NMe_2)\}_2]$ gave a τ value of 648 ms, corresponding to a Q_{Tb}^{Tb} quantum yield around 14% on assuming a radiative lifetime of 4.7 ms.[93] The analogous Dy(III) compound resulted much less luminescent, despite the fact that the typical $^4F_{9/2} \rightarrow {}^6H_J$ transitions can be observed by excitation with UV light, the most intense around 577 nm corresponding to J = 13/2. The relative energy of the $^4F_{9/2}$ level is 20960 cm^{-1},[55] similar to that of Tb(III), but the gap with the closest lower energy spin-orbit level is inferior, 7850 cm^{-1} (14800 cm^{-1} for Tb), this enhancing the non-radiative decay routes.

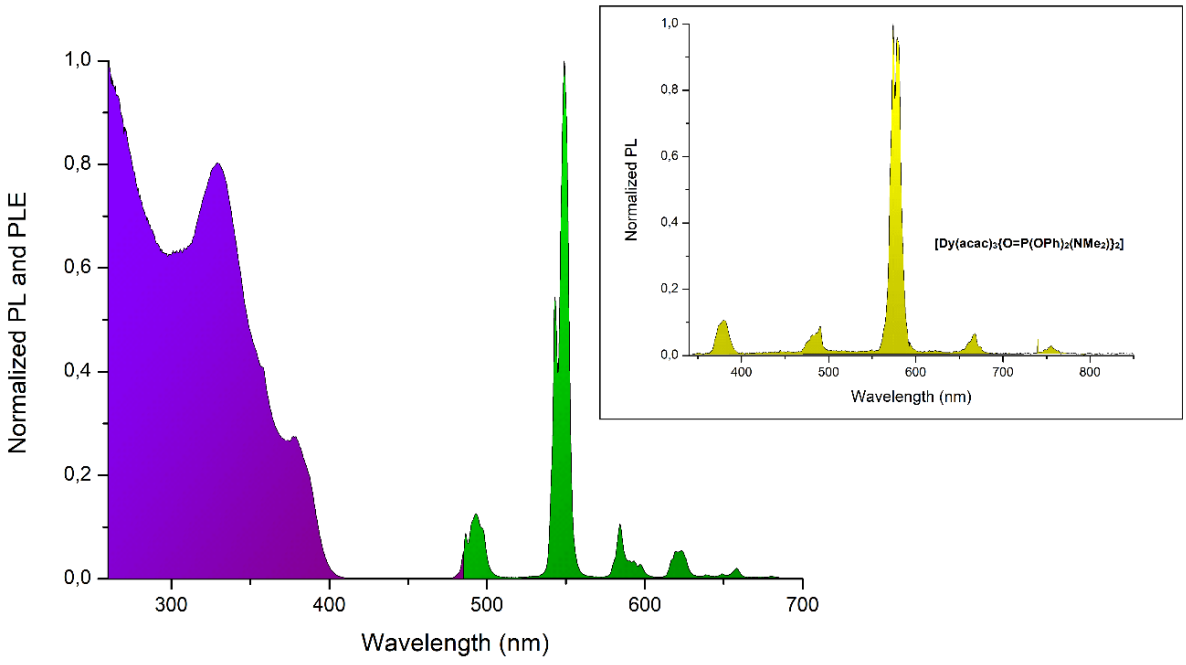

Figure 47. Normalized PL and PLE spectra of $[Tb(acac)_3\{O=P(OPh)_2(NMe_2)\}_2]$. Inset: PL of $[Dy(acac)_3\{O=P(OPh)_2(NMe_2)\}_2]$.

4. CONCLUSIONS

The thesis work demonstrated that amidophosphate ligands with phenyl substituents can successfully coordinate hard metal centres such as Mn(II) and Ln(III). The experimental and computational outcomes indicate that the electron-withdrawing OPh fragments reduce the σ-donation from the [P=O]-donor moiety with respect to phosphoramide and arylphosphonic diamide ligands.

The reaction of amidophosphates with Mn(II) bromide and iodide afforded tetrahedral complexes and coordination polymers, as unambiguously demonstrated in selected cases by single-crystal X-ray diffraction. The typical green luminescence was observed, but the amidophosphates showed negligible antenna-effect. Only one chloro-complex was isolated, and spectroscopic data suggest an expansion of the first coordination sphere.

Amidophosphates revealed to be suitable ligands for the preparation of Ln(III) derivatives in combination with β-diketonates. Depending upon the steric bulk, 7- or 8-coordinated complexes were isolated and characterized. The species exhibited the typical emission bands of the chosen lanthanide centre.

Preliminary investigations suggested that the study concerning amidophosphate ligands can be extended to cyclic species, such as *o*-phenylen-dimethylphosphoramidate.

5. BIBLIOGRAFHY

[1] (a) L. Pereira, Organic Light-Emitting Diodes, J. Stanford (eds.), New York (2012). (b) H. Xu, R. Chen, Q. Sun, W. Lai, Q. Su, W. Huang, X. Lu, Chem. Soc. Rev. 43 (2014) 3259. (c) V. W.-W. Yam, K. M.-C. Wong, Chem. Commun. 47 (2011) 11579.

[2] E. Rosenberg, J.B.A. Ross, A. Sharmin, Phosphorescent Ru(II) Complexes as Probes of Model Membrane Systems, in T. Hirao, T. Moriuchi (eds.), Advances in Bioorganometallic Chemistry, Chapter 12, Elsevier, Amsterdam (2019).

[3] C. Yang, F. Mehmood, T.L. Lam, S.L-F. Chan, Y. Wu, C-S. Yeung, X. Guan, K. Li, C.Y-S. Chung, C-Y. Zhou, T. Zou, C-M. Che, Chem. Sci. 7 (2016) 3123.

[4] Q. Zhao, W. Xu, H. Sun, J. Yang, K.Y. Zhang, S. Liu, Y. Ma, W. Huang, Adv. Opt. Mater. 4 (2016) 1167.

[5] M.S. Lowry, S. Bernhard, Chem. Eur. J., 12 (2006) 7970.

[6] K.R. Mann, M. Cimolino, G.L. Geoffroy, G.S. Hammond, A.A. Orio, G. Albertin and H.B. Gray, Inorg. Chim. Acta 16 (1976) 97.

[7] (a) J.A.G. Williams, S. Develay, D.L. Rochester, L. Murphy, Coord. Chem. Rev. 252 (2008) 2596. (b) J.Kalinowski, V. Fattori, M. Cocchi, J.A.G. Williams, Coord. Chem. Rev. 255 (2011) 2401. (c) K.M.-C. Wong, V.W.-W. Yam, Coord. Chem. Rev. 251 (2007) 2477. (d) C. Bronner, O. S. Wenger, Dalton Trans. 40 (2011) 12409. (e) W.P. To, D. Zhou, G.S.M. Tong, G. Cheng, C. Yang, C.M. Che, Angew. Chem. Int. Ed. 56 (2017) 14036.

[8] D.V. Scaltrito, D.W. Thompson, J.A. O'Callaghan, G.J. Meyer, Coord. Chem. Rev. 28 (2000) 243.

[9] S.M. Kuang, D.G. Cuttell, D.R. McMillin, P.E. Fanwick, R.A. Walton, Inorg. Chem. 41 (2002) 3313.

[10] N. Serpone, M.A. Jamieson, M.S. Henry, M.Z. Hoffman, F. Bolletta, M. Maestri, J. Am. Chem. Soc. 101 (1979) 2907.

[11] S. Otto, M. Grabolle, C. Förster, C. Kreitner, U. Resch-Genger, K. Heinze, Angew. Chem. Int. Ed. 54 (2015) 11572.

[12] M. Gaft, R. Reisfeld, G. Panczer, Modern Luminescence Spectroscopy of Minerals and Materials, Springer, Heidelberg (2015).

[13] T. Senden, E.J. van Harten, A. Meijerink, J. Lumin. 194 (2018) 131.

[14] M. Gaft, R. Reisfeld, G. Panczer, G. Boulon, S. Shoval, B. Champagnon, Opt. Mater. Express 8 (1997) 149.

[15] A. Donmez, M.B Coban, H. Kara, J. Clust. Sci. 29 (2018) 951.

[16] K.Binnemans, P.T.Jones, J. Rare Earths 32 (2014) 195.

[17] P. Li, M. Peng, L. Wondraczek, Y. Zhao, B. Viana, J. Mater. Chem. 3 (2015) 3406.

[18] (a) K. Nikolič, F. Lignou, H. Payen de la Garanderie, J. Lumin. 8 (1973) 137. (b) S. Balsamy, P. Natarajan, R. Vedalakshmi, S. Muralidharan, Inorg. Chem. 53 (2014) 6054. (c) F. A. Cotton, L. M. Daniels, P. Huang, Inorg. Chem. 40 (2001) 3576.

[19] (a) D.M.L. Goodgame, F.A. Cotton, J. Chem. Soc. (1961) 3735. (b) F.A. Cotton, D.M.L. Goodgame, M. Goodgame, J. Am. Chem. Soc. 84 (1962) 167.

[20] (a) A. Harriman, Coord. Chem. Rev. 28 (1979) 147. (b) O. Chen, D.E. Shelby, Y. Yang, J. Zhuang, T. Wang, C. Niu, N. Omenetto, Y.C. Cao, Angew. Chem. Int. Ed. 49

(2010) 10132. (c) J. Orive, J.L. Mesa, R. Balda, J. Fernández, J.R. Fernández, T. Rojo, M. I. Arriortua, Inorg. Chem. 50 (2011) 12463. (d) Z. Deng, L. Tong, M. Flores, S. Lin, J-X. Cheng, H. Yan, Y. Liu, J. Am. Chem. Soc. 133 (2011) 5389. (e) J. Lin, Q. Zhang, L. Wang, X. Liu, W. Yan, T. Wu, X. Bu, P. Feng, J. Am. Chem. Soc. 136 (2014) 4769. (f) J. Lin, L. Wang, Q. Zhang, F. Bu, T. Wu, X. Bu, P. Feng, J. Mater. Chem. C 4 (2016) 1645. (g) J. I. Zink, G. E. Hardy, G. Gliemann, Inorg. Chem. 19 (1980) 488.

[21] C. Jiang, N. Zhong, C. Luo, H. Lin, Y. Zhang, H. Peng, C.-G. Duan, Chem. Commun. 53 (2017) 5954.

[22] M. Bortoluzzi, J. Castro, F. Enrichi, A. Vomiero, M. Busato, W. Huang, Inorg. Chem. Commun. 92 (2018) 145.

[23] M. Bortoluzzi, J. Castro, J. Coord. Chem. 72 (2019) 309.

[24] M. Wrighton, D. Ginley, Chem. Phys. 4 (1974) 295.

[25] (a) Y. Zhang, W-Q. Liao, D-W. Fu, H-Y. Ye, C-M. Liu, Z-N. Chen, R-G. Xiong, Adv. Mater. 27 (2015) 3942. (b) Y. Zhang, W.Q. Liao, D.W. Fu, H.Y. Ye, Z.N. Chen, R-G. Xiong, J. Am. Chem. Soc. 137 (2015) 4928. (c) H-Y. Ye, Q. Zhou, X. Niu, W-Q. Liao, D-W. Fu, Y. Zhang, Y-M. You, J. Wang, Z-N. Chen, R-G. Xiong, J. Am. Chem. Soc. 137 (2015) 13148. (d) Y-M. You, W-Q. Liao, D. Zhao, H-Y. Ye, Y. Zhang, Q. Zhou, X. Niu, J. Wang, P-F. Li, D-W. Fu, Z. Wang, S. Gao, K. Yang, J-M. Liu, J. Li, Y. Yan, R.-G. Xiong, Science 357 (2017) 306.

[26] A.S. Berezin, M.P. Davydova, I. Yu. Bagryanskaya, O.I. Artyushin, V.K. Brel, A.V. Artem'ev, Inorg. Chem. Commun. 107 (2019) 107473.

[27] Y. Mei, H. Yu, Z. Wei, G. Mei, H. Cai, Polyhedron 127 (2017) 458.

[28] (a) M. Bortoluzzi, J. Castro, E. Trave, D. Dallan, S. Favaretto, Inorg. Chem. Commun. 90 (2018) 105. (b) Y. Wu, X. Zhang, L-J. Xu, M. Yang, Z-N. Chen, Inorg. Chem. 57 (2018) 9175.

[29] D. Hausmann, A. Kuzmanoski, C. Feldmann, Dalton Trans. 45 (2016) 6541.

[30] A.S. Berezin, K.A. Vinogradova, V.A. Nadolinny, T.S. Sukhikh, V.P. Krivopalov, E. B. Nikolaenkova, M.B. Bushuev, Dalton Trans. 47 (2018) 1657.

[31] A.V. Artem'ev, M.P. Davydova, A.S. Berezin, V.K. Brel, V.P. Morgalyuk, I.Y. Bagryanskaya, D. G. Samsonenko, Dalton Trans. 48 (2019) 16448.

[32] M. Bortoluzzi, J. Castro, A. Gobbo, V. Ferraro, L. Pietrobon, S. Antoniutti, New J. Chem. 44 (2020) 571.

[33] A. Gobbo. Synthesis and characterization of new phosphoramide ligands for the preparation of luminescent manganese and f-block metal complexes; Master's degree thesis, Ca' Foscari university of Venice, 2019

[34] S. Favaretto. Sintesi di composti fotoluminescenti di manganese(II) con leganti ossigeno-donatori a base di fosforo pentavalente. Bachelor's degree thesis, Ca' Foscari university of Venice, 2016.

[35] (a) C.K. Jørgensen, The Inner Mechanism of Rare Earths Elucidated by Photo-Electron Spectra, Springer, Berlin/Heidelberg (1973). (b) I. McGill, Rare Earth Elements, Wiley, Chichester (2005).

[36] S. Cotton, Lanthanide and Actinide Chemistry, in Derek Woollins, Wiley, Chichester (2016).

[37] V.W.W. Yam, K.K.W. Lo, Coord. Chem. Rev. 184 (1999) 157.

[38] A. Beeby, S.W. Botchway, I.M. Clarkson, S. Faulkner, A.W. Parker, D. Parker, J.A.G. Williams, J. Photochem. Photobiol. B. Biol. 57 (2000) 83.

[39] (a) G.M. Davies, S.J.A. Pope, H. Adams, S. Faulkner, M.D. Ward, Inorg. Chem. 44 (2005) 4656. (b) S. Faulkner, S.J.A. Pope, B.P. Burton-Pye, Appl. Spectros. 40 (2005) 1. (c) S. Aime, M. Botta, D. Parker, J.A.G. Williams, J. Chem. Soc., Dalton Trans. 1 (1996) 17. (d) C.M.G. dos Santos, P.B. Fernandez, S.E. Plush, J.P. Leonard, T. Gunnlaugsson, Chem. Commun. 32 (2007) 3389.

[40] (a) S.I. Klink, G.A. Hebbink, L. Grave, F. Van Veggel, D.N. Reinhoudt, L.H. Slooff, A. Polman, J.W. Hofstraat, J. Appl. Phys. 86 (1999) 1181. (b) B.H. Bakker, M. Goes, N. Hoebe, H.J. Van Ramesdonk, J.W. Verhoeven, M.H.V. Werts, J.W. Hofstraat, Coord. Chem. Rev. 208 (2000) 3. (c) T.J. Foley, B.S. Harrison, A.S. Knefely, K.A. Abboud, J.R. Reynolds, K.S. Schanze, J.M. Boncella, Inorg. Chem. 42 (2003) 5023. (d) S. Quici, M. Cavazzini, G. Marzanni, G. Accorsi, N. Armaroli, B. Ventura, F. Barigelletti, Inorg. Chem. 44 (2005) 529. (e) S. Quici, G. Marzanni, A. Forni, G. Accorsi, F. Barigelletti, Inorg. Chem. 43 (2004) 1294.

[41] (a) D. Guo, C.Y. Duan, F. Lu, Y. Hasegawa, Q.J. Meng, S. Yanagida, Chem. Commun. (2004) 1486. (b) S. Faulkner, S.J.A. Pope, J. Am. Chem. Soc. 125 (2003) 10526. (c) I.A. Kamenskikh, N. Guerassimova, C. Dujardin, N. Garnier, G. Ledoux, C. Pedrini, M. Kirm, A. Petrosyan, D. Spassky, Opt. Mater. 24 (2003) 267. (d) N.M. Shavaleev, S.J.A. Pope, Z.R. Bell, S. Faulkner, M.D. Ward, Dalton Trans. (2003) 808.

[42] (a) Y. Oshishi, T. Kanamori, T. Kitagawa, S. Takashashi, E. Snitzer, G.H. Sigel, Opt. Lett. 16 (1991) 1747. (b) L.H. Slooff, A. Polman, M.P.O. Wolbers, F. van Veggel, D.N. Reinhoudt, J.W. Hofstraat, J. Appl. Phys. 83 (1998) 497.

[43] K. Kuriki, Y. Koike, Y. Okamoto, Chem. Rev. 102 (2002) 2347.

[44] K. Nakamura, Y. Hasegawa, H. Kawai, N. Yasuda, N. Kanehisa, Y. Kai, T. Nagamura, S. Yanagida, Y. Wada, The J. Phys. Chem. A. 111 (2007) 3029.

[45] A. Beeby, L.M. Bushby, D. Maffeo, J.A.G. Williams, J. Chem. Soc., Dalton Trans. 1 (2002) 48.

[46] S.I. Weissman, J. Chem. Phys. 10 (1942) 214.

[47] M. Latva, H. Takalo, V.-M. Mukkala, C. Matachescu, J.C. Rodriguez-Ubis, J. Kankare, J. Lumin. 75 (1997) 149.

[48] T. Förster, Discuss. Faraday Soc. 27 (1959) 7.

[49] D.L. Dexter, J. Chem. Phys. 21 (1952) 836.

[50] Y. Hasegawa, Y.W.S. Yanagida, J. Photochem. Photobiol A. 5 (2004) 183.

[51] (a) D-E. Henrie, R-L. Fellows, G.R. Choppin, Coord. Chem. Rev. 18 (1976) 199. (b) H.A. Hussain, A.A. Ansari, K. Iftikhar, Spectrochim. Acta A. 60 (2004) 873. (c) M. Hatanaka, S. Yabushita, Chem. Phys. Lett. 504 (2011) 193. (d) K. Bukietyńska, A. Mondry, E. Osmęda, J. Inorg. Nucl. Chem. 43 (1981) 1311.

[52] M. Bortoluzzi, A. Reolon, A. Scrivanti, F. Enrichi, Chem. Pap. 72 (2018) 809.

[53] J.-C.G. Bünzli, S.V. Eliseeva, Chem. Soc. Rev. 39 (2010) 189.

[54] R.G. Pearson, J. Chem. Educ. 45 (1968) 581.

[55] K. Binnemans, Chem. Rev. 109 (2009).

[56] (a) I. B. Liss, W. G. Bos, J. Inorg. Nucl. Chem. 39 (1977) 443. (b) J. M. Koehler, W.G. Bos, Inorg. Nucl. Chem. Lett. 3 (1967) 545.

[57] N. Filipescu, W. F. Sager, F. A. Serafin, J. Phys. Chem. 68 (1964) 3324.

[58] (a) D. Guillaumont, H. Bazin, Chem. Phys. Chem. 8 (2007) 480. (b) R. Rodriguez-C., F. Avecilla, Inorg. Chem. 41 (2002) 21. (c) D. Guillaumont, H. Bazin, J. M. Benech, M. Boyer, G. Mathis, Chem. Phys. Chem. 8 (2007) 480.

[59] (a) B.M. Alsaadi, F.J.C. Rossotti, R.J.P. Williams, J. Chem. Soc., Dalton Trans. (1980) 597. (b) B.M. Alsaadi, F.J.C. Rossotti, R.J.P. Williams, J. Chem. Soc., Dalton Trans. (1980) 813.

[60] S. Trofimenko, Scorpionates: The Coordination Chemistry of polypyrazolilborate Ligands, Imperial College Press., London (1999).

[61] K. W. Bagnall, A. C. Tempest, J. Takatas, A. P. Masino, Inorg. Nucl. Chem. Lett. 12 (1976) 555.

[62] (a) Z-F. Li, L. Zhou, J-B. Yu, H-J. Zhang, R-P. Deng, Z-P. Peng, Z-Y. Guo. J. Phys. Chem. C. 111 (2007) 2295. (b) Z. Li, J. Yu. J. Lumin. 143 (2013) 169. (c) G. Qian, Z. Yang, M. Wang. J. Lumin. 96 (2002) 211. (d) V.I. Verlan, M.S. Iovu, I. Culeac, Y.H. Nistor, C.I. Turta, V.E. Zubareva. J. Non-Cryst. Solids 21 (2013) 360. (e) M. Bortoluzzi, E. Bianchin, S. Roppa, V. Bertolasi, F. Enrichi. Dalton Trans. 43 (2014) 10120.

[63] Y. Zhou, H. Li, T. Zhu, T. Gao, P. Yan, J. Am. Chem. Soc. 141 (2019) 19634.

[64] (a) J.T. Donoghue, D.A. Peters, J. Inorg. Nucl. Chem. 31 (1969) 467. (b) N. B. Mikheev, A.N. Kamenskaya, N.A. Konovalova, T.A. Zhilina, Russ. J. Inorg. Chem. 22 (1977) 955.

[65] Y. Makioka, T. Hayashi, M. Tanaka, L.B. Hao, Novel phosphonamides, process for producing the same, and use thereof, WO 2003/074538.

[66] (a) F.A. Silva Jr., H. A. Nascimento, D.K.S. Pereira, J. Braz. Chem. Soc. 24 (2013) 601. (b) B.V. Bukvetskii, A.G. Mirochnik, P.A. Zhikhareva, J Lumin. 32 (2016) 341. (c)

M. Bortoluzzi, A. Gobbo, A. Palù, F. Enrichi, A. Vomiero, Chem. Pap. (2019). https://doi.org/10.1007/s11696-019-00799-6.

[67] X. Huang, Y. Xu, K. Fan, S. Bao, M. Kurmoo, L. Zheng, Angew. Chem. 57 (2018) 8577.

[68] (a) K.E. Laintz, E. Tachikawa Anal. Chem. 66 (1994) 2190. (b) I. Fidelis, J. Inorg. Nucl. Chem. 32 (1970) 997.

[69] L.R. Matthews, E.T. Knobbe, Chem. Mater. 5 (1993) 1697.

[70] (a) B. Yan, H. J. Zhang, S.B. Wang, J.Z. Ni, Mater. Chem. Phys. 51 (1997) 92. (b) W. Strek, L. Sokolnicki, J. Legendziewicz, K. Maruszewski, R. Reisfeld, T. Pavich, Opt. Mater. 13 (1999) 41.

[71] C. Sanchez, F. Ribot, New J. Chem. 18 (1994) 1007.

[72] D. Sendor, U. Kynast, Adv. Mater. 14 (2002) 1570.

[73] K. Binnemans, V. Pecharsky, Handbook on the Physics and Chemistry of Rare Earths, 35, Elsevier, Amsterdam (2005).

[74] (a) J. Boyaval, F. Hapiot, C. Li, N. Isaert, M. Warenghem, P. Carette, Mol. Cryst. Liq. Cryst. 330 (1999) 1387. (b) J. Boyaval, C. Li, F. Hapiot, M. Warenghem, N. Isaert, Y. Guyot, G. Boulon, P. Carette, Mol. Cryst. Liq. Cryst., 359 (2001) 337. (c) K. Binnemans, D. Moors, J. Mater. Chem. 12 (2002) 3374.

[75] W.L.F. Armarego, D.D. Perrin, Purification of laboratory chemicals, Butterworth-Heinemann, Oxford (1996).

[76] S. Ryu, J.A. Jackson, C.M. Thompson, J. Org. Chem. 56 (1991) 4999.

[77] (a) J. Perregaard, E.B. Pedersen, S.O. Lawesson, Recl. Trav. Chim. Pays-Bas 93 (1974) 252. (b) J.H. Näsman, N. Kopola, Synth. Commun. 22 (1992) 2491.

[78] H. Kovache, H. Jean, G. Garnier, Chim. et Industr. 64 (1950) 287.

[79] (a) J-D. Chai, M. Head-Gordon, Dalton Trans. 41 (2012) 5526. (b) J-D. Chai and M. Head-Gordon, Phys. Chem. Chem. Phys. 10 (2008) 6615. (c) I.C. Gerber, J.G. Ángyán, Chem. Phys. Lett. 415 (2005) 100.

[80] F. Weigend, R. Ahlrichs, Phys. Chem. Chem. Phys. 7 (2005) 3297.

[81] (a) M. Cossi, N. Rega, G. Scalmani, V. Barone, J. Comput. Chem.24 (2003) 669. (b) V. Barone, M. Cossi, J. Phys. Chem. A. 102 (1998) 1995.

[82] F. Jensen, Introduction to Computational Chemistry, Wiley, Chichester (2007).

[83] (a) F. Neese, WIREs Comput. Mol. Sci. 2 (2012) 73. (b) F. Neese, WIREs Comput. Mol. Sci. 8(2018) e1327.

[84] T. Lu, F. Chen, J. Comput. Chem. 33 (2012) 580.

[85] L. Yang, D.R. Powell, R.P. Houser, Dalton Trans. (2007) 955.

[86] E. F. Schubert, Light-emitting Diodes, Cambridge University Press, Cambridge (2006) 292.

[87] (a) R. Bianchi, G. Gervasio, D. Marabello, Inorg. Chem., 39 (2000) 2360. (b) C. Lepetit, P. Fau, K. Fajerwerg, M.L. Kahn, B. SIlvi, Cord. Chem. Rev. 345 (2017) 150.

[88] S.E. Pipko, Y.V. Balitsky, A.D. Sinitsa, Y.G. Gololobov, Tetrahedron Lett. 355 (1994) 165.

[89] M. Bortoluzzi, A. Gobbo, J. Coord. Chem 72 (2019) 1524.

[90] M. Llunell, D. Casanova, J. Cirera, P. Alemany, S. Álvarez. SHAPE, v. 2.1, Universitat de Barcelona and The Hebrew University of Jerusalem, Barcelona and Jerusalem (2013).

[91] K. Binnemans, Coord. Chem. Reviews 295 (2015) 1.

[92] J-C.G. Bünzli, Chem. Rev. 110 (2010) 2729.

[93] J.L. Vázquez-Ibar, A.B. Weinglass, H.R. Kaback, Proc. Natl. Acad. Sci. 6 (2002) 3487.

6. SUPPLEMENTARY MATERIALS

The study of pentavalent phosphorous based ligands was extended to the possible coordination of the [P=S] fragment to trivalent lanthanides ions. In particular, the conjugate base of bis(diphenylphosphino)methane disulphide was considered, trying to extend the study initiated during the Bachelor's thesis.[a]

It is worth noting that the coordination behaviour of sulphur-donor ligands towards Ln^{3+} as metal ions had been poorly explored in the past.[b] Because of the softness of sulphur as donor atom, the formation of complexes with hard metal centres, such as trivalent lanthanide ions, represents a difficult challenge.

The compounds $K[Eu(dppmS_2)_4]$ and $[Eu(dppmS_2)_3(phen)]$ (Scheme S1) were prepared from anhydrous Eu(III) triflate, the potassium salt of bis(diphenylphosphino)methane disulphide $K[dppmS_2]$ and 1,10-phenanthroline (phen) in THF. IR and NMR data are in line with those previously reported.[a] Among the new measurements on these compounds, the proposed formulae $K[Eu(dppmS_2)_4]$ and $[Eu(dppmS_2)_3(phen)]$ were confirmed by magnetic measurements, in line with the common value for the magnetic moment of Eu(III) at room temperature, 3.3 BM.

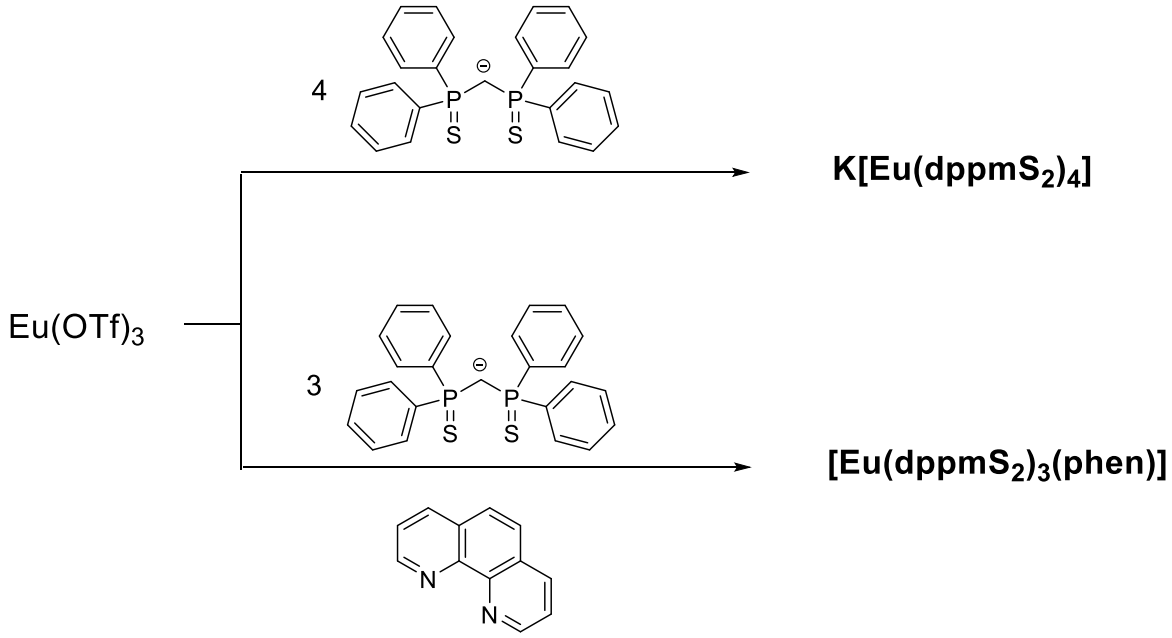

Scheme S1. Synthesis of $K[Eu(dppmS_2)_4]$ and $[Eu(dppmS_2)_3(phen)]$.

The new photoluminescence measurements confirmed that the emission from these compounds is mainly related to the excited states of the coordinated ligands, rather than the Eu(III) f-shell (see for instance Fig. S1). Wide emission bands were detected in the visible range, related to excitation in the near-UV region. It is therefore likely to suppose that the excited states of coordinated $[dppmS_2]^-$ have too low relative energy for an efficient sensitization of Eu(III).

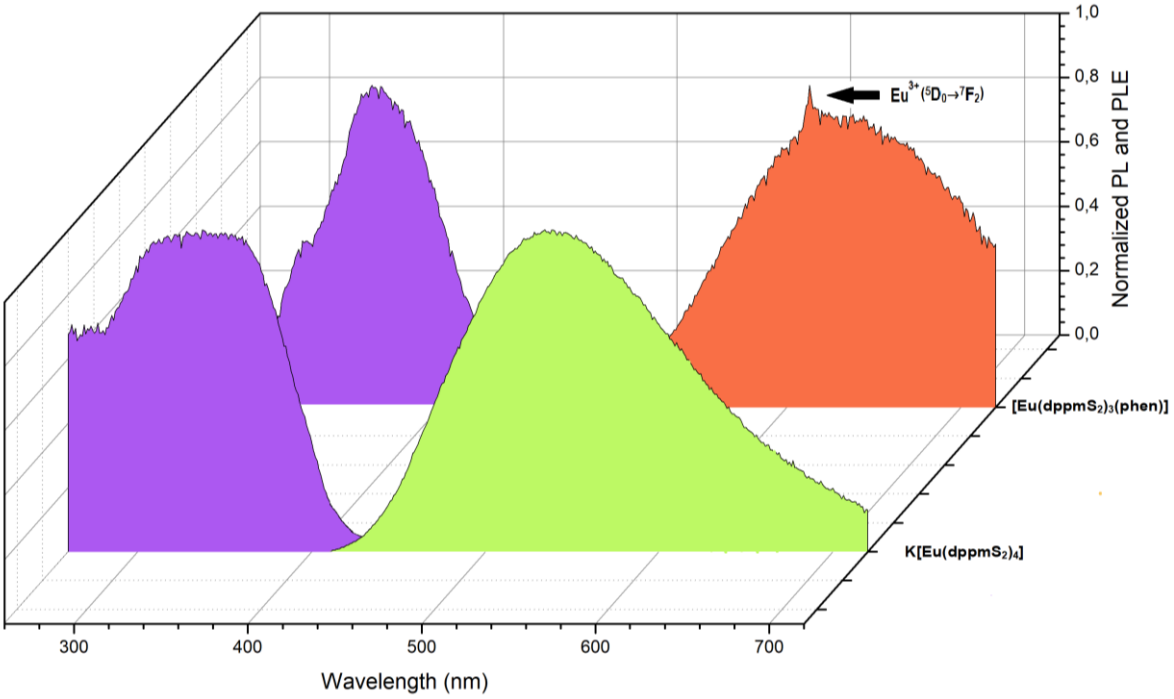

Figure S1. Normalized PL and PLE spectra of $K[Eu(dppmS_2)_4]$ and $[Eu(dppmS_2)_3(phen)]$

The unusual luminescence of these compounds prompted to complete the study trying to obtain structural information. As previously stated, Ln(III) complexes with sulphur atoms in the first coordination sphere are very rare in the literature. Unfortunately, despite all the attempts the poor stability of the Eu-S bond prevented the formation of crystals suitable for X-ray diffraction.

[a] A. Di Vera. “Sintesi e caratterizzazione di nuovi complessi di lantanidi con leganti antenna zolfo e ossigeno donatori”, Bachelor’s degree thesis, Ca’ Foscari university of Venice, 2017.

[b] (a) M.D. Regulacio, M. H. Pablico, J. A. Vasquez, P.N. Myers, S. Gentry, M. Prushan, S-W. Tam-Chang, S. L. Stoll, Inorg. Chem. 47 (2008) 1512. (b) W. M. Faustino, O. L. Malta, E.E.S. Teotonio, H.F. Brito, A.M. Simas, G.F. de Sa´, J. Phys. Chem. A. 110 (2006) 2510. (c) K. E. Laintz, E. Tachlkawa, Anal. Chem. 66 (1994) 2190.